PB84-229756

In Situ Analysis of Corrosive and Passive Surfaces by Laser-Excited Raman Spectroscopy

Rhode Island Univ., Kingston

Prepared for

Municipal Environmental Research Lab.
Cincinnati, OH

Aug 84

U.S. Department of Commerce
National Technical Information Service
NTIS

PB84-229756

EPA-600/2-84-133
August 1984

IN SITU ANALYSIS OF CORROSIVE AND PASSIVE SURFACES BY LASER-EXCITED RAMAN SPECTROSCOPY

by

Chris W. Brown
University of Rhode Island
Kingston, Rhode Island 02881

Grant No. CR807291010

Project Officer

Marvin C. Gardels
Drinking Water Research Division
Municipal Environmental Research Laboratory
Cincinnati, Ohio 45268

MUNICIPAL ENVIRONMENTAL RESEARCH LABORATORY
OFFICE OF RESEARCH AND DEVELOPMENT
U.S. ENVIRONMENTAL PROTECTION AGENCY
CINCINNATI, OHIO 45268

REPRODUCED BY
NATIONAL TECHNICAL
INFORMATION SERVICE
U.S. DEPARTMENT OF COMMERCE
SPRINGFIELD, VA. 22161

TECHNICAL REPORT DATA
(Please read Instructions on the reverse before completing)

1. REPORT NO.	2.	3. RECIPIENT'S ACCESSION NO.
EPA-600/2-84-133		PB84 229756

4. TITLE AND SUBTITLE	5. REPORT DATE
IN SITU ANALYSIS OF CORROSIVE AND PASSIVE SURFACES BY LASER-EXCITED RAMAN SPECTROSCOPY	August 1984
	6. PERFORMING ORGANIZATION CODE

7. AUTHOR(S)	8. PERFORMING ORGANIZATION REPORT NO.
Chris W. Brown	

9. PERFORMING ORGANIZATION NAME AND ADDRESS	10. PROGRAM ELEMENT NO.
Department of Chemistry University of Rode Island Kingston, RI 02881	11. CONTRACT/GRANT NO. CR807291010

12. SPONSORING AGENCY NAME AND ADDRESS	13. TYPE OF REPORT AND PERIOD COVERED
Municipal Environmental Research Laboratory-Cinti, OH Office of Research and Development U.S. Environmental Protection Agency Cincinnati, OH 45268	14. SPONSORING AGENCY CODE EPA/600/14

15. SUPPLEMENTARY NOTES

Project Officer: Marvin C. Gardels - (513)684-7236

16. ABSTRACT

From both laboratory and field investigations it has been found that protective films can be formed or deposited on lead and asbestos-cement pipes. The purpose of the present project was to determine the chemical and/or crystalographic composition of surface films on these pipes. Both laboratory and field samples of lead were investigated by Raman and infrared spectroscopy. A number of laboratory samples were investigated in situ using laser-excited Raman spectroscopy. A limited number of field samples of asbestos-cement pipes were studied using infrared spectroscopy. In addition, surface films from field samples of galvanized iron pipes were measured.

The results on lead pipes indicate that the surface films are primarily composed of lead monoxide, PbO. This compound exists in two crystalographic forms, orthorhombic and tetragonal. The latter should be the stable form under ambient conditions; however, orthorhombic is "stabilized" by some type of impurities and is the dominant form present at pH values below 7. Due to its unstable nature, orthorhombic PbO has a strong tendency to enter the water column. The stable tetragonal form of PbO was observed at pH values greater than 7.5. This form appears to be much more protective of the surface, i.e., it acts as a protective film.

Variations in the chemical composition of asbestos-cement pipes make it impossible to identify the composition of surface films using spectroscopic techniques; however, surface films on field samples of galvanized iron were identified as zinc carbonates using infrared spectroscopy.

17. KEY WORDS AND DOCUMENT ANALYSIS

a. DESCRIPTORS	b. IDENTIFIERS/OPEN ENDED TERMS	c. COSATI Field/Group

18. DISTRIBUTION STATEMENT	19. SECURITY CLASS *(This Report)*	21. NO. OF PAGES
Release to Public	Unclassified	144
	20. SECURITY CLASS *(This page)*	22. PRICE
	Unclassified	

EPA Form 2220-1 (9-73)

DISCLAIMER

Although the information described in this document has been funded wholly or in part by the United States Environmental Protection Agency through assistance agreement number CR807291010 to the University of Rhode Island, it has not been subjected to the Agency's required peer and administrative review and therefore does not necessarily reflect the views of the Agency and no official endorsement should be inferred.

FOREWORD

The U.S. Environmental Protection Agency was created because of increasing public and government concern about the dangers of pollution to the health and welfare of the American people. Noxious air, foul water, and spoiled land are tragic testimonies to the deterioration of our natural environment. The complexity of that environment and the interplay of its components require a concentrated and integrated attack on the problem.

Research and development is that necessary first step in problem solution, and it involves defining the problem, measuring its impact, and searching for solutions. The Municipal Environmental Research Laboratory develops new and improved technology and systems to prevent, treat, and manage wastewater and solid and hazardous waste pollutant discharges from municipal and community sources, to preserve and treat ublic drinking water supplies, and to minimize the adverse economic, social, health, and aesthetic effects of pollution. This publication is one of the products of that research and is a most vital communications link between the researcher and the user community.

In the present investigation, the chemical composition of fibers formed on the surface of lead, asbestos/cement, and galvanized-iron pipes have been studied. In particular, the surface of lead pipes were monitored *in situ* to determine the conditions for forming and the compositions of protective films.

Francis T. Mayo
Director
Municipal Environmental Research
Laboratory

ABSTRACT

For both laboratory and field investigations it has been found that protective films can be formed or deposited on lead and asbestos-cement pipes. The purpose of the present project was to determine the chemical and/or crystalographic composition of surface films on these pipes. Both laboratory and field samples of lead were investigated by Raman and infrared spectroscopy. A number of laboratory samples were investigated in situ using laser-excited Raman spectroscopy. A limited number of field samples of asbestos-cement pipes were studied using infrared spectroscopy. In addition, surface films from field samples of galvanized iron pipes were measured.

The results on lead pipes indicate that the surface films are primarily composed of lead monoxide, PbO. This compound exists in two crystalographic forms, orthorhombic and tetragonal. The latter should be the stable form under ambient conditions; however, orthorhombic is "stabilized" by some type of impurities and is the dominant form present at pH values below 7. Due to its unstable nature, orthorhombic PbO has a stronger tendency to enter the water column. The stable tetragonal form of PbO was observed at pH values greater than 7.5. This form appears to be much more protective of the surface, i.e., it acts as a protective film.

Variations in the chemical composition of asbestos-cement pipes make it impossible to identify the composition of surface films using spectroscopic techniques; however, surface films on field samples of galvanized iron were identified as zinc carbonates using infrared spectroscopy.

This report was submitted in fulfillment of Grant No. CR807291010 by the University of Rhode Island under the sponsorship of the U.S. Environmental Protection Agency. The report covers the period August 11, 1980 to November 10, 1983, and work was completed as of November 10, 1983.

CONTENTS

Foreword iii
Abstract. iv
Acknowledgments vi

1. Introduction. 1
   Problem 1
   Molecular Spectroscopy. 1
      Infrared Absorption Spectroscopy. 2
      Raman Spectroscopy. 2
2. Experimental. 3
   Raman Spectra 6
   Infrared Spectra. 6
   Chemicals 7
   Corrosion Meter 7
   In-Situ Raman Cells 8
3. Results 8
   Lead. 10
      Standard Raman Spectra of Lead Compounds 10
      Flow-thru Cell Experiments 10
         Experiment 1 11
         Experiment 2 11
         Experiment 3 12
         Experiment 4 13
         Experiment 5 13
         Experiment 6 14
         Experiment 7 14
         Experiment 8 15
         Experiment 9 16
         Experiment 10 16
         Experiment 11 17
      Field Samples of Lead Pipes. 17
         Experiment 17 18
         Experiment 31 18
         Experiment 32 18
         Experiment 33 18
         Experiment 34 19
         Experiment 32A. 19
         Experiment 33A. 19
   Asbestos Cement Pipes -- Field Samples. 19
   Galvanized Pipes -- Field Samples 19
4. Discussion. 20

Appendix. 21
Tables. 23
Figures 27
References. 38

ACKNOWLEDGMENTS

This report represents major contributions from Patricia F. Lynch and Gregory Thomas. Assistance of Elizabeth A. Burny and Susan Myette in preparing the final draft is gratefully acknowledged. Finally, the technical advice and timely assistance of Marvin C. Gardels during the entire project is greatly appreciated.

I. INTRODUCTION

PROBLEM

In some of the major cities in the United States, drinking water is delivered to residences and businesses through lead or asbestos cement (A/C) pipes (1). Both of these materials present known potential health hazards. Lead can form water soluble compounds, and even insoluble compounds can be suspended in the flowing water. The cement in A/C pipes can corrode, leaving asbestos particles protruding from the surface. These particles can be disengaged by the flowing water and reach the consumer as particulate matter. The primary goal of the present research project is to identify the chemical composition of surface films formed under known conditions.

Ultimately, this information will help us reach our final goal of finding some reasonable chemical conditions that will form protective films on the surfaces of both lead and A/C pipes. We have attempted to provide information, where possible, under in-situ flow-through conditions similar to those in actual water supply systems.

The present research deals mainly with lead pipes, since we had considerable previous experience with the analysis of films on lead surfaces. The methodology was developed several years before and was tested on numerous samples (2,3).

The composition of films formed on metal surfaces can be predicted from thermodynamic data (2,4,5). A plot of the predicted composition as a function of pH and electrochemical potential is called a Pourbaix diagram, and such a diagram for lead appears in Figure 1. The dashed lines a and b define the stability region for water: Below a hydrogen evolves, and above b oxygen evolves. The region on the bottom of the diagram labeled Pb is the immune region in which lead should exist without the formation of any surface films. In the upper left (labeled Pb), lead ionizes and goes into solution. In the other regions, the oxides shown on the diagram should form, but these are the thermodynamically favored forms and may not be the forms observed. For example, in an earlier study (2), we explored the pH's of 7 and 10 as a function of the potential difference E. The results are shown on the diagram as i for immune, c for carbonate, and o for orthorhombic PbO. Two of the samples were found to be immune in the immune region, but two samples proved to be carbonates. The rest of the observations showed orthorhombic PbO, but as will be shown later, we should not have observed orthorhombic PbO.

Our secondary goal in the present program was to develop the methodology for analyzing surface films on A/C pipes. Since the compositions of these films were completely unknown, new approaches had to be tested. As a third objective, we explored the possibilities of analyzing surface films on galvanized-iron pipes. As it turned out, difficulties with A/C and galvanized pipes were similar.

The analyses were performed with the optical spectroscopic techniques of Raman and infrared spectroscopy. These complementary techniques provide qualitative information about chemical composition from the characteristic spectral fingerprint of each chemical. This fingerprint can identify and, under appropriate conditions, quantify the amount of material present.

MOLECULAR SPECTROSCOPY -- INFRARED AND RAMAN

It is generally easier for the novice to understand infrared spectroscopy since many scientists are somewhat familiar with the optical absorption process. Thus we will begin the discussion of molecular spectroscopy with infrared absorption and then move on to Raman spectroscopy.

We refer to this section as molecular spectroscopy since the interaction of light is with the molecular motions of the molecules. Both rotational and vibrational motions can be affected by the interaction; but, in solids, we are only concerned with vibrations, and our discussion will be confined to these motions.

Infrared Absorption Spectroscopy

Molecules can exist in certain discrete vibrational energy states referred to as quantum states or levels. An example of two energy levels appears in Figure 2, but many potential vibrational levels exist in a molecule. Molecules can undergo a transition from one level to another by absorbing or emitting one quantum of radiation. Under ambient conditions, we are generally concerned with absorption of radiation.

When a diatomic molecule absorbs radiation and goes to a higher vibrational state the molecule simply vibrates faster (note that molecules always possess a minimum amount of vibrational energy). For larger molecules the complexity of the motions can also change. For example, the water molecule has two hydrogen atoms bound to an oxygen atom, and the bonds are separated by an angle of 105°. Each bond can be treated as a spring that is continually expanding and contracting. The two bonds can expand and contract together in an in-phase fashion that we refer to as a symmetric vibration. They can also move out of phase, which we refer to as an antisymmetric motion. A third vibrational motion is defined by the expansion and contraction of the angle between the two bonds. Thus water has three vibrational motions: two stretching and one bending.

For any non-linear polyatomic molecule, there are (3N-6) possible vibrational motions, where N is the number of atoms. Not all of these will be accessable by absorbing infrared radiation, and we will discuss the selection rules below. However, if we assume that many of these vibrations can interact with infrared radiation, we soon see the possible complexity of the problem. This can be simplified by the fact that rather specific frequencies can be assigned to certain chemical group motions. For example, most $-CH_2-$ groups in organic molecules undergo a transition to the anti-symmetric stretching level at a frequency of 2936 to 2916 cm^{-1}. If there were ten $-CH_2-$ groups, each would absorb at approximately the same frequency and produce one absorption band rather than ten bands.

In much of this investigation, we were studying molecules that are in a crystalographic environment. In such an environment, each individual molecule is affected by neighboring molecules. For example, one of the more important molecules in this study was PbO. As we showed above, the vibration of a diatomic is very simple. However, in a crystallographic form the vibrational frequency of one molecule is affected by the positions and motions of other molecules in the proximity of the original molecule. The coupling between nearby molecules can cause frequency shifts and splittings of bands. An example of the latter effect might be the coupling of vibrations of two polar molecules located parallel to each other in a unit cell. In-phase motions could produce to one vibrational frequency and out-of-phase motions to another.

Infrared radiation is absorbed by a molecule only when there is a change in dipole moment. Homonuclear diatomic molecules cannot interact with infrared radiation since they do not have dipole moments in the ground or excited states. Many symmetric molecules such as methane do not have dipole moments in the ground state; however, they are distorted in an excited state to induce a dipole and they can absorb radiation in the transition process.

The most important feature of vibrational spectroscopy in chemical analysis is the uniqueness of the spectral pattern. The chemical composition and the physical state combine to cause a unique spectral pattern, i.e., each chemical material has its distinctive pattern and this pattern is different for the gaseous, liquid, and solid states. The unique pattern acts as a fingerprint for the material in question. The identity of this material can be determined by searching libraries of spectra fingerprints of known material. Today, there are a number of rapid, accurate computer searching algorithms available.

Raman Spectroscopy

Raman spectroscopy provides molecular information that complements the information provided by infrared spectroscopy; however, the proceses are entirely different. As discussed above, infrared involves the

absorption of a photon by a molecule undergoing a quantum transition from a lower to a higher energy state. Raman spectroscopy involves a light scattering process. Relatively high energy photons incident upon a sample are scattered elastically or inelastically. Elastically scattered (same energy) photons are referred to as Rayleigh scattering, whereas inelastically scattered (different energy) photons are referred to as Raman scattering.

In the Raman scattering process, the incident photon with frequency induces a dipole moment in the molecule and forces the molecule to a pseudo energy state. This is shown in the center portion of the energy level diagram in Figure 3 by the energy transition ν_o from v=0 to the "dashed" (pseudo) energy state. Typically, the energy of ν would correspond to 20,000 cm^{-1}, whereas the energy difference between the lowest two vibrational levels, ν_i, is on the order of 2000 cm^{-1}. The excited molecule can release a photon of the same energy and return to the v=0 state (Rayleigh), or it can retain some of the energy and return to a higher energy state such as v=1 (Raman). The energy of the latter photon is $\nu_o - \nu_i$ or (20,000 - 2000 = 18,000 cm^{-1}). Raman transitions which originate in the ground state (v=0) and end in an upper state (v=1) are referred to as Stokes scattering. Raman transitions can also originate in an excited state (e.g., v=1) and end in the ground state (v=0). These are referred to as anti-Stokes. The intensities of the transitions depend upon the number of molecules in the original energy state. This follows a Boltzman distribution and, for the population of molecules in an excited state, it decreases with increasing energy differences between the ground and excited states at constant temperature. The intensity of anti-Stokes scattering decreases with the frequency of the transition; thus, Stokes scattering is normally used. As mentioned above, the incident photon induces a temporary dipole moment in the molecule. For part of the energy to be retained by the molecule causing Raman scattering, the selection rules require that there be a change in polarizability in the molecule in going from the ground (v=0) to excited (v=1) state. The polarizability is associated with the electron (charge) distribution; thus, for Raman scattering, the electron "cloud" must be going through some distortion in the excited vibrational state.

Since the interaction of light with matter in Raman spectroscopy depends upon the polarizability, the ease at which an electron can interact depends upon the magnitude of the polarizability. Generally, molecules with large atoms having loosely held electrons are the strongest Raman scatterers. Lead is one such atom and its compounds are strong Raman scatterers.

There are certain inherent advantages to Raman spectroscopy. Water is a weak Raman scatterer; therefore, spectra of other materials can be obtained by passing the incident and scattered beams through water. Generally, Raman spectra are excited with visible light sources; thus, cells and containers can be made of glass. This greatly reduces any fabrication problems. Raman spectra are excited with a laser beam so that minimum sample sizes are required. Since Raman is a scattering effect,

any geometrical configuration can be used. However, for surface samples, the scattered signal is maximized at certain experimentally determined incident angles.

As has been shown previously, Raman spectroscopy offers an ideal method for probing the nature of surface films. Spectra can be obtained *in situ* without disturbing the environment. All other surface analysis techniques require that samples be removed from the aqueous environment and, in many cases, the samples have to be subjected to ultra high vacuum. Thus, Raman spectroscopy is ideally suited for determining the composition of surface films on lead, and it was the primary analytical tool used in this program.

II. EXPERIMENTAL

RAMAN SPECTRA

A schematic of the Raman spectrometer is shown in Figure 4. A Coherent Radiation Laboratory Model 52 (CR-3) 3-watt Argon Ion laser is used as the excitation source. The laser radiation is optically filtered with an Anaspec Model 300-S tunable laser monochromator. Typical laser power at the sample is in the range of 200 to 500 m-watts. The Raman scattering is collected at 90° to the laser excitation and directed into a Spex Industries Model 1401 3/4-meter Czerny-Turner double monochromator-spectrometer with f/6.8 optics and a stepper motor grating drive. A photomultiplier/photon counting system is used for detection.

The Raman spectrometer is interfaced directly to a Data General NOVA 3/12 Computer. The stepper motor on the spectrometer grating drive can be controlled by the computer or independent of the computer. Under computer control, multiple scans can be made of the same spectral region. The spectrometer can be manually set at a certain frequency, and the operator informs the computer of the frequency range, scan speed and the number of scans. The computer provides the stepper motor pulses to scan forward. At the end of the scan range, pulses are sent to reverse the stepper motor and the grating drive is returned to its initial frequency and another scan is initiated.

The detection system on the spectrometer is also interfaced to the computer through an A/D converter. The analog signal from the photon counting rate meter is converted to a digital signal. The stepper motor control is set so that the analog signal is converted to a digital number one time per cm^{-1} (wavenumber).

The digital data acquired by the computer can be subjected to the following algorithms:

1. Signal average
2. Spectral subtraction
3. Spectral addition
4. Spectral expansion
5. CRT display
6. Hard copy graphing

We will demonstrate some of these algorithms in the results section.

Raman spectra were measured of samples *in situ* (the cells will be discussed below), as surface films after removing from the aqueous environment, as powders in capillary tubes or as powders pressed in a KBr matrix. The latter method consists of grinding the powder, adding powdered KBr, mixing and forming a pellet by pressing in a die at 20,000 lbs.

INFRARED SPECTRA

Infrared spectra of samples were measured on a Beckman Model 4260 infrared spectrometer. This spectrometer is interfaced to the same NOVA-3 computer. In this case, frequency pulses from the spectrometer "interrupt" the computer and cause an analog to digital conversion of the voltage signal representing the % transmission of the spectrometer. All of the algorithms listed above for Raman are applicable to infrared spectra.

Spectra of samples as pressed KBr pellets were measured. Generally, the powdered sample was obtained from an *in situ* pipe sample by scraping the surface.

CHEMICALS

Two types of lead samples were used in this study:

1) 1.5 mm thick foil obtained from Alfa Chemical having a listed purity of 99.995%.
2) 5 mm thick, 20 mm I.D. pipe provided by the Environmental Protection Agency Laboratory - Cincinnati.

The lead sections were cut away from the foil or pipe with a band saw. To insure the lead surface to be monitored did not contain any lead oxides or other interfering species prior to the initiation of an experiment, the following cleaning techniques were employed:

1) polishing with steel wool followed by fine emery paper,
2) immersion into dilute nitric acid for 5 to 10 minutes,
3) immersion into warm concentrated ammonium acetate for 5 to 10 minutes.

The immersion techniques were designed to remove any lead surface film by producing soluble lead species. At the completion of one or more of these applications, the lead surface was washed with distilled water, dried with Kimwipes, and washed a second time with the aqueous flow-thru medium to be used in the experiment. After the final wash, the lead electrodes were positioned in the cell and the experiment was initiated immediately. These cleaning techniques were used interchangeably with no apparent effect on the formation of surface films.

All other chemicals used in this study were reagent grade.

CORROSION METER

A Petrolite Corporation Model M-3010 Corrosion Meter was used to monitor the rate of corrosion in mils per year (mpy). The device employs the PAIR technique and requires three electrodes of identical material referred to as reference, test and auxillary electrodes. In our case, all three electrodes are lead. The methodology and the conversion of the meter reading to actual lead corrosion are discussed in the Appendix.

IN-SITU RAMAN CELLS

Two types of in-situ flow-thru Raman cells were employed in this investigation. The first is a miniature cell with lead electrodes formed from 1 inch squares of lead foil. The cell container was a 325 ml Pyrex crystallizing dish. Water was pumped through the cell by a parastaltic pump from a 2 liter reservoir. A schematic of this cell is shown in Figure 5.

The second in-situ flow-thru Raman cell consisted of electrodes made from the 1 inch OD lead pipe. In this case the electrodes were set in a flow-thru configuration attached to a 100 gal. reseroir with a centrifugal pump flowing water at the rate of 7 gal. per minute. A number of "cell" configurations were designed and built. The first design is shown in Figure 6. The cell consisted of three sections of 1 inch lead pipe separated from each other by Tygon tubing, and connected to the reservoir pump by Tygon tubing. The test electron (pipe) in the first design had a sampling window in the shape of a diamond cut into it. Our intentions were to seal a half cylindrical section of Pyrex glass over the opening, but we could not make an adequate seal.

The second design for the flow-through pipe cell is shown in Figure 7. The auxillary and reference electrodes were embedded inside Tygon tubing. The test electrode was embedded inside of a glass tube which was connected to the remaining sections of the cell by Tygon tubing. Electrical leads to all electrodes were sealed with silicone glue. Moreover, both ends of each lead electrode (pipe) were covered with silicone glue so as to limit the corrosion of the inner cylindrical section of the pipes. This cell worked well as far as not leaking. However, the overall configuration of the three electrodes in a row and the shape of the sampling window in the test electrode made it extremely difficult to obtain suitable Raman spectra.

To solve the configuration problems another cell was designed and built. A schematic of this cell is shown in Figure 8. This new cell was a modification of the one shown in Figure 7. In this case, the test electrode is held in a 90 glass tube which was located between the reference and auxillary electrodes. As noted in the schematic, the 90

glass tube containing the text electrode has a flat glass plate at one corner for the laser beam to enter; this eliminates possible optical distortion of the beam. The Raman scattering is collected through the cylindrical surface at 90 to the input beam. A schematic of the entire system including the cell, pump and 100 gal. reservoir is shown in Figure 9. During normal operation, the cell was placed in an empty 100 gal. reservoir, which was used to catch any leaking water. To measure Raman spectra the cell was moved from this container to the Raman sample compartment.

III. RESULTS

LEAD

The primary goal of this investigation was to relate the composition of surface films formed on lead to the exposure conditions. Raman spectra of surface films were measured *in situ* and after removal from the aqueous environment. Moreover, Raman spectra of field samples supplied by EPA were measured. The compositions of these films were determined by comparison with standard spectra of known chemicals; thus, we will discuss the standard spectra first.

Standard Raman Spectra of Lead Compounds

Raman spectra were measured of standard samples in capillary tubes when possible. We resorted to KBr pellets when decomposition by the laser radiation was apparent. Spectra were measured at a spectral slit width of 6 cm^{-1}. All spectra were acquired by the computer and stored on magnetic disks; these data could then be used at a later date for comparison purposes or subjected to other data processing routines. Moreover, for weakly scattering samples, the scattering intensities could be signal averaged to improve the signal to noise ratio. An example of this process is shown in Figures 10-12. The Raman spectrum of a single scan of $PbCl_2$ powder from 0 to 250 cm^{-1} is shown in Figure 10, the average of 9 scans in Figure 11 and the 2X expansion of the 9 scan average in Figure 12. The improvements in the signal to noise ratio are obvious.

Standard spectra of $PbCl_2$ and $PbBr_2$ on the same frequency scale are shown in Figure 13. Spectra of $PbSO_4$ and $(PbCO_3)_2$ $Pb(OH)_2$ are shown in Figure 14 and 15, respectively.

The major components expected on the surface of lead pipes are the oxides; thus, we tried to obtain satisfactory spectra of all of the oxides. From the Pourboix diagram in Figure 1, it is anticipated that PbO will be the most significant component in the pH region of practical importance (pH = 6 to 10). PbO exists in two crystallographic forms: tetragonal and orthorhombic. Below 488°C the tetragonal structure is the thermodynamically stable form. However, in an earlier study we found that orthorhombic PbO is apparently stabilized by impurities and remains in that form indefinitely.

The Raman spectrum of orthorhombic PbO is shown in Figure 16. We tried to purchase tetragonal (referred to as "litharage") but the spectrum was always that of orthorhombic. However, in the process of making a KBr pellet of orthorhombic PbO, the grinding or pressure converted some of the orthorhombic to tetragonal. The spectrum of orthorhombic PbO as a powder in a capillary tube is compared to a rigorously ground sample in a KBr pellet in Figure 17. Obvious differences can be seen. These are even more apparent in the expanded spectrum shown in Figure 18. We subtracted the O-spectrum from the O & T spectrum and the result is given as T in Figure 19. The spectral differences between the two crystallographic forms are clear from this figure.

The Raman spectra of the other oxides were also difficult to obtain. The spectrum of one oxide, Pb_3O_4, as a powder in a capillary tube is shown in Figure 20. Spectra labeled A through D represent four successive scans. The relative decrease in the intensity of the band at 150 cm should be noted. When Pb_3O_4 was ground and made into a KBr pellet, an entirely different spectrum was obtained as is shown in Figure 21. The heat of the laser beam could decompose the powdered Pb_3O_4, possibly into Pb_2O_3 and orthorhombic PbO with the broad band between 400 and 600 cm^{-1} due to Pb_2O_3 and the sharp one at 150 cm^{-1} due to orthorhombic PbO.

On a number of occasions during the last several years we have attempted to obtain the Raman spectrum of PbO_2. This dark brown material turned to a tan color under the laser beam and the Raman spectrum was very similar to orthorhombic PbO. The Raman spectrum of PbO_2 in a KBr pellet was finally obtained using low laser power (less than 100 m-watts) and it is shown in Figure 22 where it is compared to that of orthorhombic PbO. The major differences in the spectra are the relative intensities and the exact peak frequencies. In the spectrum of orthorhombic PbO the peaks are at 84, 99, 154, 302 and 398 cm^{-1}, whereas in PbO_2 the peaks are at 83, 91, 146, 286 and 384 cm^{-1}. The closeness of the peak frequencies makes it difficult to distinguish between orthorhombic PbO and PbO_2. In a number of samples we will discuss, both compounds could be present.

Flow-Thru Cell Experiments

One of our objectives was to determine the similarities and differences between the large flow-through pipe cell and the small flow-through cell. We ran a number of experiments with both cells under identical conditions. In the present discussion we will follow the chronological development independent of the cell size. A summary of the experiments listing the type of cell, duration of the experiment and conditions is given in Table 1. We will discuss each experiment separately and summarize the results at the end.

Experiment 1

In this experiment, distilled water was pumped through the small cell

using a peristaltic pump. The corrosion meter was adjusted for a full scale reading of 50 myp (mils per year) and a cycle time of 25 min. During the first 36 hours of the experiment, a large amount of a white crystalline precipitate formed in the cell, depositing on the electrodes and the bottom of the cell. A Raman spectrum of the electrodes could not be obtained through the precipitate; therefore, it was decided to discontinue the experiment. The reference electrode was removed from the cell, dryed and a Raman spectrum of the surface was measured. The precipitate was collected by filtering and the Raman spectrum of the dried material was measured. Both spectra shown in Figure 23 contained relatively sharp, strong bands. Comparison of these with the standard spectra shows them to be predominantly due to orthorhombic PbO. Figure 24 shows the result of subtracting the standard spectrum of orthorhombic PbO from the spectrum of the electrode. No residual bands are readily apparent in the result, indicating that orthorhombic PbO is indeed the predominant component on the electrode surface. The two "derivatives" seen at approximately 150 and 84 cm^{-1} are a commonly occurring artifact seen when subtracting two spectra containing intense, sharp peaks. Considering the sharpness of these bands and the slight differences in band shapes of the two spectra, these derivatives are within acceptable limits and indicate a relatively clean subtraction of orthorhombic PbO from the electrode spectrum.

The difference spectrum resulting after the Raman spectrum of orthorhombic PbO was subtracted from that of the filtrate is shown in Figure 25. Again, the subtraction is relatively clean, indicating that the filtrate is most likey orthorhombic PbO.

Experiment 2

In this experiment, laboratory tap water (pH = 5, hardness = 12 mg/liter) was pumped through the cell for 8 days. Raman spectra of the reference electrode were measured in situ. A cloudiness developed in the water during the 8 days, but no noticeable precipitate formed. Raman spectra of the surface for days 1, 4, 5, 6, and 8 are shown in Figures 26-30. Each spectrum is an average of 9 scans. Multiple scanning increased signal-to-noise ratios and "brought out" the weaker bands which would otherwise be buried in the noise of the background. In the spectra for days 1 and 4, a broad, weak band is seen between 600 and 400 cm^{-1} and a sharp band is located at about 170 cm^{-1}. These spectra are similar to those in Figure 20 which suggest that Pb_3O_4 (possible in the form of Pb_2O_3 and PbO) is present. By day 5, the broad band (possibly due to Pb_2O_3) has almost disappeared; the bands at 170 and 90 cm^{-1} have increased in intensity indicating an increase in the amount of PbO. The bands appearing in these spectra after 5 days are very much less intense than those seen after 36 hours in the distilled water.

After measuring the spectra on the 5th day, sodium bicarbonate was added to the water in the reservoir to bring its pH to approximately 7.5. Raman spectra were recorded on day 6 and 8 (Figures 29 and 30). The band between 400 and 600 cm^{-1} completely disappeared whereas the bands at

344, 170 and 90 cm $^{-1}$ increased slightly. The small bands appearing between 900 and 1000 cm^{-1} are "grating ghosts" and are due to aberrations in the gratings of the monochromator.

Initially, we thought that the spectrum of the surface film was due to orthorhombic PbO; however, on an expanded frequency scale, comparison of the spectrum of the surface film with that of tetragonal PbO, as is shown in Figure 31, indicates that the film is tetragonal.

Experiment 3

In this experiment, distilled water and tap water were mixed such that the alkalinity was 4 mg/l carbonate. These conditions were chosen to mimic the water in the city of Boston. The pH was adjusted with NaOH to 9.5. Raman spectra of the reference electrode measured on days 1, 2, 6, 9, 12, 13, 16, 19, 21, and 23 are shown in Figures 32-41. During this time, a small amount of a fluffy, yellowish-white precipitate had formed in the solution in the cell. Appearance of any band in the spectrum does not occur until after the ninth day (at approximately 175 cm). From day 9 to 23 this band increased only slightly in intensity and no other band is obvious in the spectrum.

The Raman sectrum of the surface film measured on day 28 is compared to that of tetragonal PbO in Figure 42. The similarity strongly supports the formation of tetragonal PbO under these conditions (pH = 9.5).

Corrosion meter readings were recorded throughout the 23 days. Table 2 shows the readings corresponding to each of the Raman spectra measured for experiment 3. The greatest drop in corrosion rate occurred between days 1 and 2. The readings did not drop substantially after the second day and, in fact, between day 2 and 12 the meter readings were essentially constant. There is no major change in the Raman spectra before day 12, either. Between day 12 and day 19 there was a two-fold drop in the meter readings and changes begin to occur in the Raman spectrum with the slow formation of a band around 170 cm . Between days 19 and 23, the corrosion rate was constant and the Raman spectra for these days were similar.

Experiment 4

To determine the effect of increasing the pH to 10.5, the same electrochemical cell was used in this experiment. The surfaces of the electrodes from the last experiment were mechanically cleaned with fine sand paper and remounted into the cell. Tap and distilled water were used in the same ratio as the previous experiment and the initial pH was adjusted to 10.5. The duration of the run was 10 days and Table 3 lists the corrosion readings recorded during that time. By comparing these values with those in Table 2, it can be seen that by day 2, the corrosion rate had settled to a level similar to that of day 6 in the previous experiment. At the end of the 10 day experiment, the corrosion rate leveled off to the rate reached at day 16 in the previous experiment. It is very informative to look at the Raman spectra measured during this period (Figures 43 to 47) and to compare them to those of the previous experiment. After the second day of the experiment, a lead oxide coating could be detected on the electrode surface. By day 6, intensity of the PbO bands in the Raman spectrum already exceeded those of day 28 in experiment 3.

To determine the crystal structure of the coating on the electrodes, the spectrum measured on day 8 was used. Figure 46 (top) shows the spectrum of the electrode measured with slit widths comparable to those used in the rest of this experiment. The band below 100 cm^{-1} is off scale because of the intensity of the spectrum. Therefore, to bring all the bands between 400 and 0 cm^{-1} back on scale, the slit width was reduced by a factor of 1/3. The resultant spectrum is shown in Figure 48 (bottom). Figure 48 shows the frequency expanded spectrum of tetragonal PbO (S) as well as the spectrum of the electrode surface (E). It can be seen that the bands in this spectrum corresponds to those of tetragonal PbO.

During the course of this experiment, the pH was periodically monitored. Table 3 shows that by day 6, the pH had decreased to 8.5. The reservoir was refreshed with new solution to bring the pH up to 9.5. Within 24 hours, the pH had decreased to 9.0 and on the 8th day, leveled off to 8.8. This pH change was attributed to the fact that this was an open system, which exposed the solution to the atmosphere, causing reaction with CO^2 to occur.

Experiment 5

This experiment was performed with the lage pipe cell using the 100 gal. tank with 3/1 distilled/tap water and pH of 9.3. Table 4 lists the corrosion meter readings for the duration of this experiment. It is interesting to note that while the pH remained constant in this closed system, the corrosion rate gradually decreased from day 0 to day 12, almost doubled on day 13, then slowly decreased until day 20, when it again (less drastically) increased. Between day 28 and 32, it slowly began to decrease. This could be reflective of surface conditions in the lead pipe, i.e., an alternate buildup of a protective coating and the flaking of some of this coating from the pipe. After the 34th day of the experiment, an attempt was made to measure a Raman spectrum of the surface of the lead pipe. It was found that the design of the cell (original design) made it very difficult to align the pipe in the sample compartment of the Raman spectrometer. After two hours, optimum alignment was achieved and a Raman spectrum shown in Figure 49 was obtained.

The expanded spectrum in Figure 50 shows that the bands of tetragonal PbO (A) are present in the spectrum of the surface (B) but are shifted somewhat to lower frequencies. In addition, in the spectrum of the pipe surface, bands below 75 cm^{-1} also appear along with bands above 400 cm^{-1} (see Figure 51). A search of our reference library of Raman spectra indicated that these extra bands could be due to carbonate. Figure 51 shows the reference spectrum of lead carbonate (A) and that of the lead pipe (B). The band above 1000, as well as those between 400 and 600, 200 and 300 cm^{-1} and the low frequency bands below 75 cm^{-1} correspond to the Raman bands of lead carbonate.

Experiment 6

An experiment similar to #4 was run in the small cell using a phosphate buffer to give a pH of 9.0. In this experiment, 100 ppm phosphate were added to a 3:1 mixture of distilled/tap water. This brought the pH to 9.0 and no further adjustment was made in the pH.

Table 5 shows the corrosion meter readings for the duration of the experiment (29 days). The corrosion readings for this experiment are relatively higher than those of the other experiments run to date. After approximately 15 days, the corrosion rate began to approach the levels that were seen in the first 5 days of Experiment 4 (pH = 10.5).

The Raman spectrum of the electrode surface after 12 days of exposure is shown in Figure 52. The spectrum was very strong and easily measured, in contrast to previous experiments after 12 days. Tetragonal PbO seems to predominate although there are weak bands at 203 and 128 cm which could not be assigned. The band at approximately 77 cm could be due to the presence of a small amount of orthorhombic PbO. It was at this time that problems with the laser source developed and the last spectrum we obtained from this experiment was measured at greatly reduced laser power. Figure 53 shows this spectrum of day 34. Despite the reduced power, a relatively strong spectrum was measured and the band appearing at 287 cm seems to suggest the increase of orthorhombic PbO on the surface. We could not resolve the region below 90 cm to bring out the other band due to orthorhombic PbO at 77 cm .

It does seem that the addition of phosphate ion accelerates the deposit of lead oxides on the surface and that at a pH of 9.0 the results are comparable to a system containing no phosphate and running at a pH of 10.0 or more (i.e., Experiment 4).

Experiment 7

This experiment performed on the large flow-thru pipe cell using a 100 gal. reservoir with a 3:1-distilled/tap water ratio and buffered with phosphate to a pH of 8.0. Table 6 lists the corrosion and pH values for the duration of the experiment. The pH remains constant, while the corrosion rate decreases during days 4 to 6, oscillates about 0.3 mpy during days 6 to 19, increases during days 19 to 26, and finally decreases during days 26 to 32. These increases and decreases could be caused by a protective coating building up on the pipe surface then being flaked off by the flowing water. This experiment was terminated due to the fact that movement of the cell would cause the electrode wires, which enter through the Tygon tubing, to shift producing leaks in the system. By day 34 the leaks were impossible to seal.

Raman spectra were measured several times through the duration of the experiment, but only on days 12 and 19 were satisfactory spectra measured in the cell. These spectra are shown in Figures 54 and 55. By using high laser power obtainable with a new laser tube, and many hours of alignment only the strongest peak at 145 cm^{-1} of the lead oxide on the surface was resolvable. The peaks above 145 cm^{-1} are most likely grating ghosts, which are possible when using high laser power. Raman spectra of the test, auxiliary, and reference lead pipe-electrodes measured directly off the surface after dismantling the cell are shown in Figures 56-58. These spectra indicate tetragonal PbO, verified by the peaks at 77, 145, and 343 cm^{-1}, with no apparent presence of orthombic PbO, which has peaks at 83, 141, and 290 cm^{-1}. This is interesting because in experiment 5, which had no phosphate, the spectrum of the electrode surface at day 34 had peaks indicating that both tetragonal and orthombic PbO were present.

Experiment 8

In this experiment the small cell was used with a 3:1 mixture of distilled/tap water. It was buffered with 100 ppm phosphate and the pH was adjusted to 10.4 using sodium hydroxide. This pH was selected for comparison with experiment 4, which had approximately the same pH (10.5) but no phosphate, and experiment 6, which had 100 ppm phosphate but lower pH (9.0). Table 7 shows the corrosion rates and pH values for the duration of the experiment (24 days). These readings might indicate, as in the case of experiment 7, that a coating was building up on the surface and the flaking away. This experiment was terminated at day 24 because of troubles with the electrode connections, making the corrosion rates somewhat unreliable. If comparisons are made, after 18 days the corrosion rate began to approach that of experiment 6 at 23 days, but the overall trends are different. This suggests that by increasing the pH, with 100 ppm phosphate concentation the same surface coating forms faster.

Raman spectra of the electrode surface at 1, 3, 6, 9, 13, and 24 days of the experiment are shown in Figures 59-64. By comparing the 13 day spectrum to the 12 day spectrum of experiment 6 (Figure 52), there seems to be a similiarity in the relative intensities. This does not mean that the amount of coating on the surfaces was equal, but it does indicate that the phosphate has as much of an effect as pH on the rate of formation of the surface film. The spectra of days 1 thru 24 indicate the formation of tetragonal PbO, which is interesting because of the fact that in all the flow-thru experiments using phosphate the major, if not only, surface film detectible is tetragonal PbO.

Experiment 9

In this experiment the small flow-thru cell was used with a 3:1 mixture of distilled and tap water which was buffered with 50 ppm phosphate. This caused the pH to be elevated to 8.6. These conditions, which differ from the other flow-thru experiments, were chosen for further comparison of the effects of phosphate on the surface film formation. Table 9 shows the corrosion rates and pH values. These readings indicate the same behavior as previously encountered. After an initial

build up, we see the rate decrease to day 5 then increase to day 8, subsequently decreasing to day 13. These oscillations in the corrosion rate have been observed repeatedly through the course of this and other experiments.

Raman spectra of lead electrode surfaces at days 2, 6, 9, 12, 14, 26, 30, and 36 are shown in Figures 65-73. These periodic measurements show the same pattern as past phosphate buffered experiments. These spectra indicate the formation of tetragonal PbO, with no peaks indicating the presence of any orthohombic PbO. Tetragonal PbO is verified by peaks at 77, 145, and 343 cm^{-1} and orthorhombic by peaks at 83, 141, 290, and 395 cm^{-1}. By comparing the 12 day spectrum to the 36 day spectrum in Figure 74, we see no changes other than the overall intensities.

Experiment 10

In this experiment, the 100 gal. reservoir was filled with a 3 to 1 ratio of distilled/tap water which was buffered with phosphate to a pH of 7.8. The new large cell reduced the amount of distortion of the laser beam upon entering the cell. However, manipulation of the cell to position it in the Raman sample chamber was still a very tedious task. Another disadvantage is the large amount of water the laser beam must travel through. One major difference in this flow-thru system is the area of the electrode surface which is being exposed. Because the corrosion rate is related to the electrode surface area we decided to decrease the size of the surface area to see if this would cause a reduction in the signal-to-noise ratio of the corrosion meter readings. Figure 75 shows an enlargement of two corrosion meter readings for typical lead electrodes having a surface area of approximately 2 in , characteristic of most experiments to date, and 1 cm , which was used in this experiment. Table 9 lists the corrosion rates and pH values for the duration of the experiment (47 days). The pH remained constant, while the corrosion rate oscillated, and gradually decreased as the experiment continues. Therefore, even with the smaller electrode we see the same overall behavior as in previous experiments.

Electronic malfunctions in the laser supply and thermocouple pressure sensor caused the laser unit to be inoperative for a major segment of this experiment. These problems were corrected however, and a Raman spectrum was measured. Figure 76 shows the spectrum at day 46. This spectrum indicates the presence of tetragonal PbO with no evidence of any other species. This might indicate that the surface film had proceeded in a similar manner as previous phosphate buffered systems.

Experiment 11

In this experiment, a large flow-thru cell was used with a mixture of distilled and tap water in a 3:1 ratio. Phosphate buffer was not used in this experiment. The pH was adjusted to 8.4 by the addition of sodium hydroxide. The flow-thru medium travelled thru the glass cell which supported three lead electrode pipe sections having exposed surface areas of 1 cm each. The aqueous medium passed thru this cell and subsequently was recirculated thru a 100 gal. reservoir. Table 10 lists the corrosion

rates and pH values encountered during the course of the experiment (40 days). The pH was maintained at approximately 8.4 with the periodic addition of small quantities of sodium hydroxide. The corrosion rate readings were indicative of all previous experiments. The rate varied for the first few days, leveling off at day 7 and then oscillating about .5 mpy for the duration of the experiment. Again, the trend is best explained by the repeated action of the surface film building up on the lead and subsequently flaking off.

Raman spectra measured from the surface of one of the lead electrodes on days 14, 32, 37, and 40 are shown in Figures 77-80. The spectra were all originally measured between 0 and 2500 cm^{-1} revealing no resolvable bands above approximately 400 cm^{-1}; therefore, the scans shown in these spectra are in the range of 0 to 600 cm^{-1}. The spectrum in Figure 77, which was measured near the beginning of the experiment, shows a small band at approximately 160 cm^{-1}. As the experiment progresses and the surface film builds, we see the formation of other bands in Figures 78-79. These spectra indicate the presence of only tetragonal PbO, which is the same surface film found on the other flow-thru experiments using buffered media and approximately the same pH.

Field Samples of Lead Pipes

Periodically during the course of this investigation, lead pipe samples were submitted from E.P.A -- Cincinnati, and Raman spectra of the surface films were measured, and compared with our standard library of spectra and spectra of lead surfaces in our flow-thru system.

Experiment 17

This pipe sample was labelled "phosphate." A cross section was cut away and a Raman spectrum was measured of the inside of the section. The spectral region between 1200 and 0 cm^{-1} is shown in Figure 81. The spectrum resembles a weak spectrum of tetragonal PbO.

Experiment 31

A Raman spectrum of a section of this pipe was measured. It had extremely intense bands, and therefore the slits were cut to approximately 1/2 of the width usually used for the lead surfaces. The spectrum of the pipe is compared to the reference Raman spectrum of orthorhombic PbO in Figure 82. As can be seen, the comparison suggests that the surface of pipe labelled "Exp 31" is coated with orthorhombic PbO rather than tetragonal PbO.

Experiment 32

The inner wall of the pipe labelled "Exp 32" contained two different coated sufaces. Figure 83 shows the inside of a cross-section of pipe. A tan strip, 1 to 2 cm wide stretched parallel to the direction of the pipe, whereas the rest of the surface had a faint white appearance.

Figure 84 shows the Raman spectrum measured directly from the tan strip. The bands suggest the presence of a coating of orthorhombic PbO.

Experiment 33

It was very difficult to obtain a spectrum of the surface of this pipe. Figure 85 shows that the spectrum at the peak of 150 cm^{-1} suggest that it is the spectrum of tetragonal PbO. The other peaks between 900 and 1100 cm^{-1} are probably due to grating ghosts.

Experiment 34

This pipe was labeled pH-8.5; 20mg/l CaCO; 0.5 mg/l PO . A cross-section was cut away and a Raman spectrum was measured from the inner surface. Figure 86 shows the region between 400 and 0 cm^{-1}, but the sample was originally scanned from 2000 to 0 cm^{-1} which produced no peaks above 400 cm^{-1}. This spectrum indicates the presence of tetragonal PbO. This sample and the experiment 17 lead sample, which was also labeled phosphate, both have spectral peaks signifying tetragonal PbO.

Experiment 32A

This lead pipe sample was exposed to pH 7.00 0.05, alkalinity of 22 mg/l and phosphate of 0.3 - 0.5 mg/l. A cross-section of the pipe sample was cut away and a Raman spectrum was measured from the inner surface. Figure 87 shows the region between 600 and 0 cm^{-1}, but the spectrum was originally scanned between 2000 and 0 cm^{-1}, which produced no resolvable peaks above 400 cm^{-1}. The surface film was very thin, smooth, and reflective, which made it difficult to obtain a satisfactory spectrum. After many attempts a relatively weak spectrum was obtained, and this indicated the presence of tetragonal PbO.

Experiment 33A

The lead pipe sample was exposed to pH of 8.00 0.05, alkalinity of 15 mg/l Ca^{2+} and 0.35-0.5 mg/l phosphate. A cross-section of this pipe sample was cut away and a Raman spectrum was measured from the inner surface. Figure 88 shows the region from 600 to 0 cm^{-1}; bands were not observed above 400 cm^{-1}. This surface film also gave a spectrum indicating tetragonal PbO. By comparing the surface films in experiments 32A and 33A we noted that they physically appeared different, although their Raman spectra and medium in which they were exposed were similar. This may be caused by the fact that when the experiments were terminated, the surface film was beginning to flake away as might be the case in experiment 33A, or the film had just been uniformly formed as might be the case in experiment 32A. Another possibility which should be considered is that the conditions in experiment 32A caused the formation of a good protective surface.

ASBESTOS CEMENT PIPES -- FIELD SAMPLES

Approximately 15 field samples of asbestos cement (A/C) pipes were supplied by EPA Cincinnati. Numerous attempts were made to obtain the Raman spectra of surface films on these pipe samples; however, all attempts were unsuccessful. The major problem appeared to be the fact that the A/C material is a thermal insulator and heat from the laser beam

decomposed or melted anything on the surface. We could see visible changes in the surface films. We tried to scrape off surface films and measure their Raman spectra in capillary tubes or in KBr pellets. However, these endeavors were unsuccessful.

Since we could not obtain Raman spectra of A/C pipes, we made the surface scrapings into KBr pellets for infrared analysis. Infrared spectra of two samples are shown in Figures 89 and 90. The spectrum in Figure 89 is of the scrappings from a clean surface and the one in 90 from a pipe labeled "6" A/C pipe (hardness = 20 mg/l, pH = 5.5). Our intentions were to determine the difference between the two samples by subtracting the spectrum of the "clean surface" from the "6" A/C pipe spectrum. However, the major difference in the spectra is the appearance of the relatively intense band at ~1500 cm^{-1} in the spectrum of the "clean surface." The appearance of this band suggests that the surface of A/C pipes may not be chemically identical (or homogeneous). Thus, spectral differences may not be due to the presence of surface films and may not indicate their composition.

GALVANIZED PIPES -- FIELD SAMPLES

Five galvanized pipe samples were supplied by EPA Cincinnati. A cross-section of each was cut away, and we tried to measure Raman spectra using three different methods: (1) directly off of the surface, (2) scraping the surface and pressing it into a KBr pellet, and (3) scraping the surface and inserting a powder into a capillary tube. All of these methods were ineffective in providing Raman spectra.

Good infrared spectra were obtained by making scrapings of the surface into KBr pellets. Spectra of the five samples are shown in Figures 91-95. Since carbonates were present in at least some of the aqueous environments, we measured the infrared spectrum of pure zinc carbonate ($ZnCO_3$) as a pellet; this is shown in Figure 96. The strong doublet at 1300-1600 cm^{-1} is very distinctive. It definitely appears in Figures 91 and 93, and to a lesser extent in the other three spectra. Thus, the $ZnCO_3$ appears to be one of the major components on the surfaces of galvanized pipes.

IV. DISCUSSION

The analytical results on lead pipes indicate that corrosion is minimized when tetragonal PbO is formed on the surface. Tetragonal PbO is the thermodynamically favored form at temperatures below 488°C; however, the other crystallographic form, orthorhombic PbO, is generally observed. There may be a number of reasons why the orthorhombic form appears. It is apparently stabilized by impurities, which will be present in every "real" system. It also appears to be produced in the decomposition of other oxides, e.g., Pb_3O_4.

Orthorhombic PbO is less protective of the surface and apparently corrodes away, i.e., gets into the water system. Some of our earlier results indicated that orthorhombic PbO may be formed in solution and redeposited on the surface. Under conditions favoring the formation of orthohombic, the oxide was found on the surface of a Pt reference electrode in the same container. Under conditions favoring tetragonal PbO, this oxide was only observed on the surface of the working lead electrode. In the present program, our goal was to determine those chemical conditions that produced tetragonal PbO using Raman spectra to monitor the surfaces. In addition, we used Raman to identify any other oxides or compounds present on a surface.

Orthorhombic PbO was produced in experiments 1 and 2 (pH <7). In both experiments a precipitate was formed, although this was more pronounced in experiment 1. In experiment 2, the pH of the aqueous medium was increased to 7.5 after the fifth day, and the spectrum of the surface was that of tetragonal PbO (see Figure 3).

The other nine experiments were performed over the pH range of 8 to 10.5. In every case, tetragonal PbO was identified as a component of the surface film. In addition, the spectrum of lead carbonate was observed in experiment 5 and there was an indication of a small amount of orthorhombic PbO in experiment 6 at day 12, which seemed to increase by day 34. The corrosion rates for this experiment ranged between 1 and 2 mpy, which is significantly higher than other experiments. It is difficult to explain the results in experiment 6 since similar conditions produced tetragonal PbO.

In experiments 6-10 phosphate was added as a buffer. With the exception of experiment 6, the addition of phosphate lowered the rate of corrosion at lower pH values. For example, the lowest overall rates were

obtained in experiment 7 (Table VI) with pH = 8 and phosphate buffer. In this case, the rate was >0.5 mpy only on one day. These results are very optimistic.

The general tendency of the corrosion rates was to start high, decrease for several days, increase rapidly, and start to decrease again. The data shown in Tables 2-10 are average values for the days listed. Data were not included for every day, since many days had identical values. Data are presented only for those days showing significant changes. In each experiment, there was a considerable amount of oscillation, i.e., increases and decreases in the corrosion rate. We suspect that initially a film freely forms on the bare metal. As the film becomes thicker, the rate decreases. At some point, the film becomes too thick and some of it flakes off, causing an abrupt increase in the rate. As a film forms on the surface, the rate decreases again.

Specific correlations between the corrosion rate and Raman spectra could not be found. For example, it was not possible to correlate the oscillations in the corrosion rate with Raman spectral intensities. Typically, the Raman intensities increased with the time of the experiment, although there were some significant changes in intensities. General correlations between corrosion and Raman spectra could be seen. For example, the corrosion rates were higher than expected in experiment 6, and orthorhombic PbO was observed. Although the conditions do not favor either of these, they correlate well together.

In summary, it appears that the tetragonal form of PbO is the more stable and protective form of the lead oxides. The rate of corrosion is decreased considerably when tetragonal PbO is present. The only apparent difficulty with the formation of tetragonal PbO is that the film may become too thick and flake off. The evidence of this flaking is not conclusive; however, it does seem reasonable in light of the fluctuations in the rate of corrosion. Tetragonal PbO was formed and the fluctuations minimized with a phosphate buffer and pH of 8.0.

APPENDIX

CORROSION RATE MONITORING BY THE PAIR TECHNIQUE

A Petrolite Corporation Model M-3010 corrosion rate meter was employed in this study. This instrument employs a three electrode system: reference, auxiliary, and test. The Petrolite Corporation calls this method of measuring the corrosion rate the PAIR technique (Polarization Admittance Instantaneous Rate) (6). This instantaneous method is derived from the more commonly known Tafel method (7).

When corrosion takes place at a metal surface, a chemical reaction occurs causing a flow of electrons. For electrochemical purposes, the electrons flow from an anode to a cathode. This causes a current flux, and the metal is referred to as polarized. There are three types of polarization: activation, concentration, and IR drop (8,9). Activation polarization is caused by a slow rate of an electron transfer reaction. In other words, the reaction which occurs at the electrode has a relatively high activation energy. Concentration polarization is caued by concentration changes near the electrodes which are induced by the electrochemical reaction. Concentration polarization can be decreased considerably with stirring. IR drop or resistance overvoltage is an ohmic (iR) drop in potential between working electrodes. This is caused by the resistance in the electrolyte surrounding the electrode and/or a product film on the surface of the electrode. The PAIR technique is designed for flowing systems; therefore, concentration polarization is eliminated.

The PAIR technique measures the corrosion rate indirectly. Figure 97 illustrates a simplified schematic of the Petrolite system. The indirect measurement is accomplished by slightly perturbing the corrosion properties of the test electrode. These perturbations are compared to the reference electrode. Initially, if there is any potential difference between the test electrode and the reference electrode, the instrument will electronically zero it. When the zeroing is complete, an adjustable current source begins to allow current flow between the test electrode and the auxiliary electrode. When this current is sufficient to maintain a potential difference of 10 mV between the test electrode and the auxiliary, compared to the reference electrode, the test electrode is considered polarized. This current reflects the corrosion rate of the test electrode since the current needed to polarize the electrode is directly proportional to the corrosion current density. This zeroing and polarizing cycle is performed continuously for each measurement.

Measurements are taken at pre-set time intervals which can be adjusted between 30 sec. and 50 min. depending on the material.

The calculations involved in this method can be shown utilizing two equations (10):

Stern-Geary Equation

$$Icorr = \frac{\Delta I}{\Delta E} \frac{\beta a \ \beta c}{2.3 \ (\beta a + \beta c)} \qquad (1)$$

where Icorr = corrosion current density (μamps/cm)

ΔI = polarizing current (μamps/cm)
ΔE = potential shift = 10 mV
βa = anodic Tafel slope (mV)
βc = cathodic Tafel slope (mV)

and Faraday's Law

$$\text{metal loss/gain (gms)} = \frac{\text{eq. wt.} * I * t}{96{,}500} \qquad (2)$$

where eq. wt. = equivalent weight (gms/eq)

I = rate of current flow (amps)

t = time (sec)

By taking into consideration the area of the electrode and the density (d) of the material, Faraday's law can be converted to solve for the corrosion rate (CR) in mils per year (mpy).

$$CR \text{ (mpy)} = \frac{0.13 \ (Icorr) \ (\text{eq. wt.})}{d} \qquad (3)$$

Mpy per year are commonly used units in corrosion. One mpy is one one-thousandth of an inch per year. By combining equations (1) and (3), a more detailed expression for the corrosion rate can be formulated:

$$CR \text{ (mpy)} = \frac{0.13 * \text{eq. wt.}}{d} * \frac{\Delta i/A}{\Delta E} * \frac{\beta a \beta c}{2.3(\beta a + \beta c)} \qquad (4)$$

where Δi = polarizing current (μamps)
A = area of the electrode (cm)

The corrosion rate readings produced by the Petrolite meter are standardized with respect to a mild steel electrode having an area of 9 cm. The meter is preset to read 1 mpy for a polarizing current equal to 5.45 amps at a potential shift of 10 mV. For mild steel the equivalent weight equals 27.95 gm/eq, and the density equals 7.86 gm/cm. Solving equation (4) for the Tafel slopes gives:

$$\frac{\beta a\, \beta c}{2.3(\beta a + \beta c)} = \frac{d * A * \Delta E * CR}{0.13 * eq.\ wt. * \Delta i} = 35.8\ mV \qquad (5)$$

The Petrolite meter plots the corrosion rate for each cycle in units of mpy. This corrosion rate is proportional to parameters of mild steel electrodes, as shown above. To calculate the corrosion rate if the material and/or the area of the electrodes are changed, the current which produced the meter reading is needed. For all reading on this meter equation (4) can be reduced to:

$$CR\ (mpy) = K * \Delta i\ (\mu amps) \qquad (6)$$

$$\text{where } K = \frac{0.13 * eq.\ wt. *}{d * \Delta E * A} \quad \frac{\beta a\, \beta c}{2.3(\beta a + \beta t)} = 0.18$$

Solving equation (5) for i gives:

$$\Delta i\ (\mu amps) = \frac{CR\ (mpy)}{0.18} \qquad (7)$$

To calculate the corrected corrosion rate in mpy from a given current, the parameters for the new electrode are inserted into equation (4). The only relatively unknown parameters are the Tafel slopes. Tamba, Gauntt, and Pye (13) have all performed polarization corrosion rate studies in which Tafel slopes were needed. The assumption that these workers used was that $\beta a = \beta b = 0.12$ volts for any metal or alloy. This assumption produced corrosion rates which differed no more than 2.2 from the actual corrosion rates (11). For corrosion studies, this is considered within acceptable limits. With this assumption the Tafel constant is:

$$\frac{\beta a\, \beta c}{2.3(\beta a + \beta c)} = 0.026\ V = 26\ mV \qquad (8)$$

The corrosion rate measurements made by the Petrolite instrument are relative to an electrode of mild steel having an area of 9 cm, as previously stated. With the information provided above, a correction can be made for changes in area and/or material. An example of the calculations involved are shown below for a lead electrode system.

When employing a Petrolite instrument with lead electrodes of any area, the following parameters hold:

eq. wt. = 103.6 gm/eq.
d = 11.3 gm/cm

$$\frac{\beta_a \beta_b}{2.3(\beta_a + \beta_c)} = 26 \text{ mV}$$

$$\Delta E = 10 \text{ mV}$$

By inserting these parameters into equation (4), the corrosion rate can be calculated in terms of the polarizing current and the area.

$$CR \text{ (corrected)} = \frac{3.1 * i}{\text{area}} \qquad (9)$$

By combining equations (6) and (7) an expression for the corrected corrosion rate in myp can be derived.

$$CR \text{ (corrected)} = \frac{17.2 * CR \text{ (meter)}}{\text{area}} \qquad (10)$$

To show that equation (10) can be used for correcting corrosion rate readings, experimental data was used. In experiments with lead electrodes having an area of 1.0 in^2, the corrosion rate on the meter was in the range of 0.20 mpy. When the area of the electrodes was decreased to 1.0 cm, with all other conditions remaining constant, the uncorrected corrosion rate approximately 0.03 mpy. Correction of these rates using equation (10) gives:

area = 1.0^2 in = 6.5 cm^2

CR = 0.20 mpy

$$CR \text{ (corrected)} = \frac{(17.2)(0.20)}{(6.45)} = .533 \text{ mpy}$$

area = 1.0 cm^2

CR = 0.03 mpy

$$CR \text{ (corrected)} = \frac{(17.2)(0.03)}{(1.0)} = .516 \text{ mpy}$$

These corrected corrosion rates show that equation (10) can be performed on experimental data.

TABLES

Table 1. Summary of Flow-Thru Cell Experiments

Experiment #	Type of Cell	Duration (days)	Conditions
1	Small	1	Distilled water
2	Small	8	Tap water, pH=5, hardness =12mg/l
3	Small	28	3/1 Distilled/Tap, alkalinity=4mg/l and pH=9.5 (with NaOH)
4	Small	10	3/1 Distilled/Tap, alkalinity=4mg/l and pH=10.5
5	Large	34	3/1 Distilled/Tap, alkalinity=4mg/l and pH=9.3
6	Small	29	3/1 Distilled/Tap, alkalinity=4mg/l and pH=9.0 with 100 ppm phosphate added as buffer
7	Large	34	3/1 Distilled/Tap, alkalinity=4mg/l and pH=8,0 with phosphate buffer
8	Small	24	3/1 Distilled/Tap, alkalinity=4mg/l, 1000 ppm phosphate, pH-10.4 (with (NaOH)
9	Small	14	3/1 Distilled/Tap, alkalinity=4mg/l, 50 ppm phosphate, pH=8.6
10	Large	47	3/1 Distilled/Tap, buffered with phosphate to pH=7.8
11	Large	40	3/1 Distilled/Tap, alkalinity=4mg/l, pH=8.4 with NaOH

Table 2. Corrosion Meter Readings for Flow-Thur Experiment 3

Day	Meter Reading (mils per year)
1	4.4-2.1
2	2.1-1.2
6	0.89
9	0.89
12	0.89-0.80
16	0.53-0.44
19	0.36
21	0.36
23	0.36

Table 3. Corrosion Meter Readings for Flow-Thru Experiment 4

Day	Meter Reading (mpy)	pH	
1	1.07	10.5	
2	0.89		
5	0.71		
6	0.71	8.5	
7	0.71	9.0	9.5
8	0.71	8.8	
9	0.71		
10	0.53		

Table 4. Corrosion Meter Readings for Flow-Thru Experiment 5

Day	Meter Reading (mpy)	pH
0		9.3
3	0.66-0.44	
4	0.444-	9.3
5	0.338	
9	0.243	
10	0.243	
11	0.267	
12	0.334	
13	0.533	
17	0.444	
18	0.489	9.3
19	0.533	
20	0.533	
21	0.604	
24	0.604	
28	0.604	
32	0.489	
33	0.489	
34	0.462	9.3

Table 5. Corrosion Meter Readings for Flow-Thru Experiment 6

Day	Meter Reading (mpy)	pH
5	1.96	9.0
7	1.78	
9	1.67	
11	1.39	
13	1.32	
15	1.17	
17	1.07	
19	1.17	
21	0.89	
23	1.00	
25	0.89	
27	1.00	
29	0.89	

Table 6. Corrosion Meter Reading for Flow-Thru Experiment 7

Day	Meter Reading (mpy)	pH
0	----	8.0
4	0.409	
6	0.329	
8	0.355	
10	0.329	
13	0.373	
16	0.355	8.0
19	0.373	
23	0.498	
26	0.515	
29	0.426	
32	0.249	8.0

Table 7. Corrosion Meter Readings for Flow-Thru Experiment 8

Day	Meter Reading (mpy)	pH
0	----	10.4
2	0.746	
5	0.729	
7	0.693	
10	0.818	
13	0.764	10.4
15	0.853	
16	0.800	
18	0.995	
20	0.899	
22	1.066	
24	0.995	10.4

Table 8. Corrosion Meter Readings for Flow-Thru Experiment 9

Day	Meter Reading (mpy)	pH
1	0.80-0.44	8.6
3	0.98	
5	0.66	
8	0.96	
13	0.73	8.6
16	0.87	
20	0.62	
21	0.80	
26	0.55	8.6
27	0.64	
29	0.48	
30	0.57	
32	0.53	
34	0.60	
36	0.50	8.6

Table 9. Corrosion Meter Readings for Flow-Thru Experiment 10

Day	Meter Reading (mpy) Uncorrected	pH
1	0.241	7.8
4	0.791	
7	0.688	
10	0.654	
12	0.619	
14	0.585	7.8
20	0.550	
23	0.585	
24	0.619	
26	0.585	7.8
27	0.550	
29	0.585	
30	0.550	
34	0.516	
36	0.550	7.8
41	0.516	
43	0.550	
44	0.516	
46	0.550	
47	0.516	7.7

Table 10. Corrosion Meter Readings for Flow-Thru Experiment 11

Day	Meter Reading (mpy) Uncorrected	pH
1	0.36-0.71	8.4
2	0.53-0.89	
6	0.36-0.71	
7	0.46	
8	0.50	
10	0.46	8.3
13	0.50	
15	0.53	
17	0.50	
19	0.53	
22	0.50	8.4
26	0.43	
27	0.46	
28	0.50	
33	0.46	8.4
35	0.50	
38	0.53	
39	0.50	
40	0.50	8.4

FIGURES

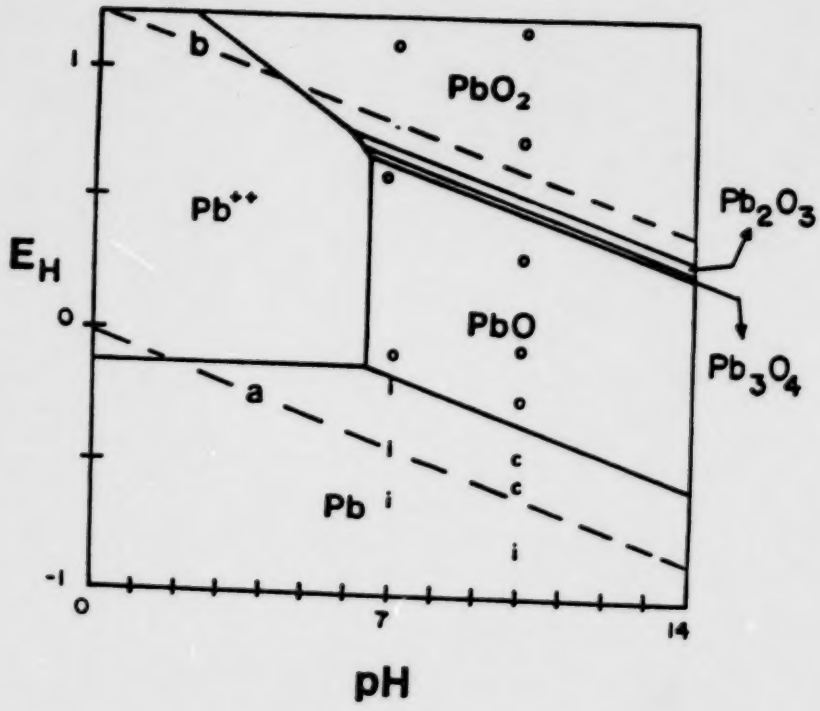

Figure 1. Calculated Pb-H_2O Pourbaix diagram using the most recent NBS data. (24) Experimental results, o=tetragonal PbO, i=apparent immunity, no spectrum observed, c = basic lead carbonate.

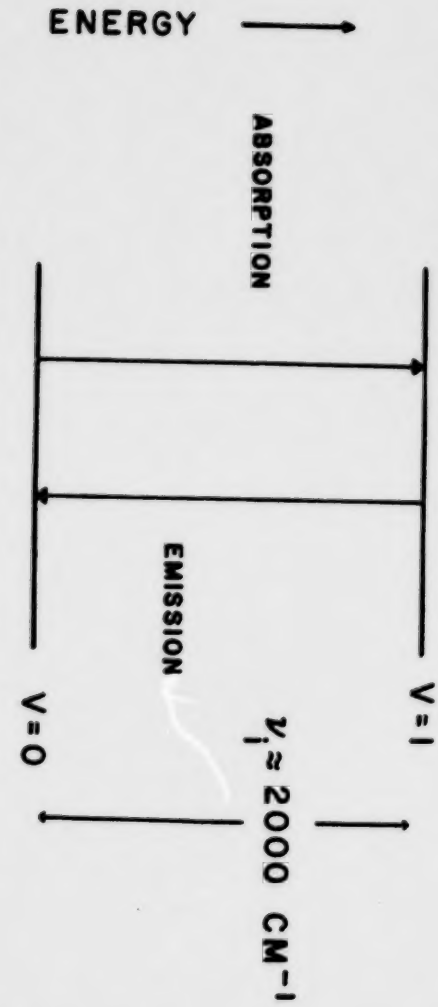

Figure 2. Vibrational energy levels of a diatomic molecule.

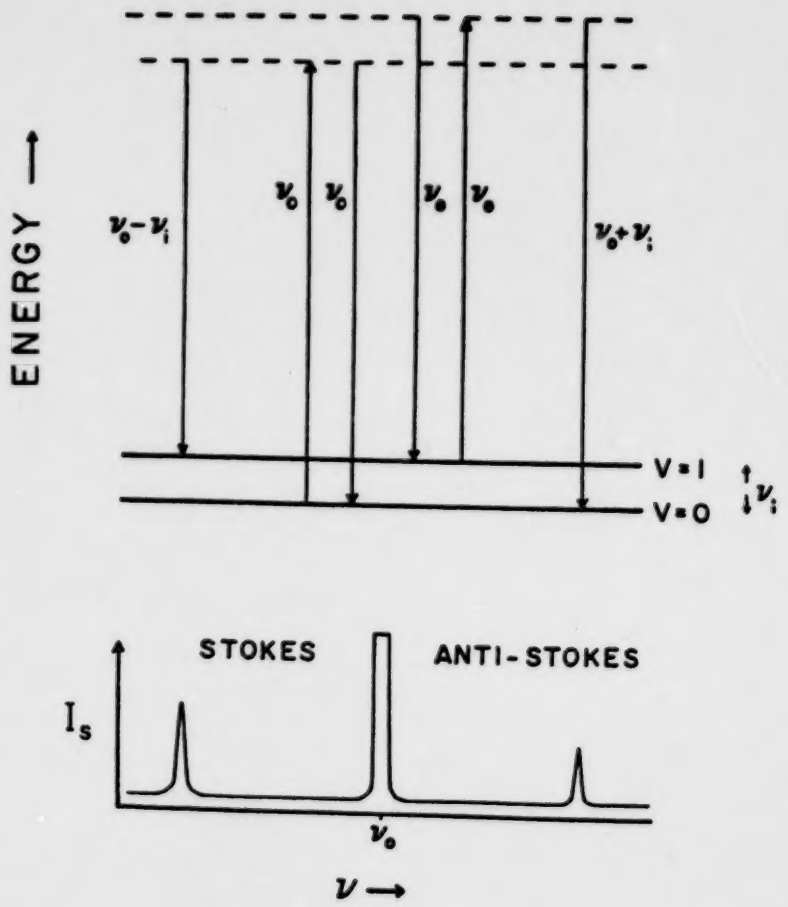

Figure 3. Energy level diagram for a typical vibrational Raman transition and the Raman spectrum resulting from such a transition.

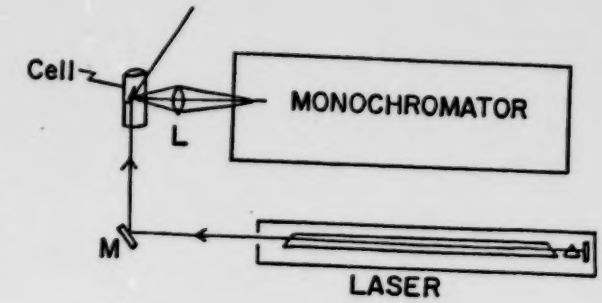

SIDE VIEW

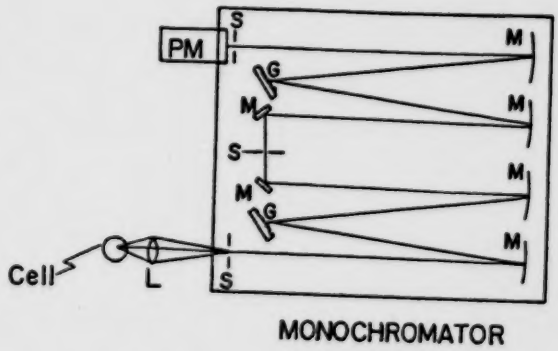

TOP VIEW

Figure 4. Schematic drawing of a laser Raman spectrometer. Mirrors are labelled M, gratings G, and slits S.

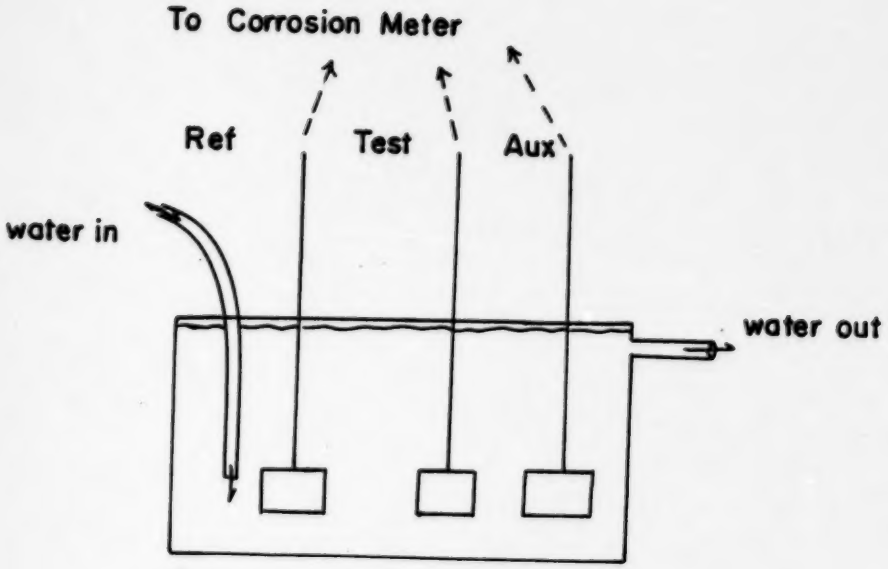

Figure 5. Electrochemical/Raman Cell - simplified.

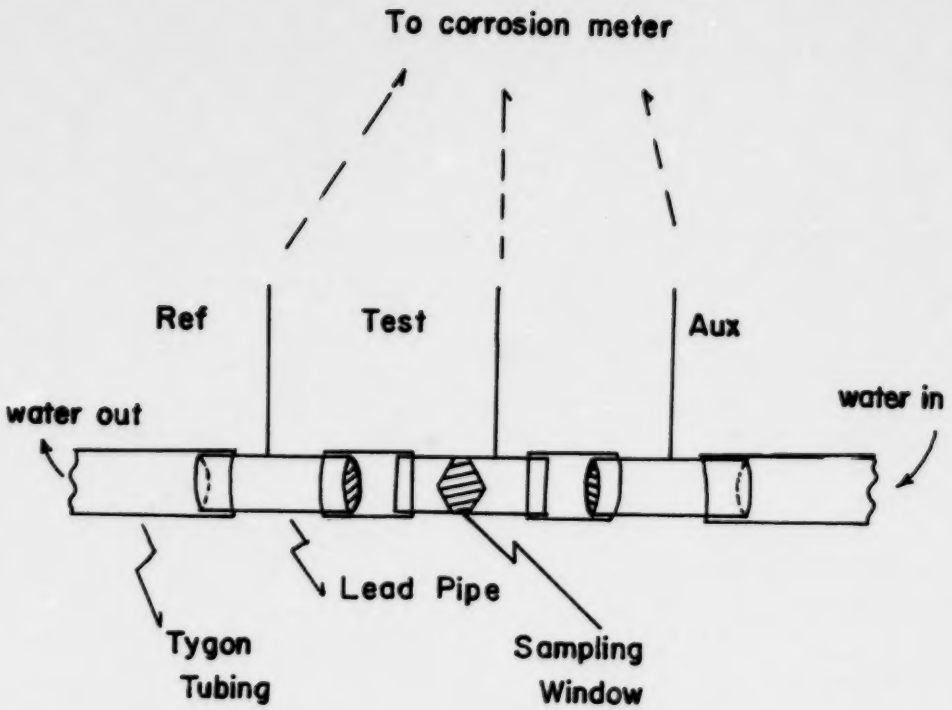

Figure 6. Original lead-pipe corrosion cell.

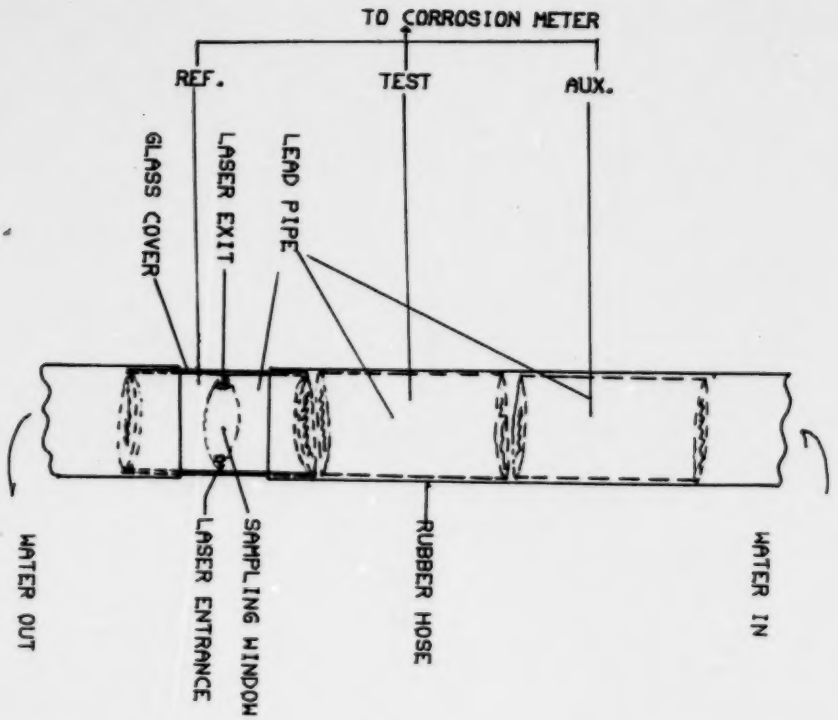

LEAD-PIPE FLOW-THRU CELL

Figure 7. Modified lead-pipe corrosion cell.

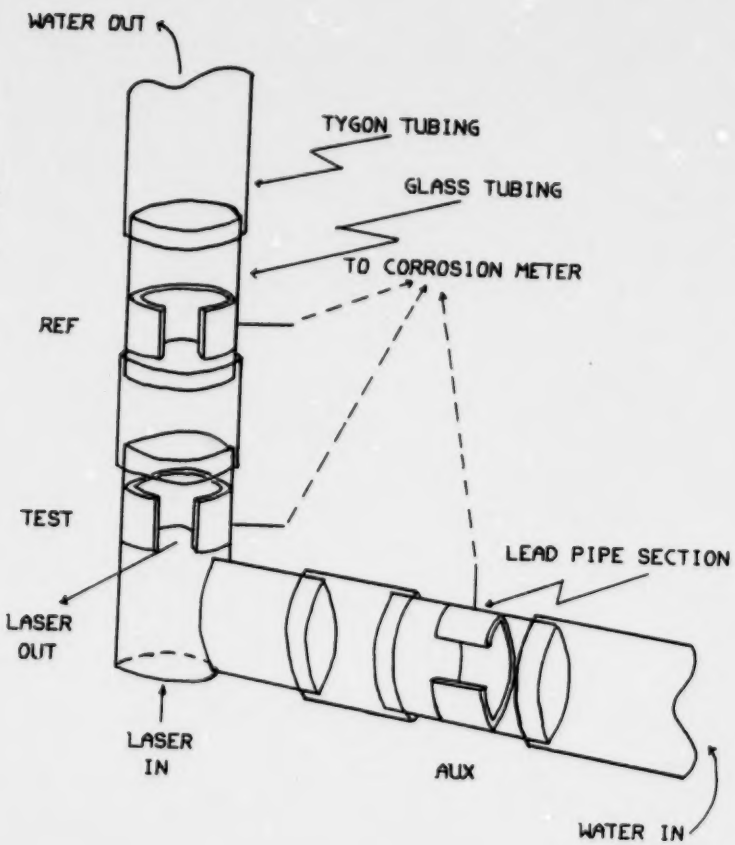

Figure 8. Final design of lead-pipe corrosion cell.

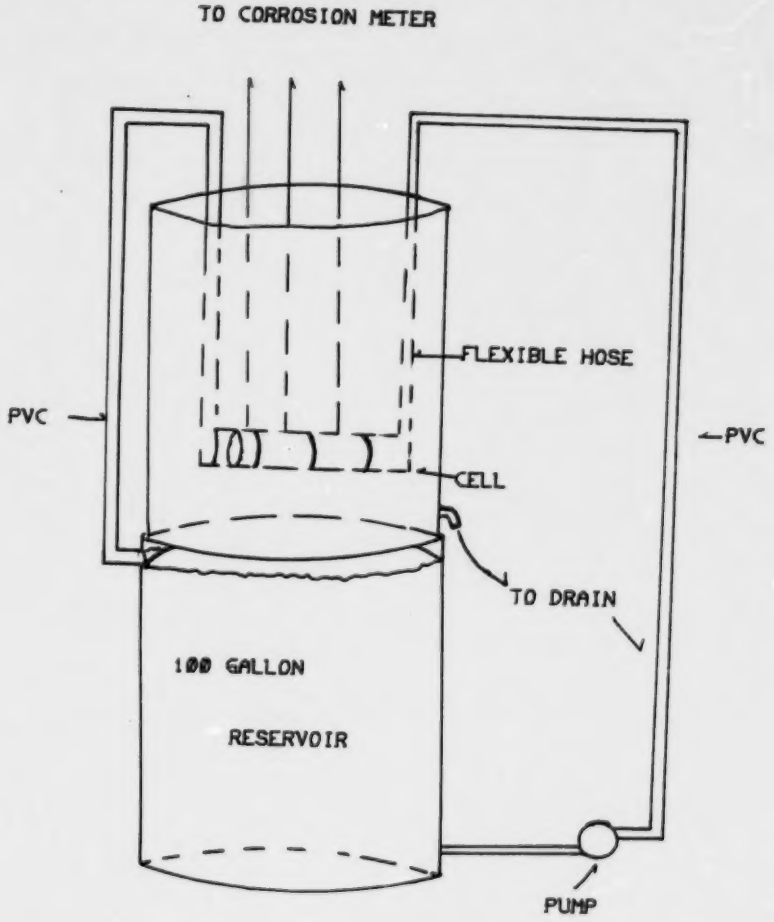

Figure 9. Schematic of entire lead-pipe flow-thru system.

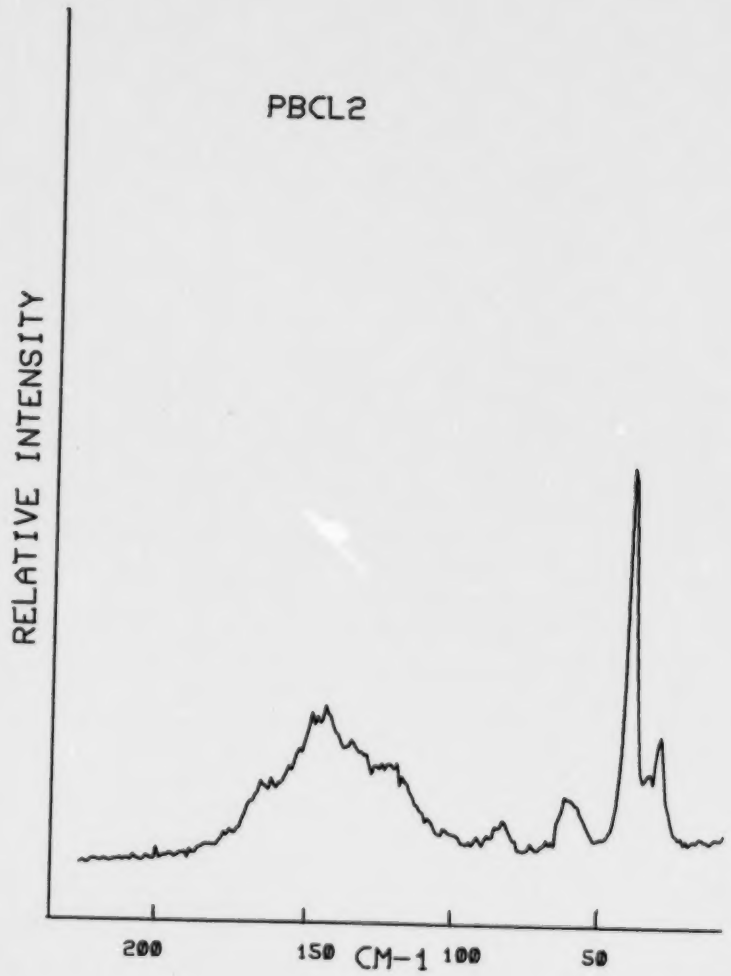

Figure 10. Raman spectrum of a single scan of $PbCl_2$.

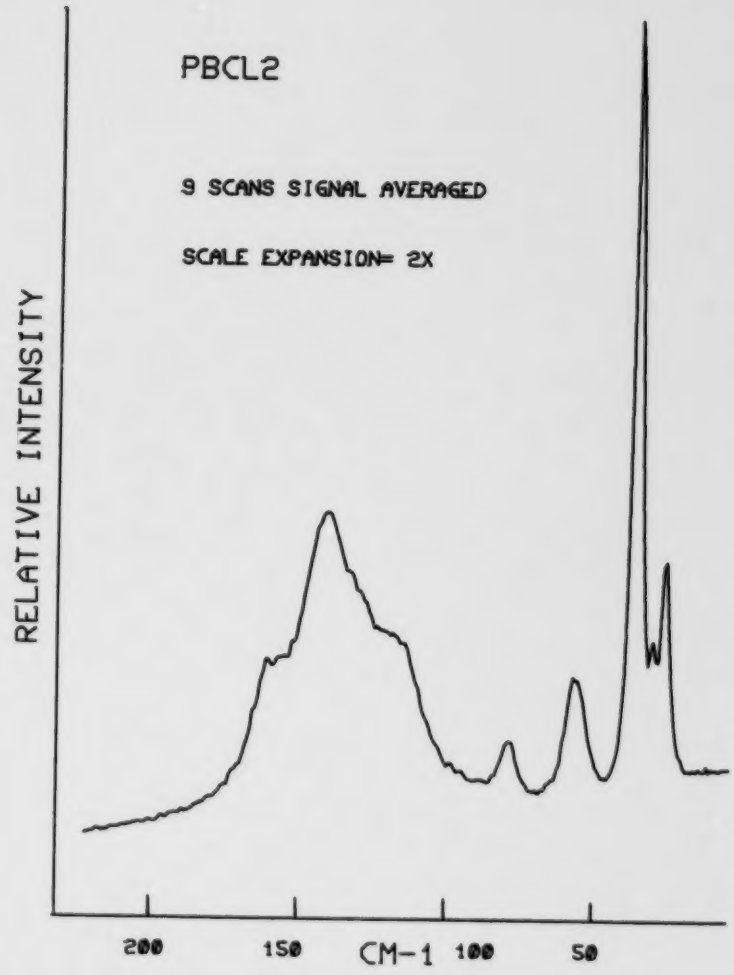

Figure 11. Signal average of nine scans of a Raman spectrum of $PbCl_2$.

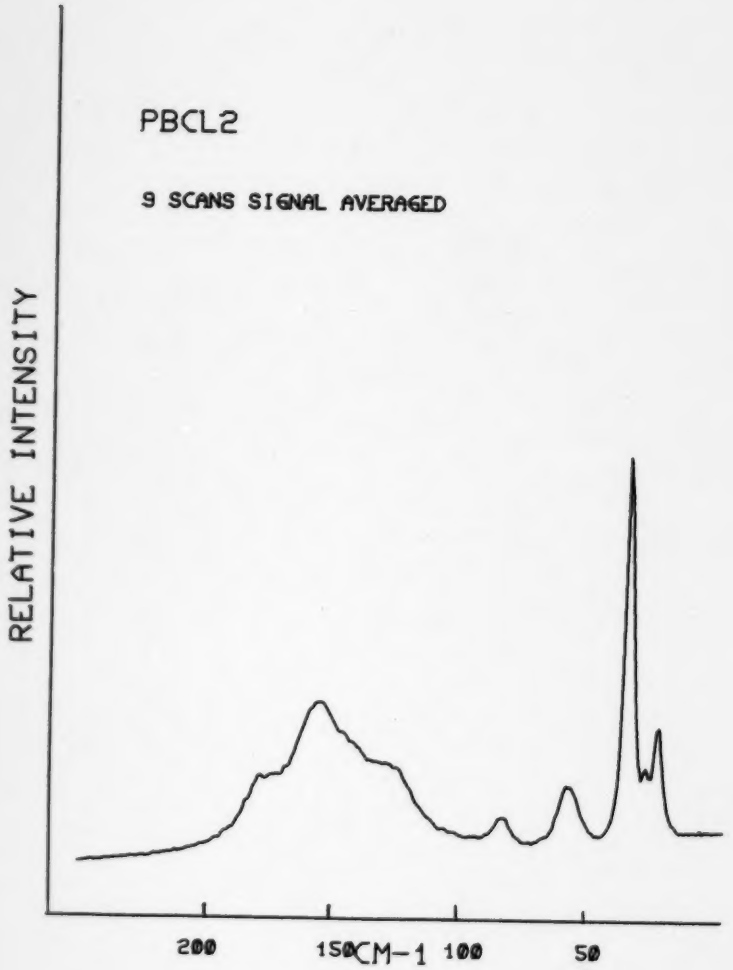

Figure 12. Expanded spectrum (2x) of Figure 11.

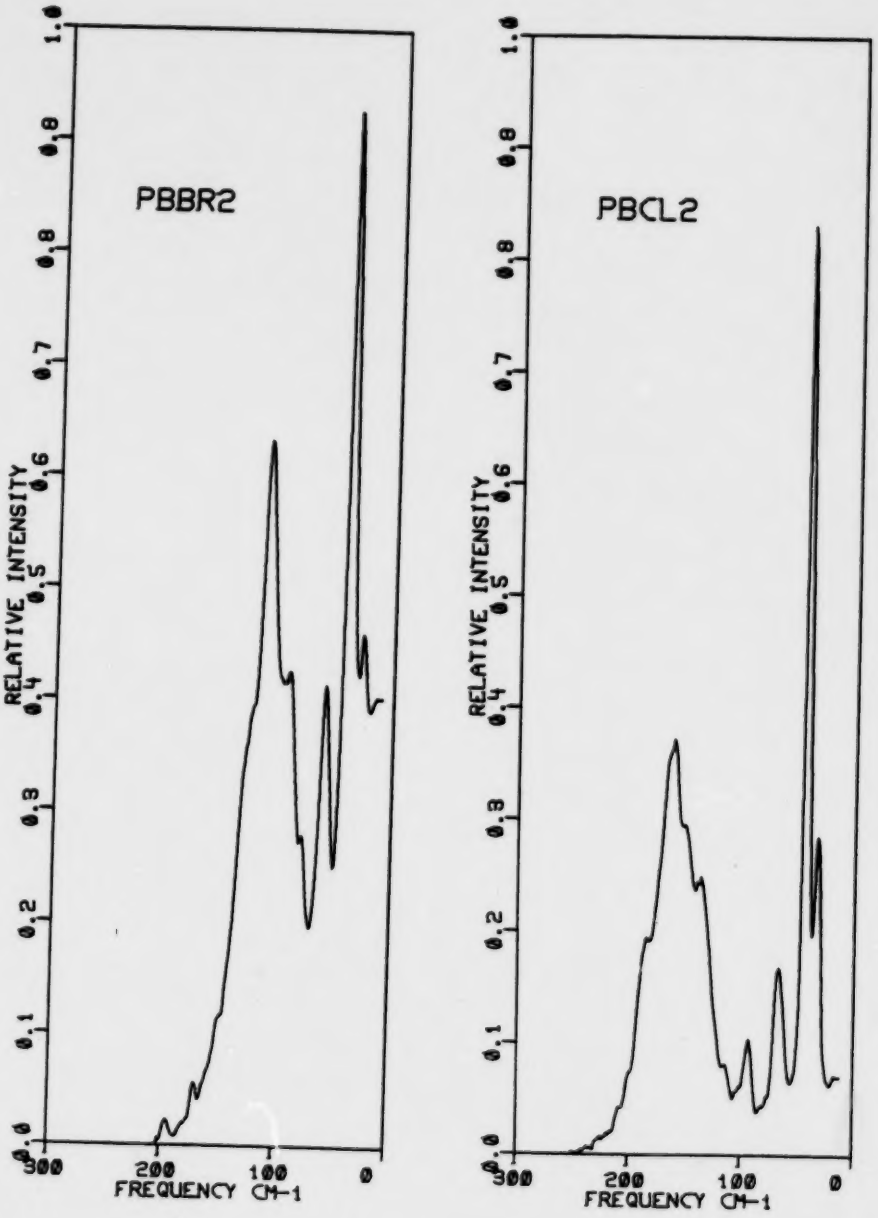

Figure 13. Raman spectra of $PbBr_2$ and $PbCl_2$

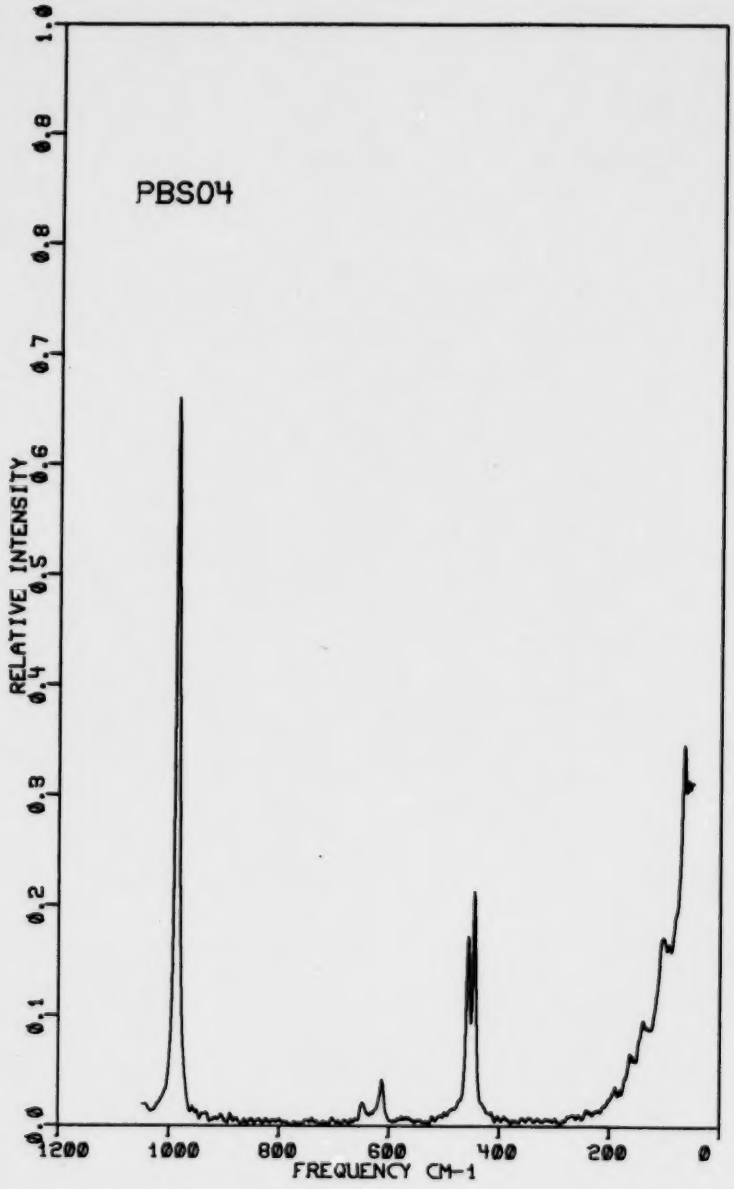

Figure 14. Raman spectrum of $PbSO_4$.

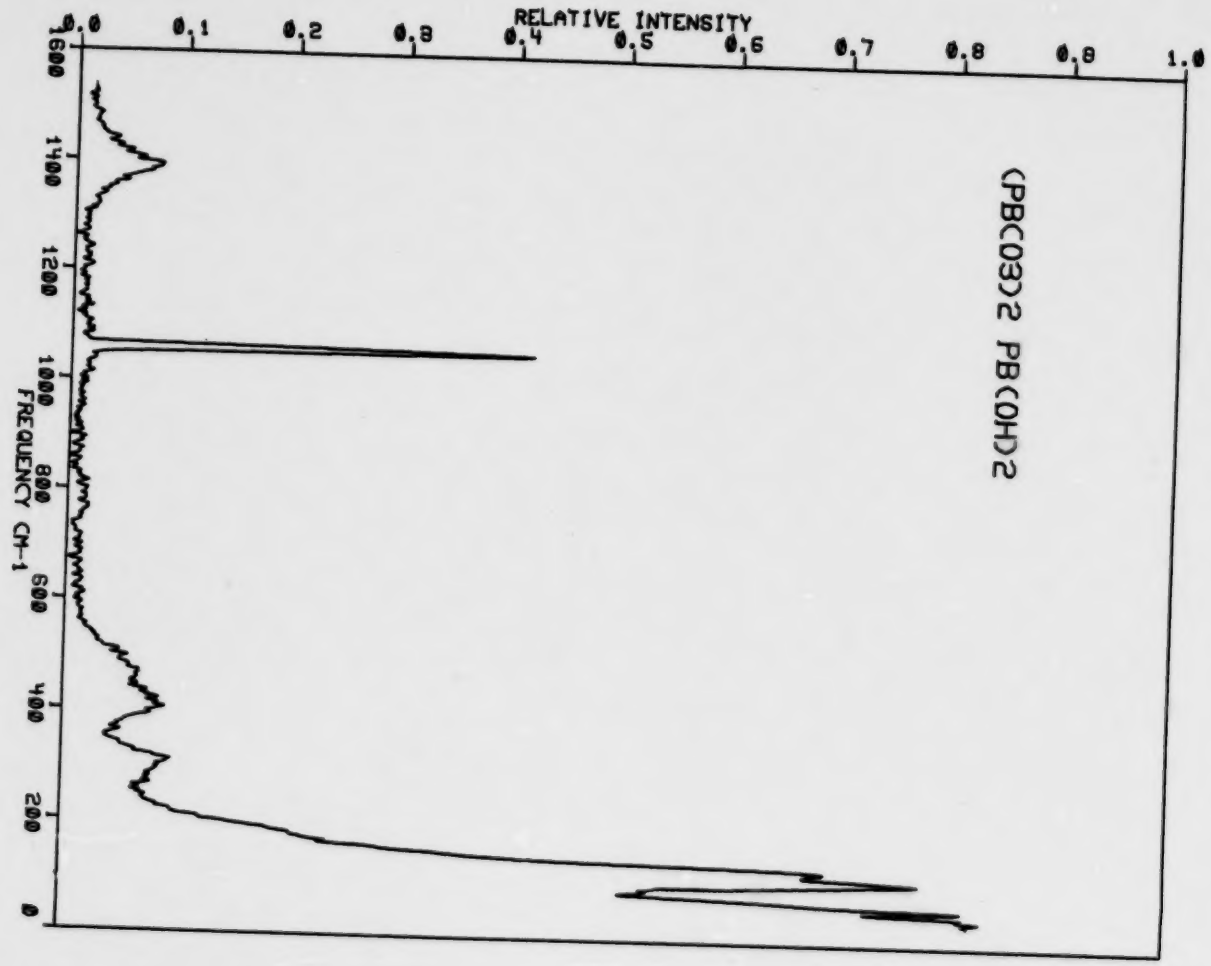

Figure 15. Raman spectrum of of $(PbCO_3)_2 \cdot Pb(OH)_2$.

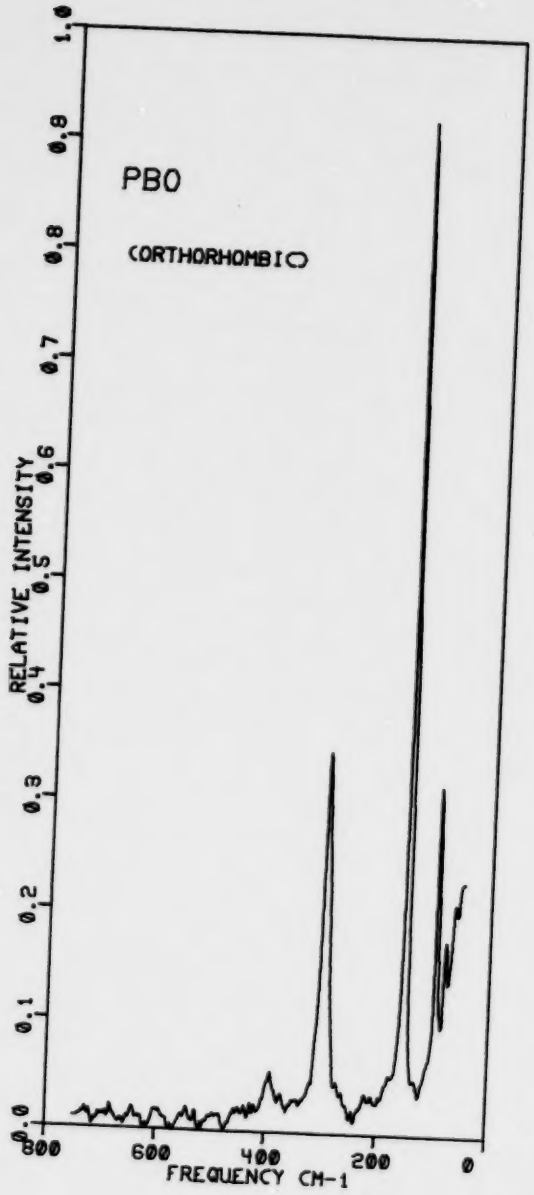

Figure 16. Raman spectrum of orthorhombic PbO.

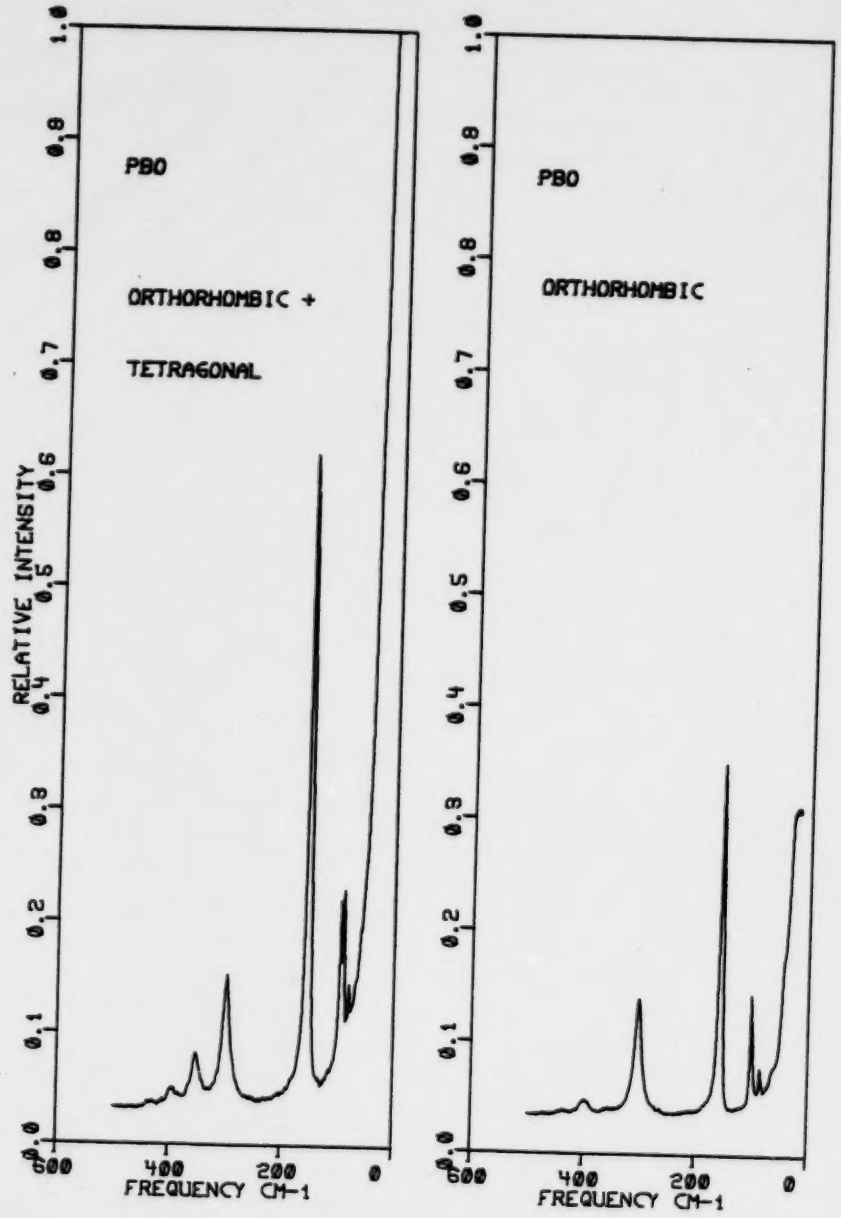

Figure 17. Raman spectra of: Left - KBr pellet of orthorhombic and tetragonal PbO.
Right - Pure orthorhombic PbO.

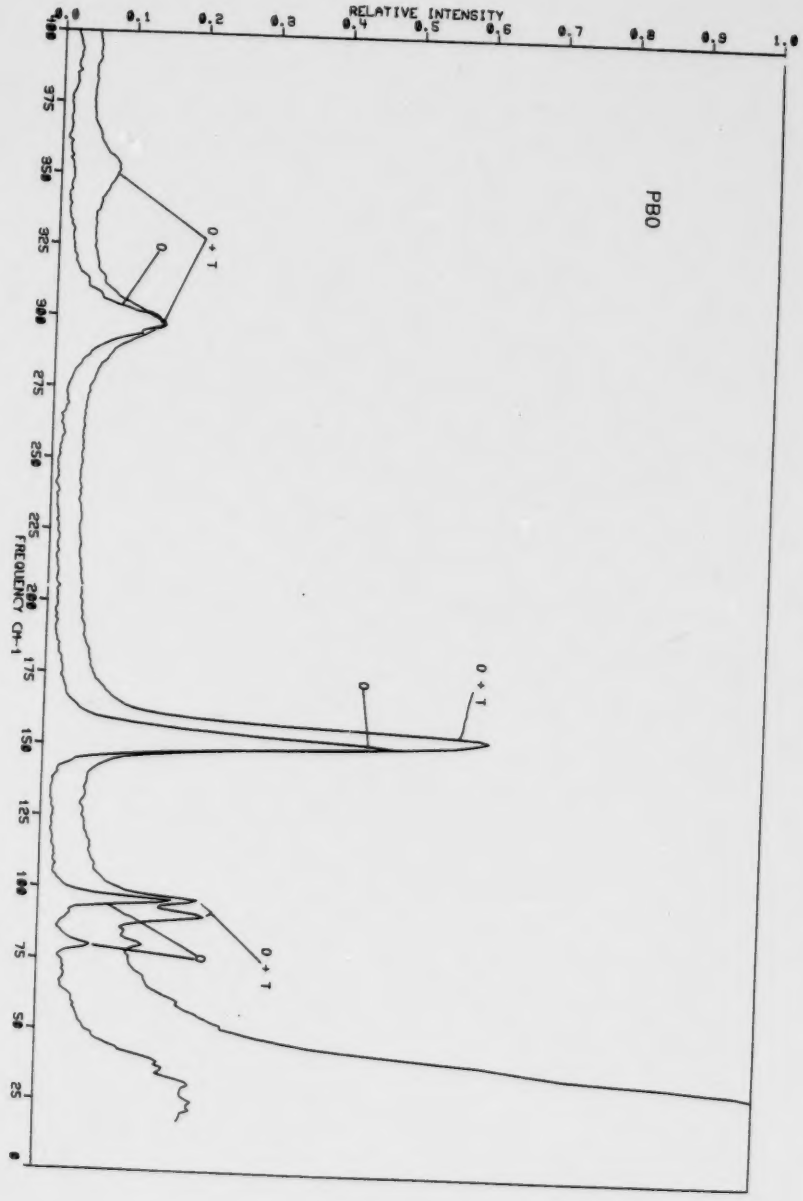

Figure 18. Raman spectra (expanded cm^{-1} axis) of:
Top - Orthorhombic + tetragonal PbO (O + T).
Bottom - Orthorhombic PbO (O).

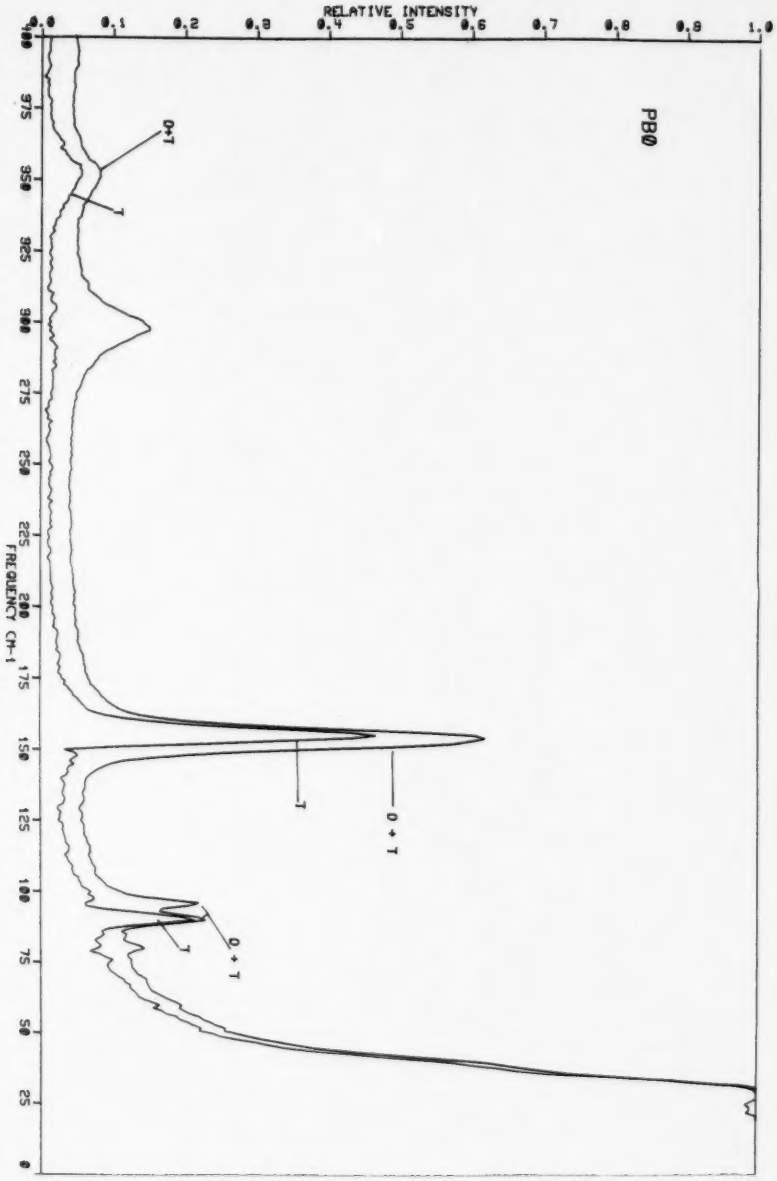

Figure 19. Raman spectra (expanded cm^{-1} axis) of:
Top - Ortho + tetragonal PbO (O + T).
Bottom - Tetragonal PbO (T).

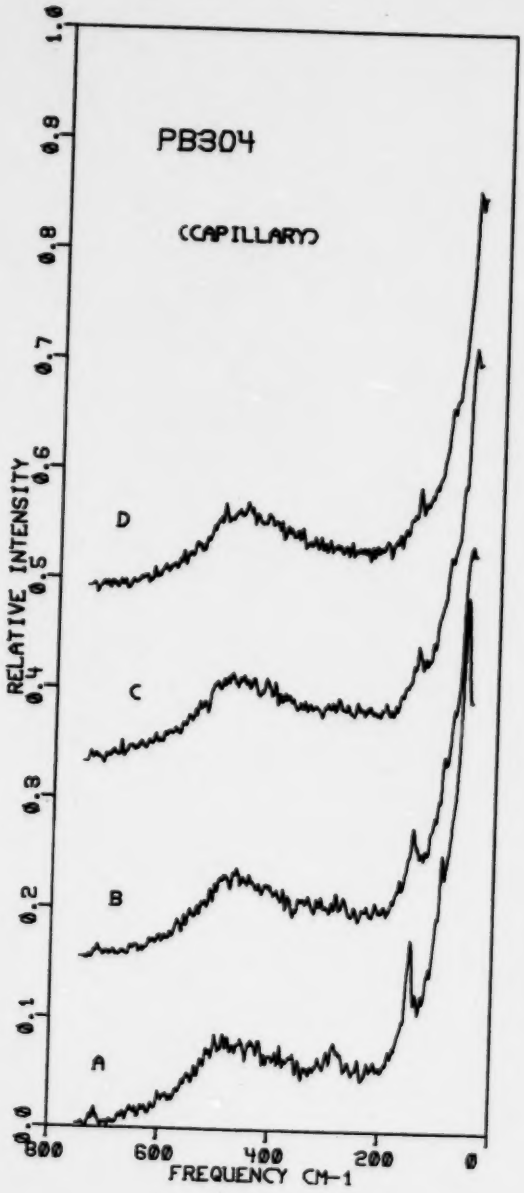

Figure 20. Raman spectrum of Pb_3O_4 powder.

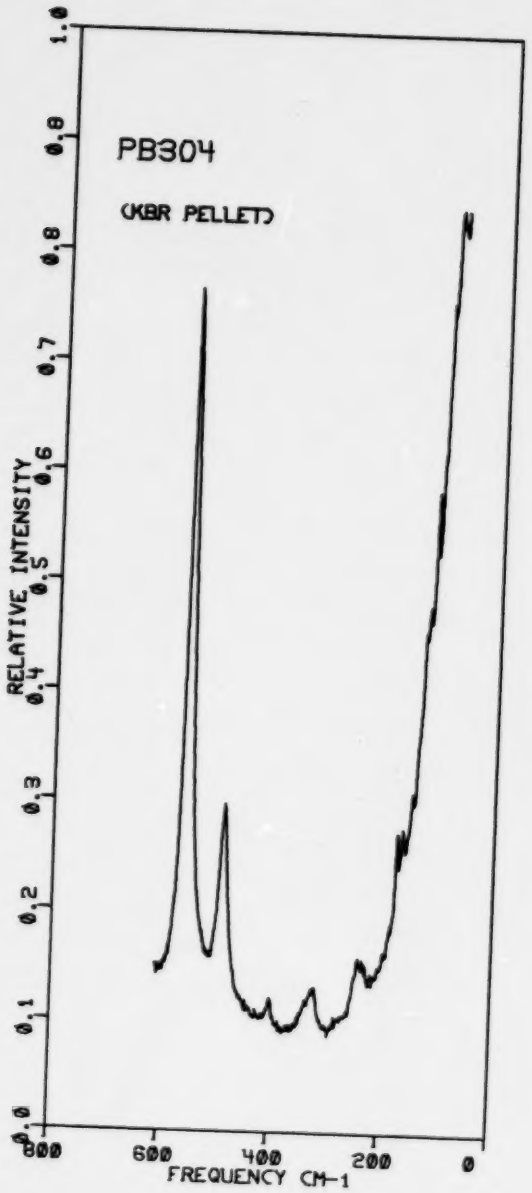

Figure 21. Raman spectrum of Pb_3O_4 in KBr pellet.

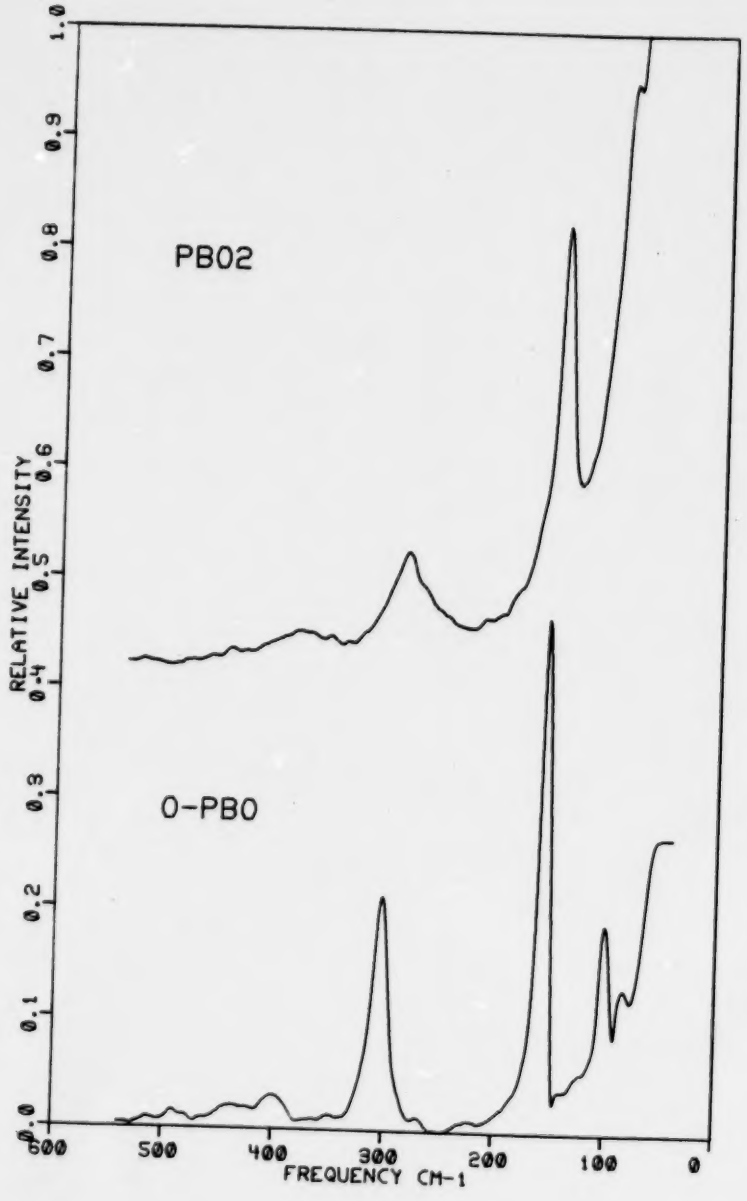

Figure 22. Raman spectra of PbO_2 and O-PbO.

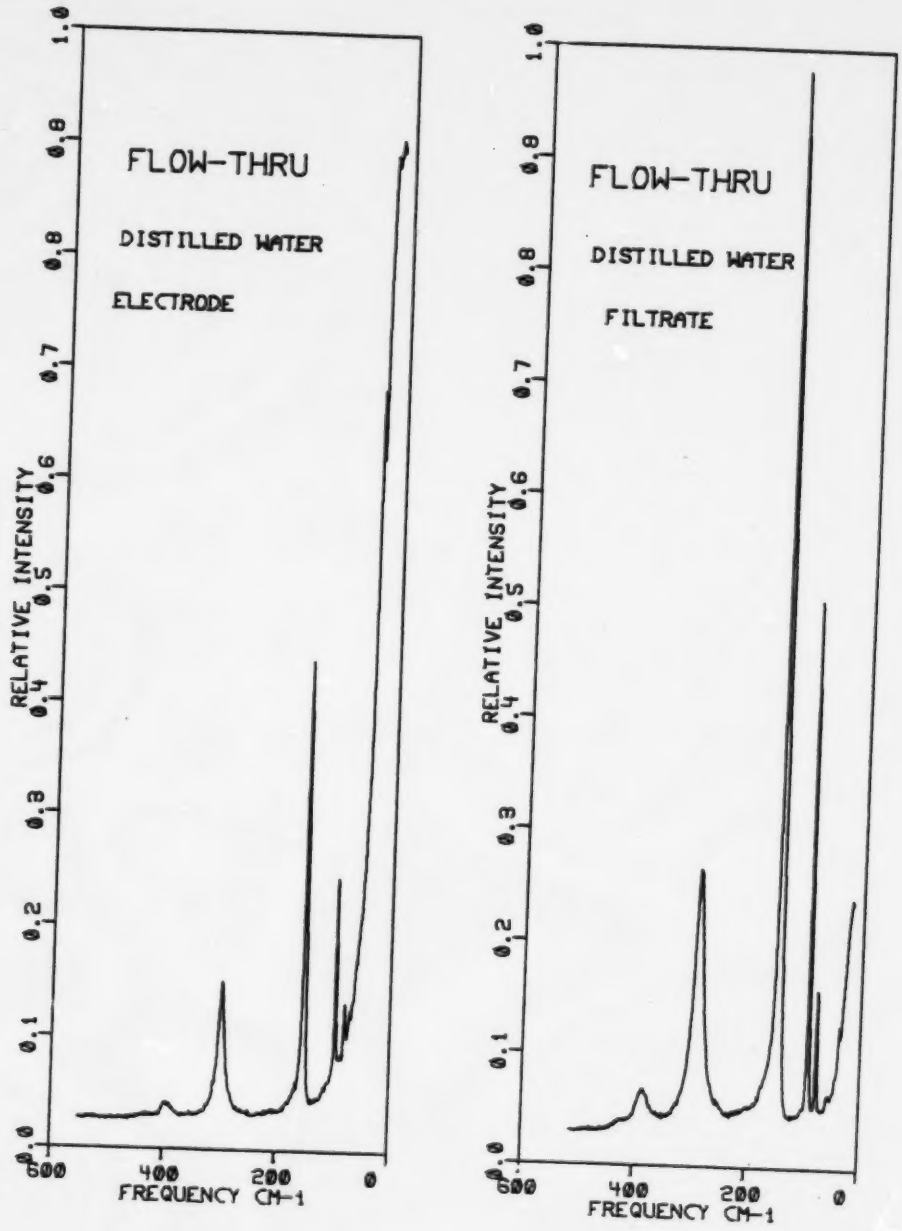

Figure 23. Raman spectrum of electrode and filtrate from Experiment 1.

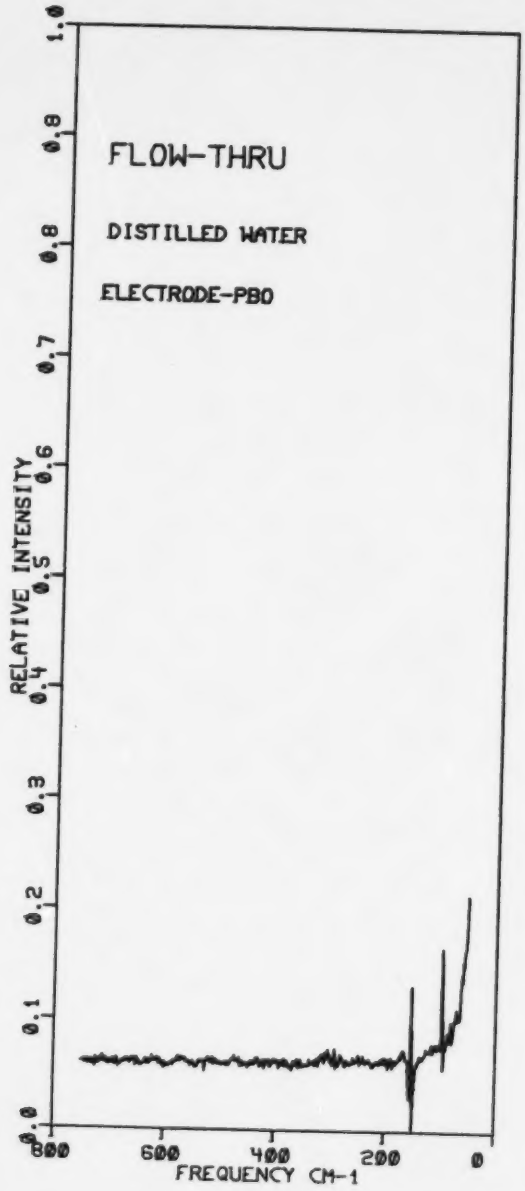

Figure 24. Difference spectrum = electrode spectrum minus O-PbO spectrum.

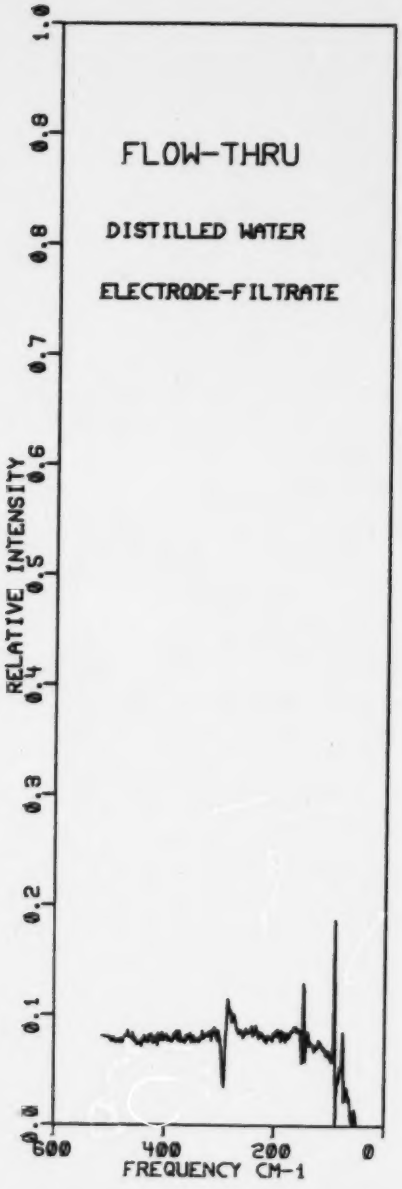

Figure 25. Difference spectrum = electrode spectrum minus filtrate spectrum.

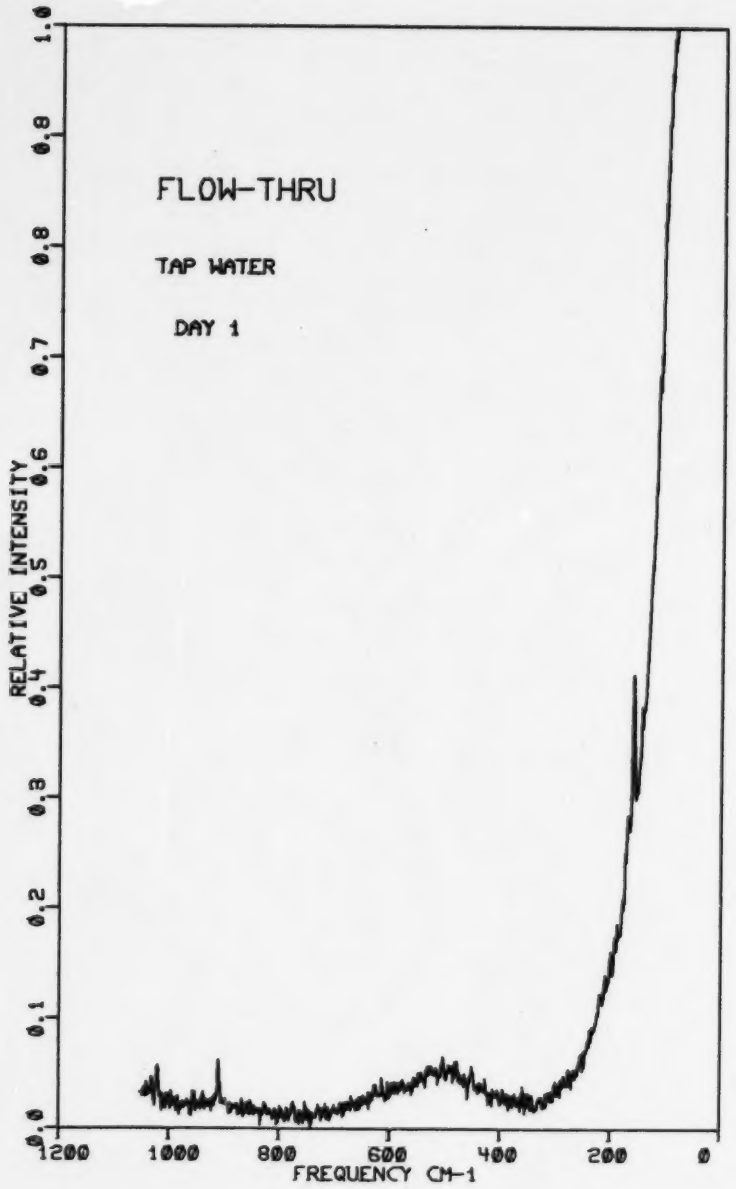

Figure 26. Raman spectrum, experiment 2, day 1.

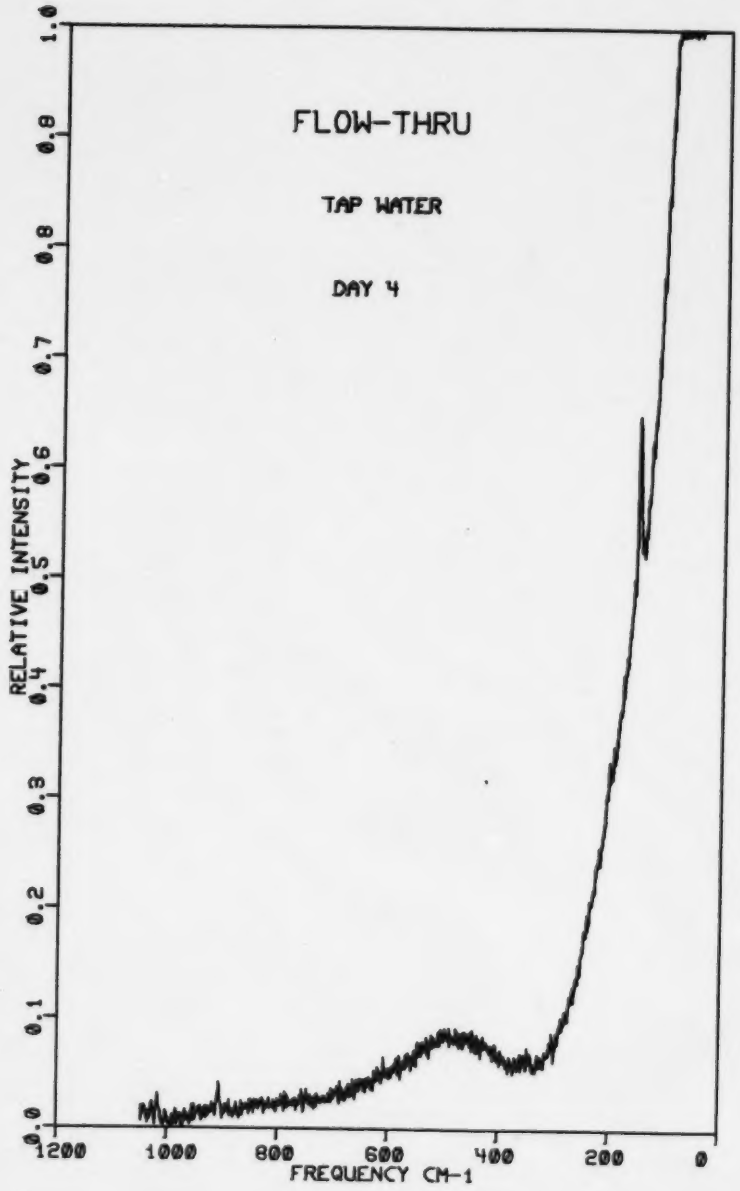

Figure 27. Raman spectrum, experiment 2, day 4.

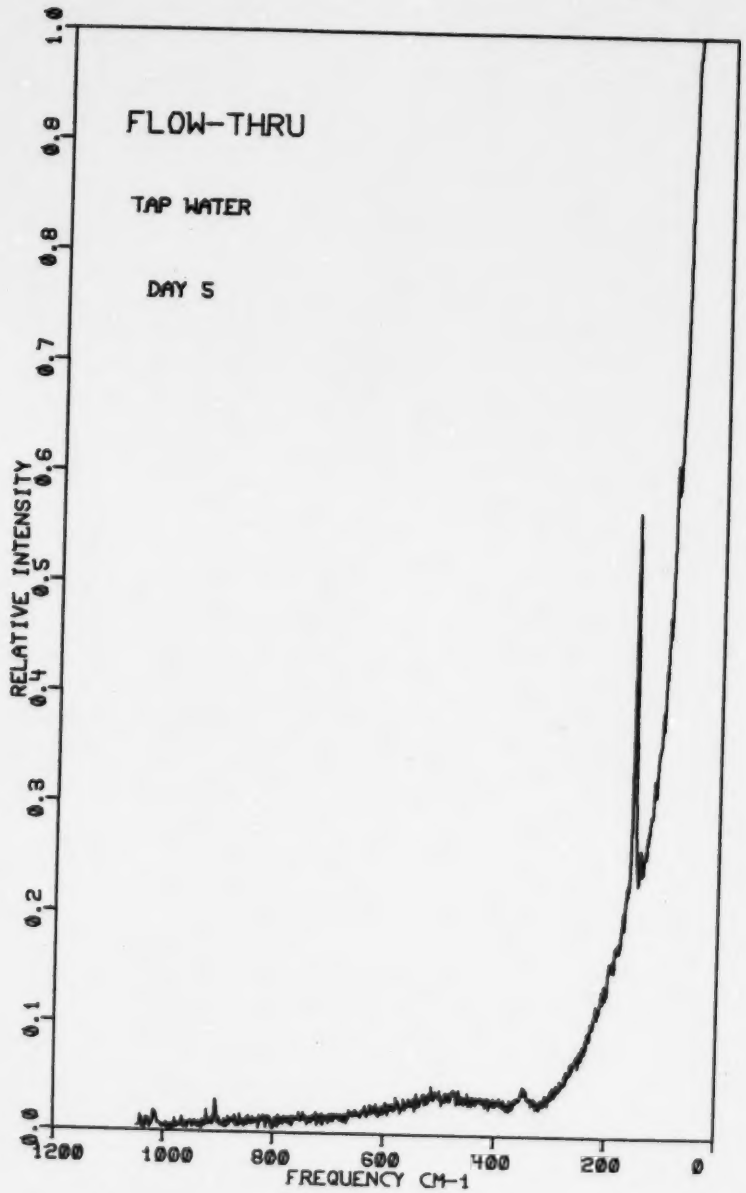

Figure 28. Raman spectrum, experiment 2, day 5.

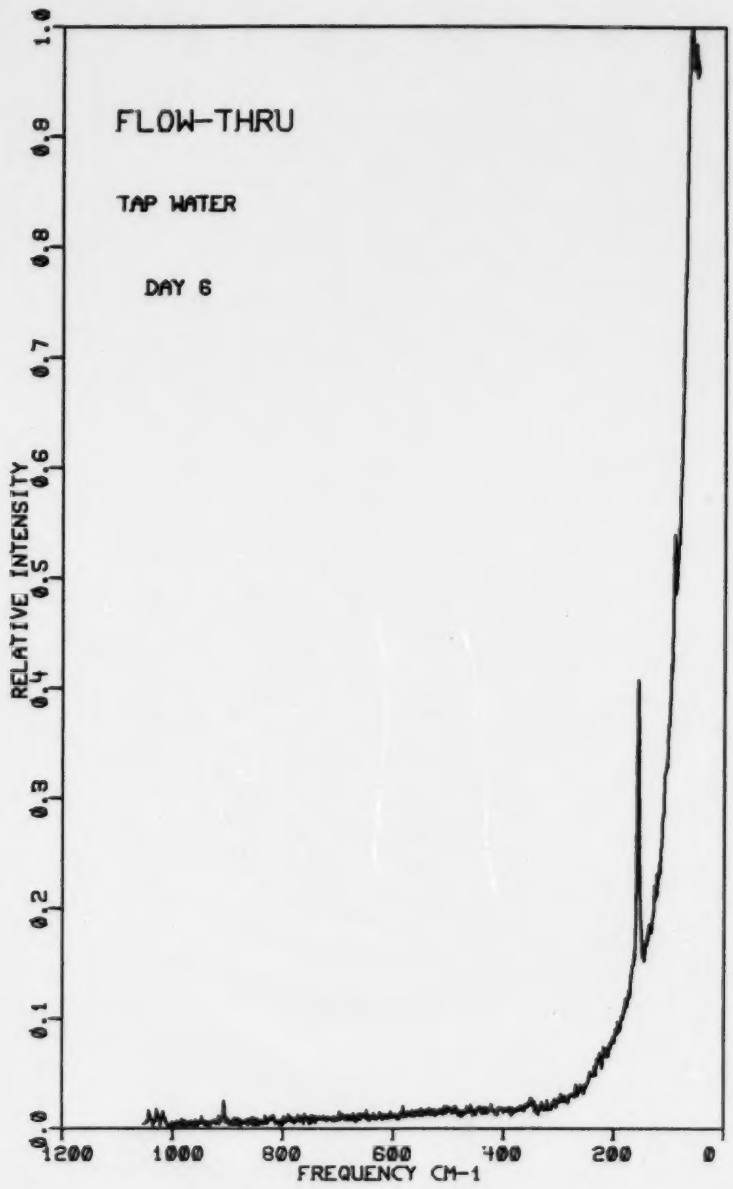

Figure 29. Raman spectrum, experiment 2, day 6.

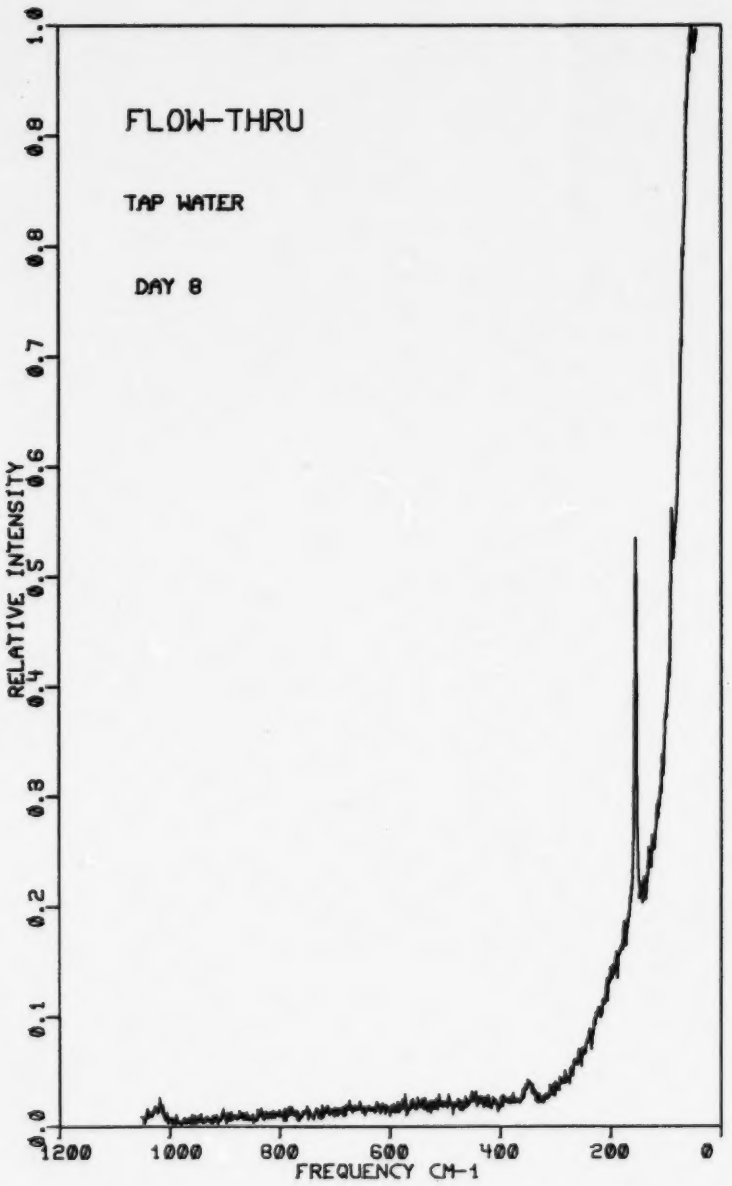

Figure 30. Raman spectrum, experiment 2, day 8.

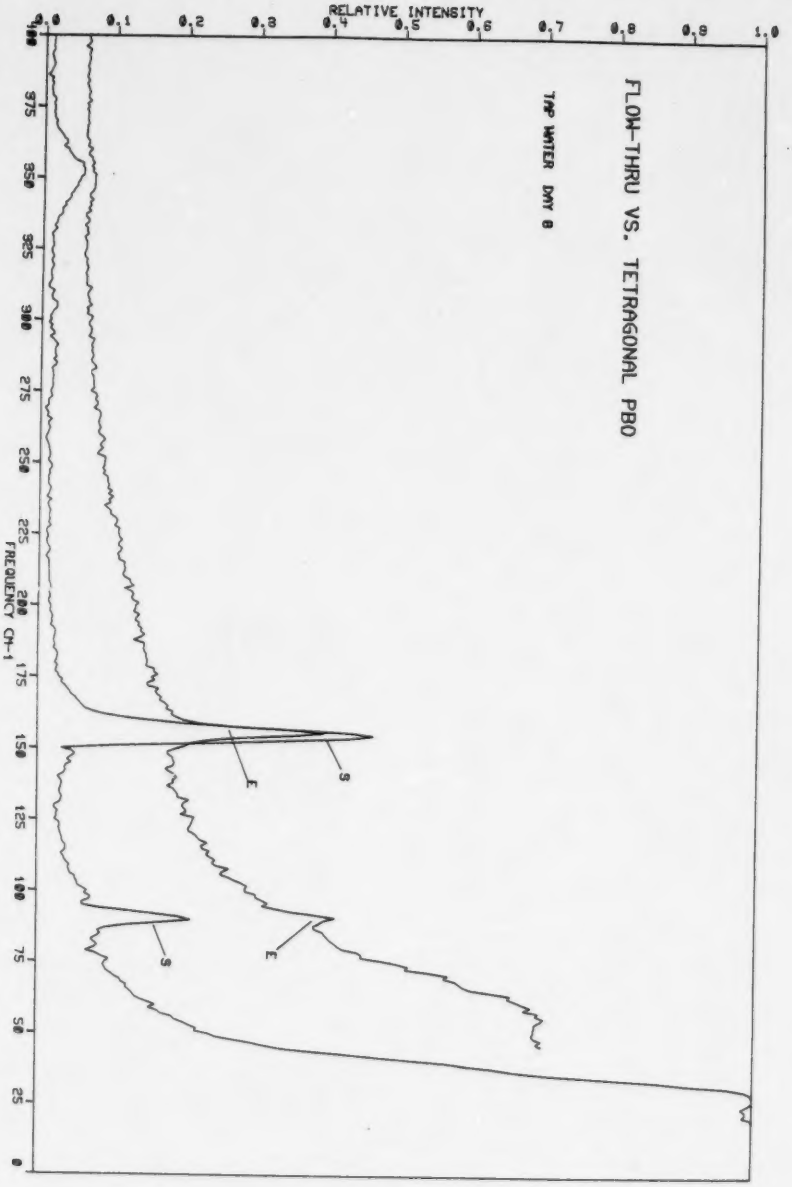

Figure 31. Raman spectra (expanded cm^{-1} axis) of:
Top - Electrode surface (E) from tap water - experiment from day 8.
Bottom - Standard spectrum (S) of tetragonal PbO.

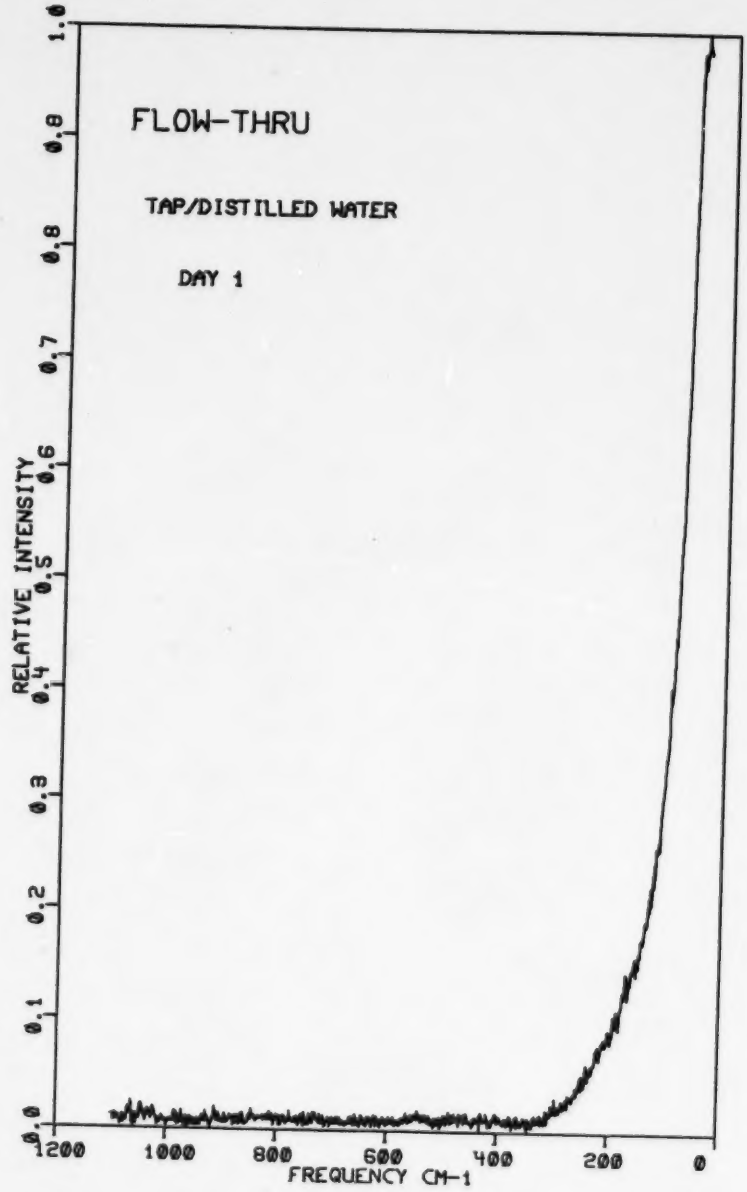

Figure 32. Raman spectrum, experiment 3, day 1.

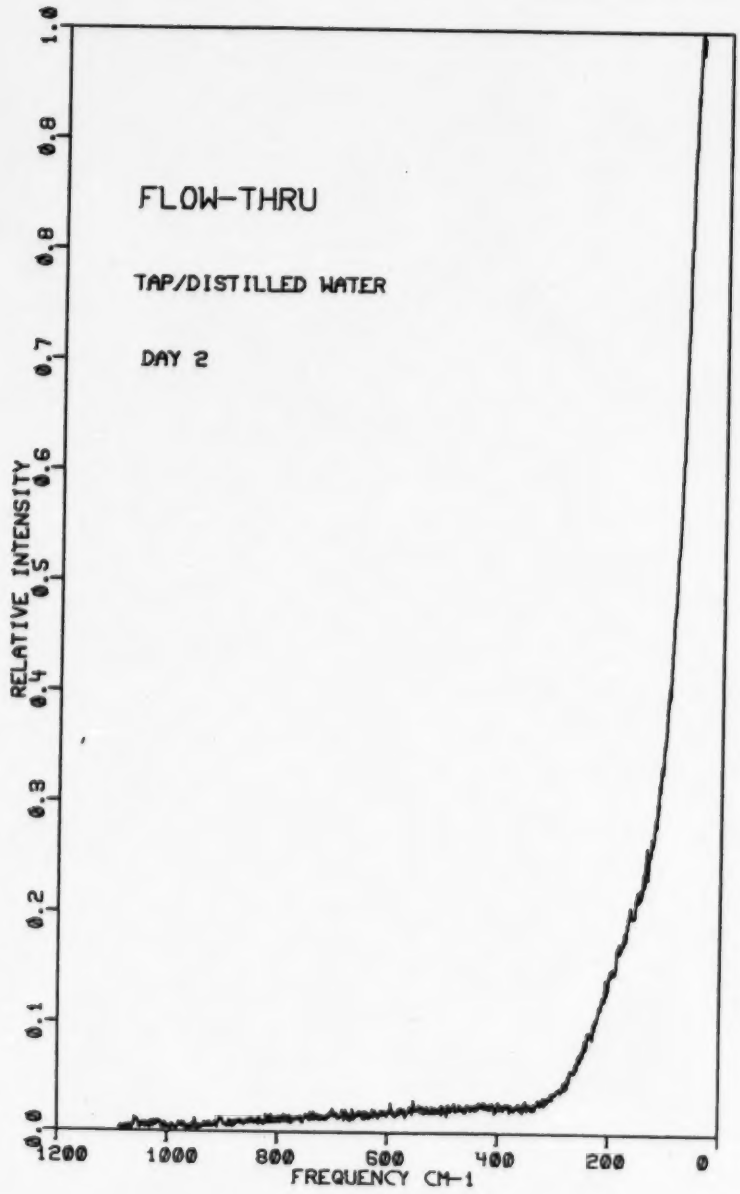

Figure 33. Raman spectrum, experiment 3, day 2.

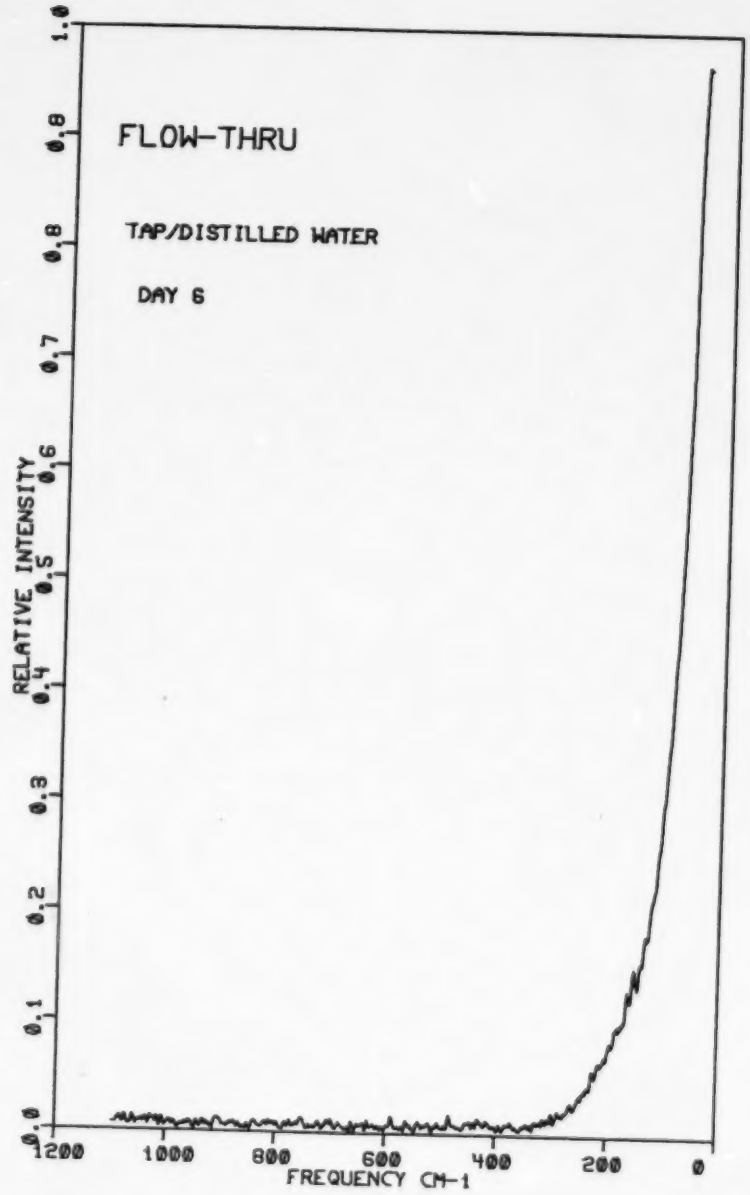

Figure 34. Raman spectrum, experiment 3, day 6.

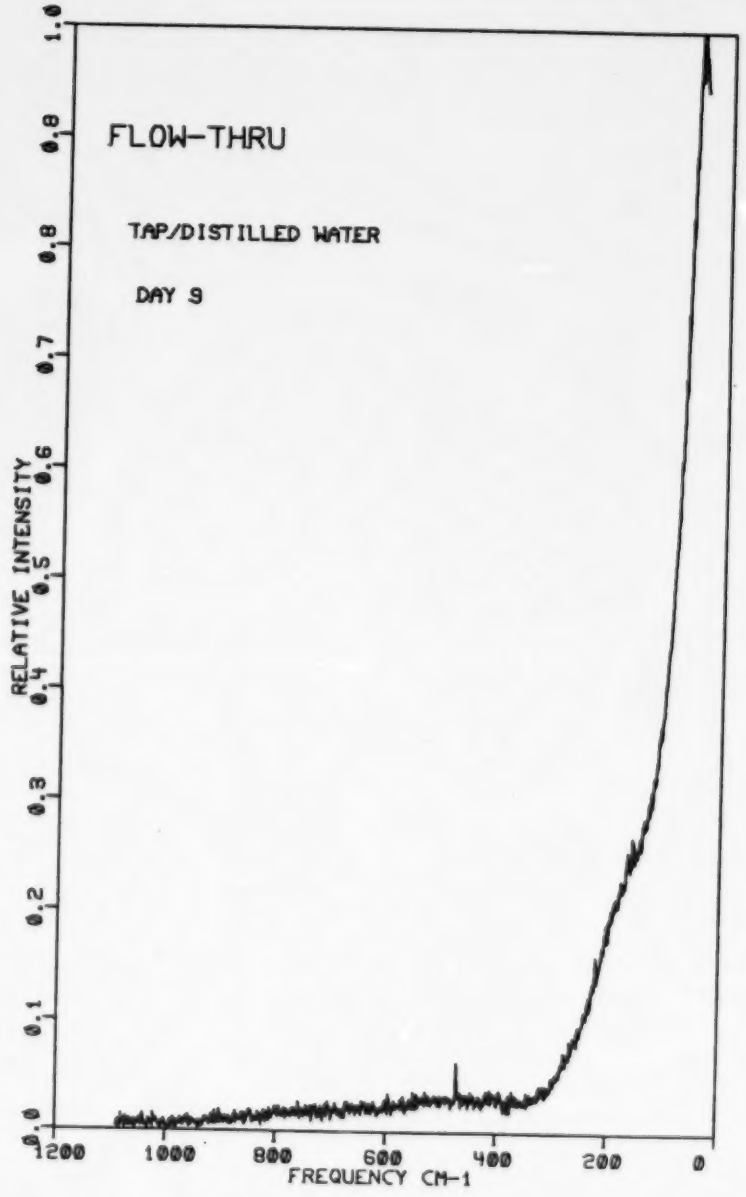

Figure 35. Raman spectrum, experiment 3, day 9.

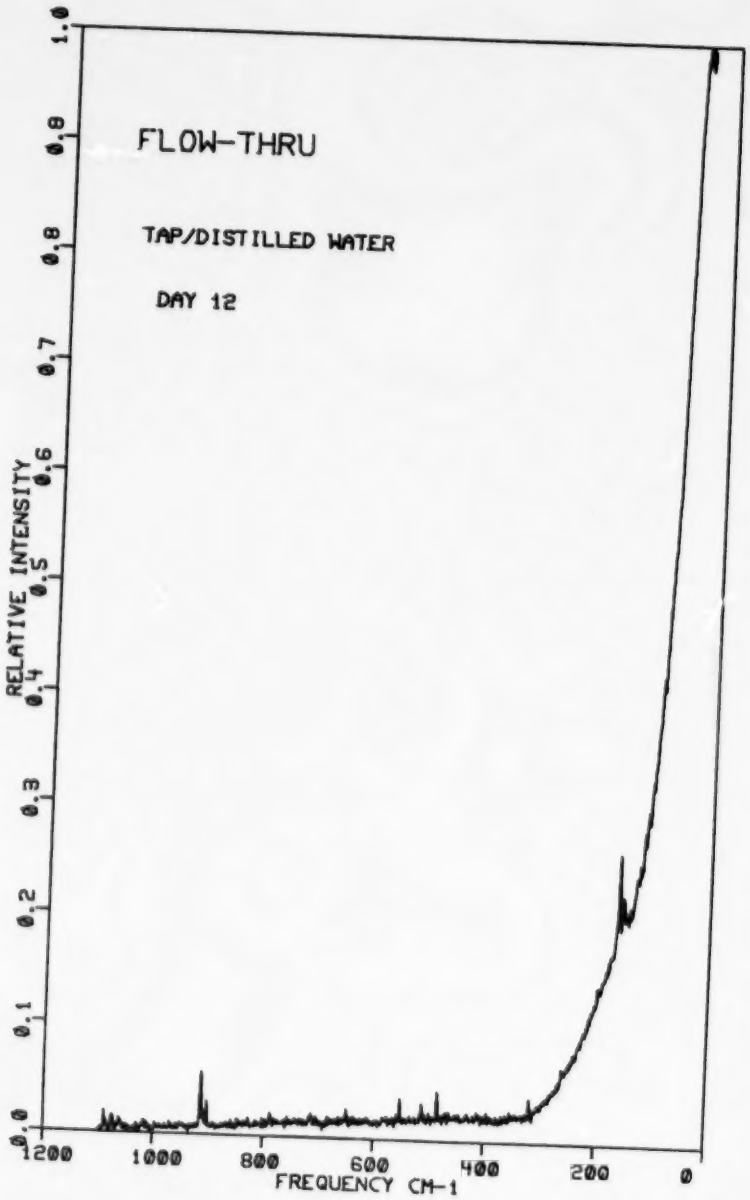

Figure 36. Raman spectrum, experiment 3, day 12.

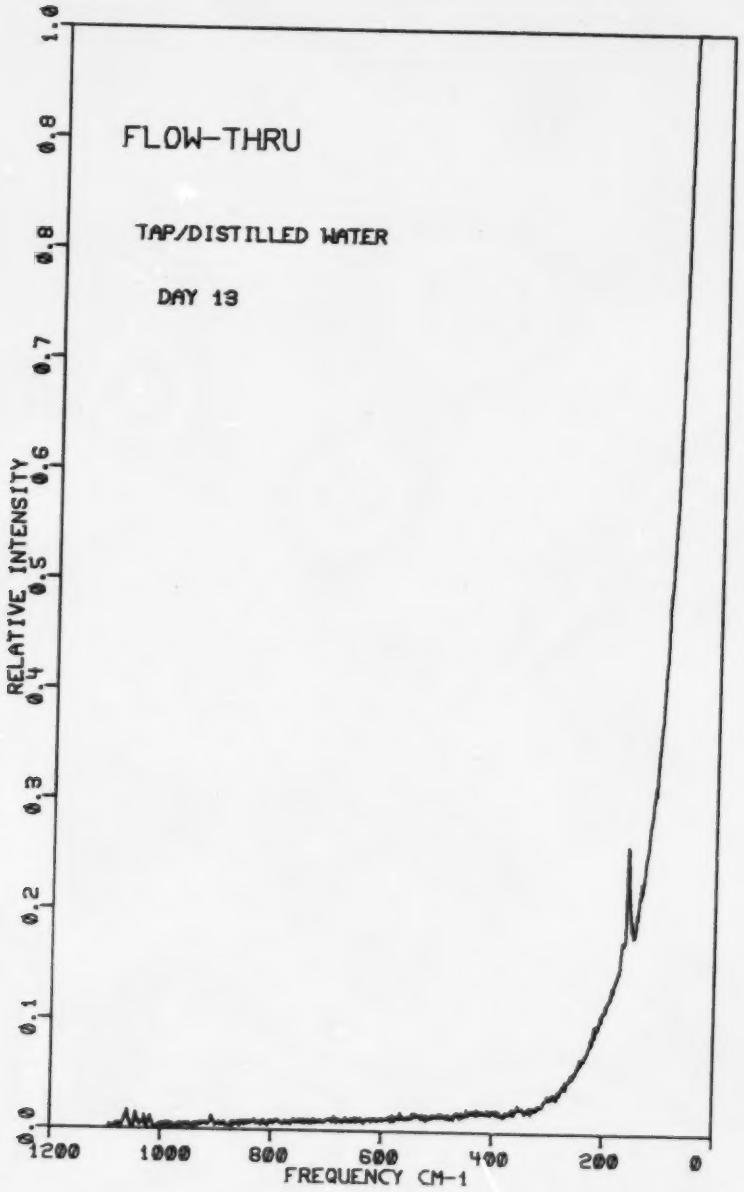

Figure 37. Raman spectrum, experiment 3, day 13.

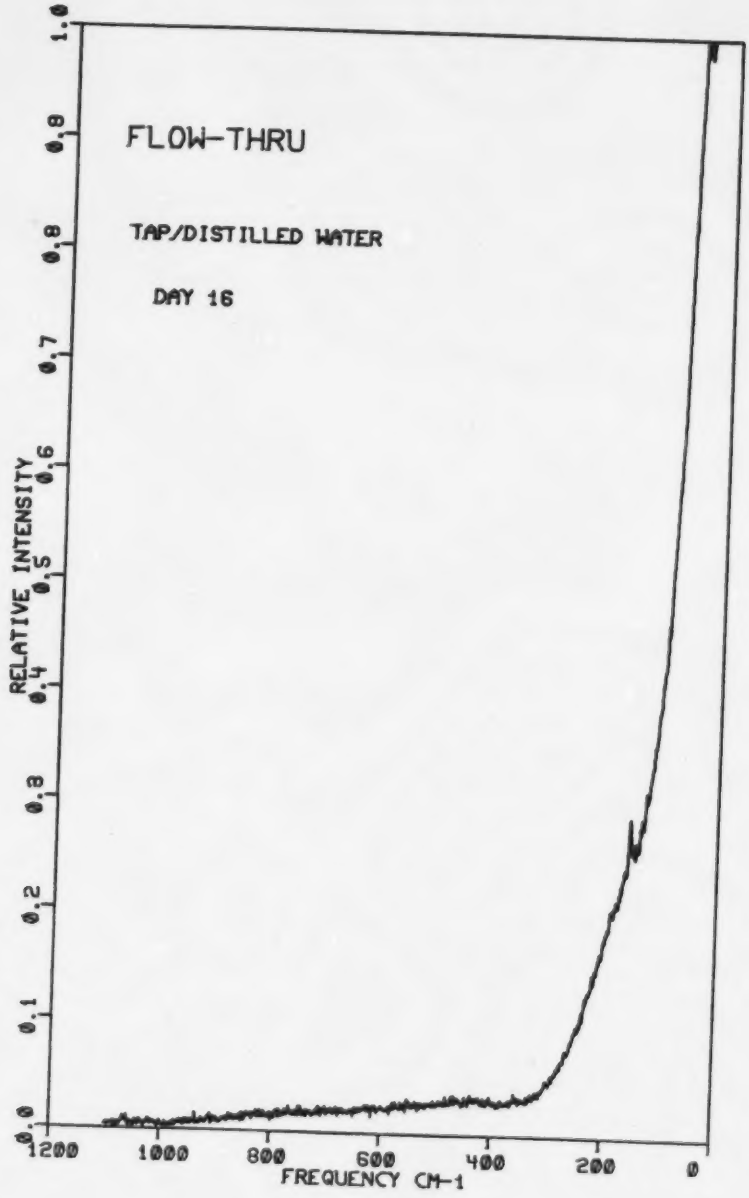

Figure 38. Raman spectrum, experiment 3, day 16.

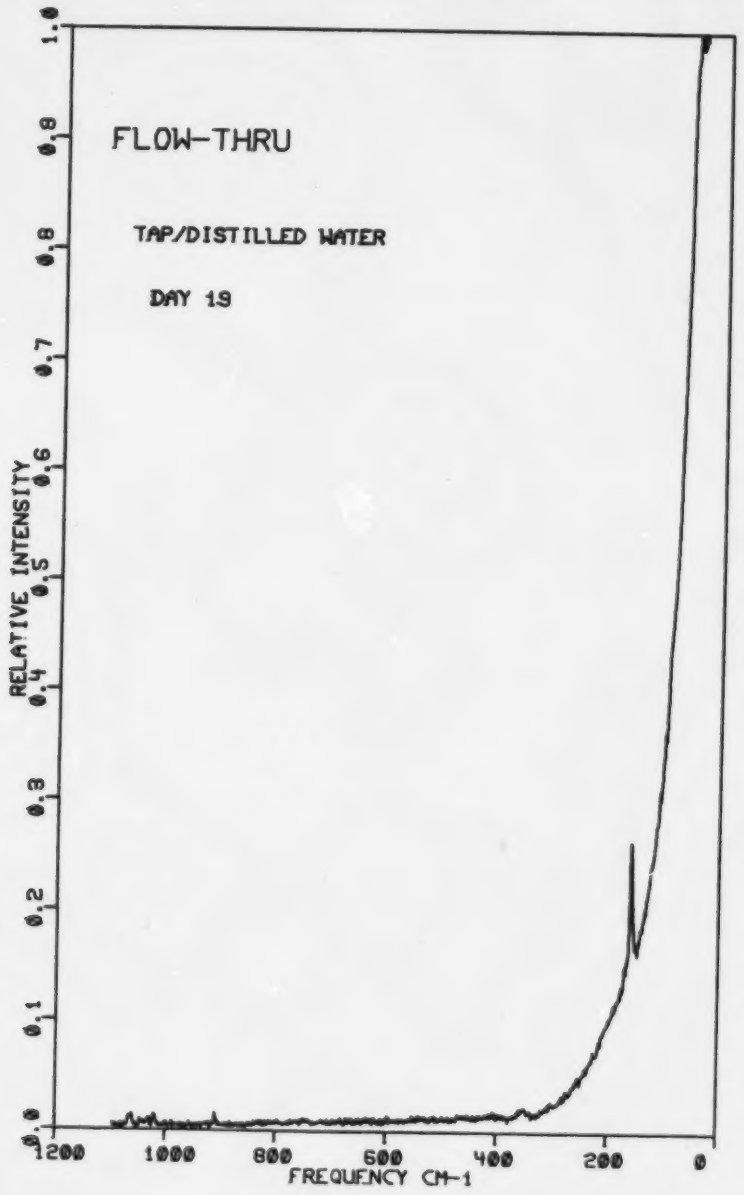

Figure 39. Raman spectrum, experiment 3, day 19.

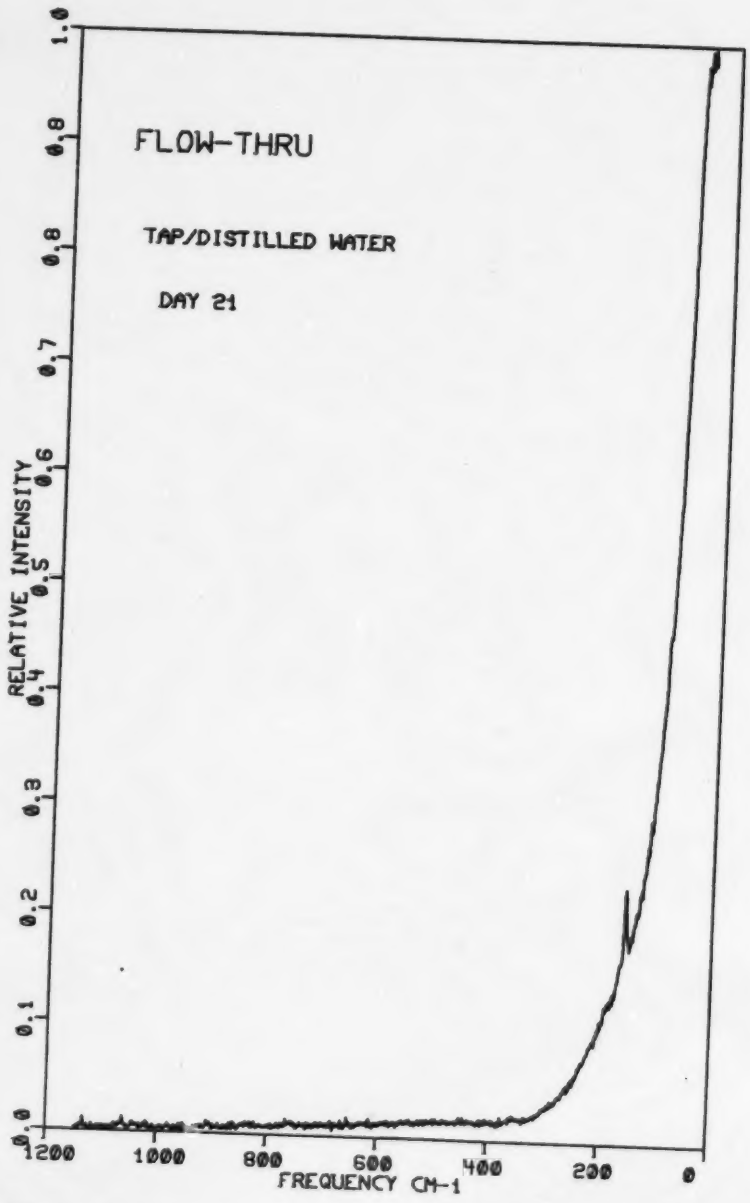

Figure 40. Raman spectrum, experiment 3, day 21.

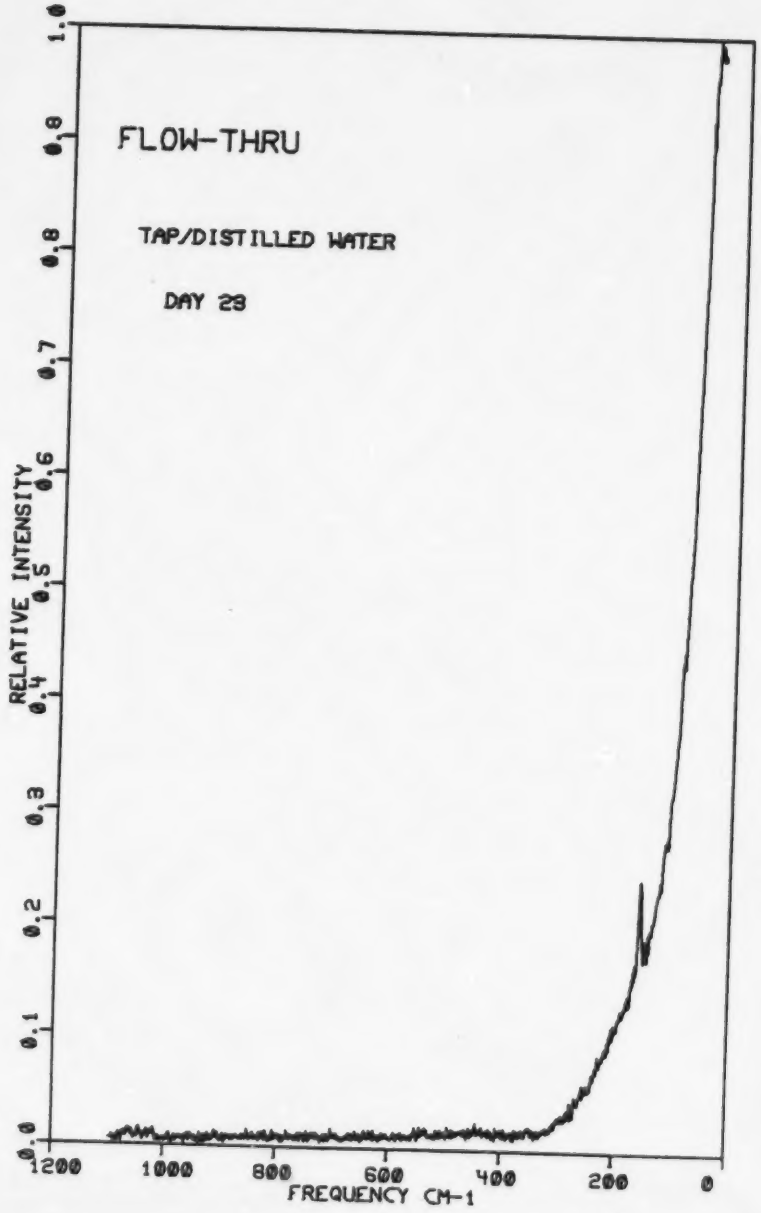

Figure 41. Raman spectrum, experiment 3, day 23.

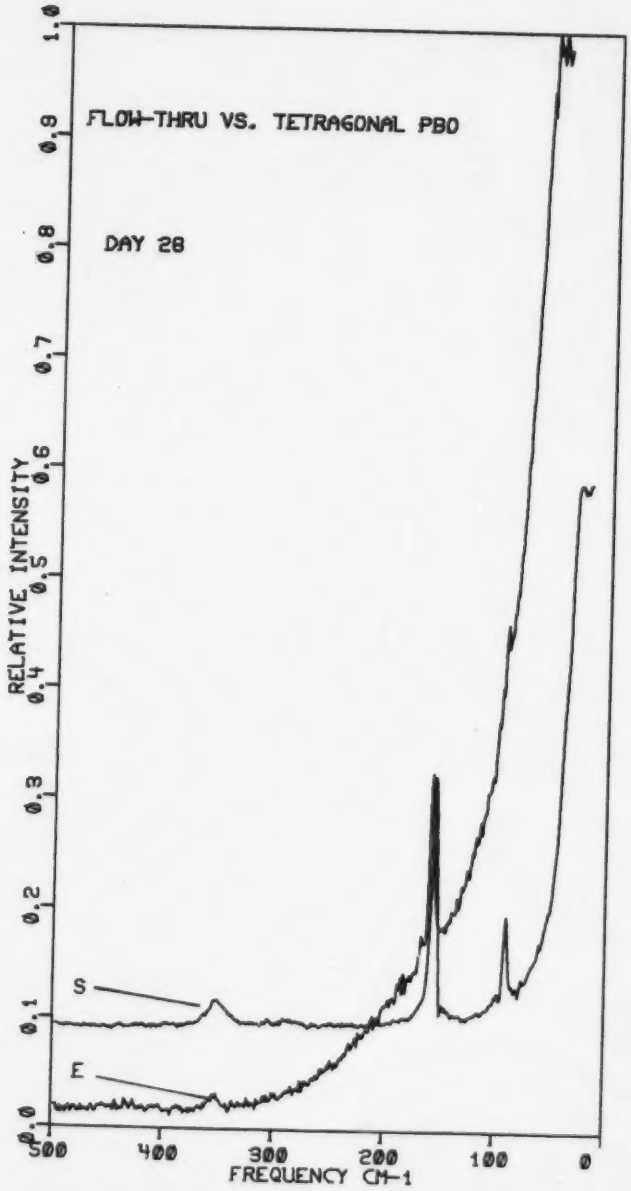

Figure 42. Raman spectra (standard cm^{-1} axis) of:
Top - Standard (S) tetragonal PbO.
Bottom - Electrode (E) surface, experiment 3, day 28, pH - 9.5.

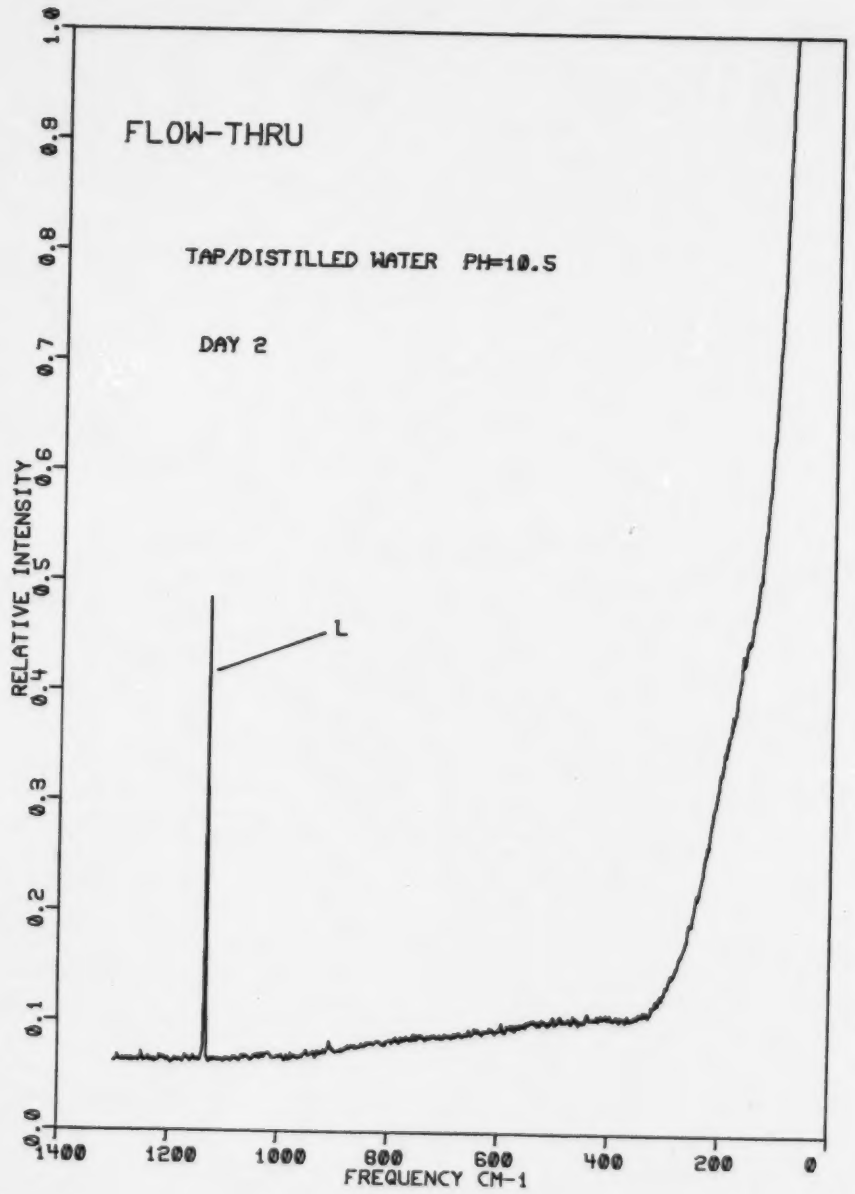

Figure 43. Raman spectrum of electrode surface in experiment 4, day 2, pH - 10.5 (L = peak due to room lights).

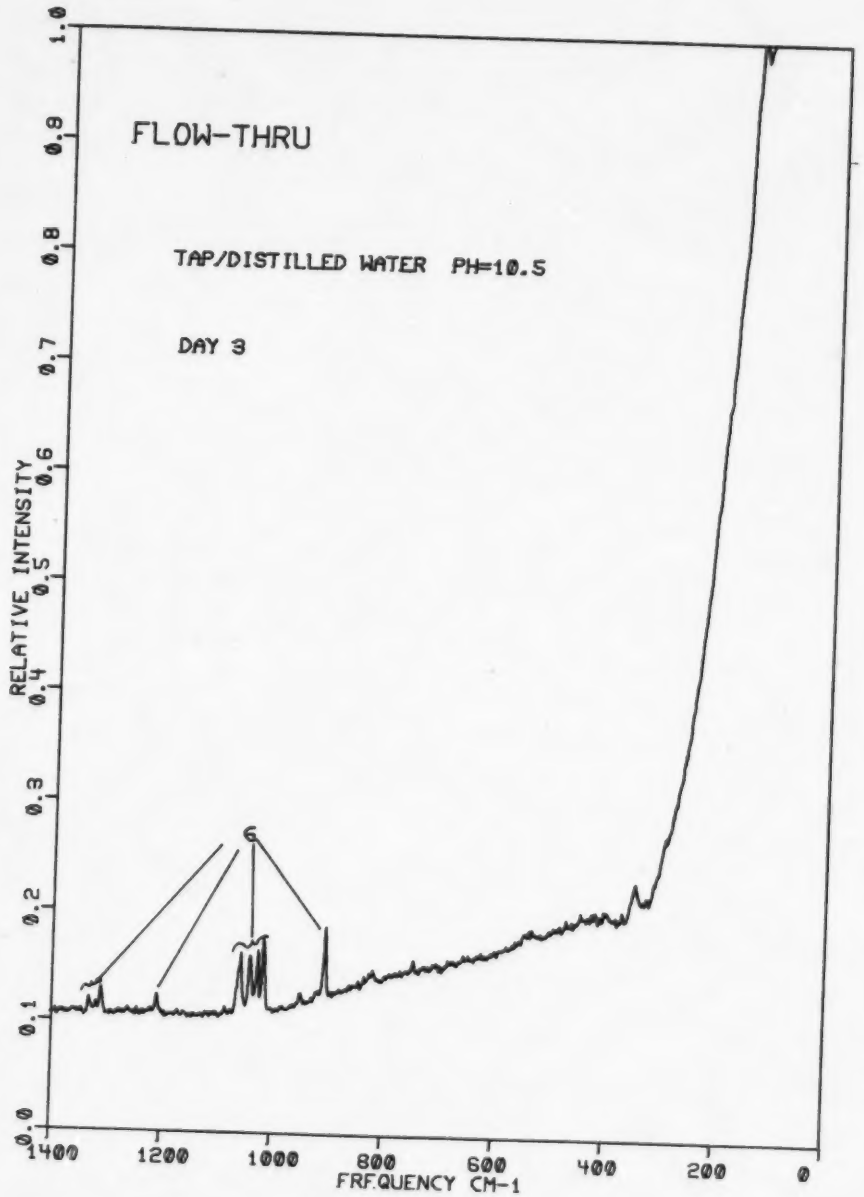

Figure 44. Raman spectrum of electrode surface in experiment 4, day 3, pH = 10.5 (G = peak due to grating ghosts).

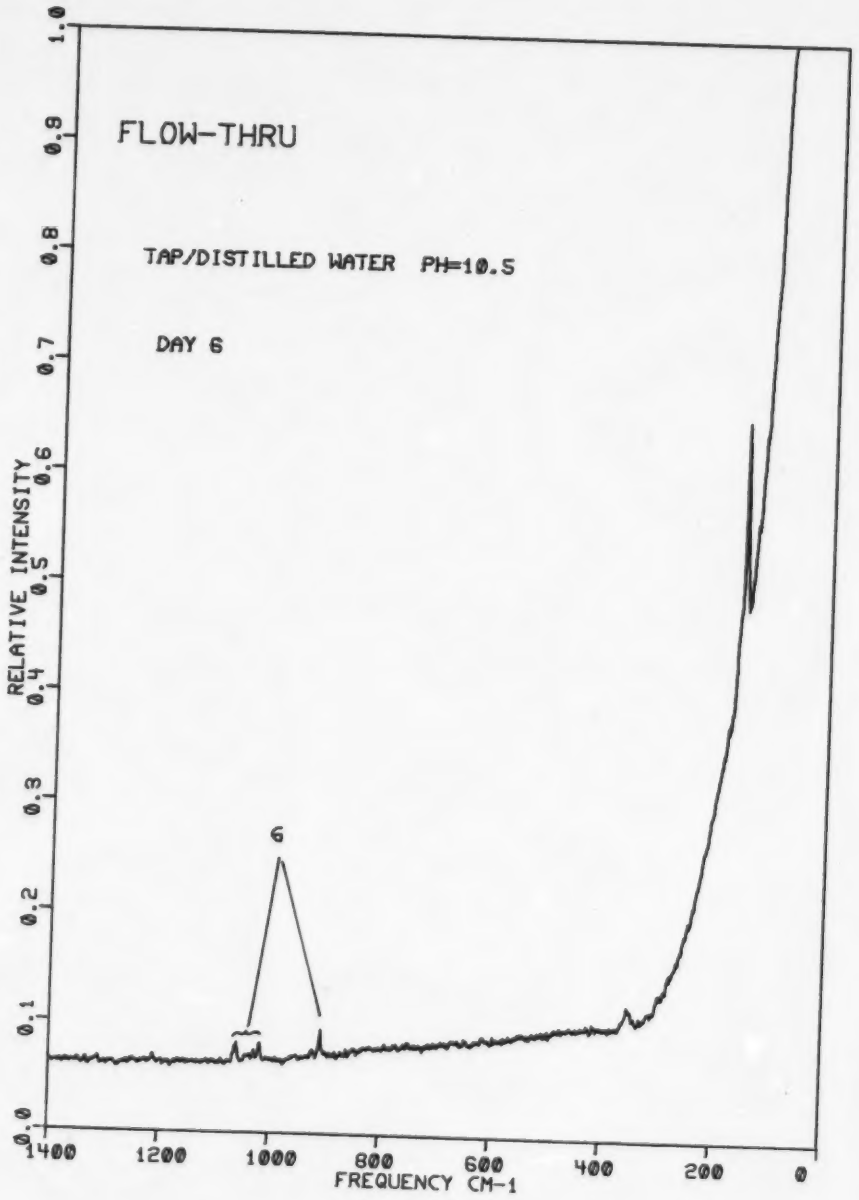

Figure 45. Raman spectrum of electrode surface in experiment 4, day 6, pH = 10.5 (G = grating ghosts).

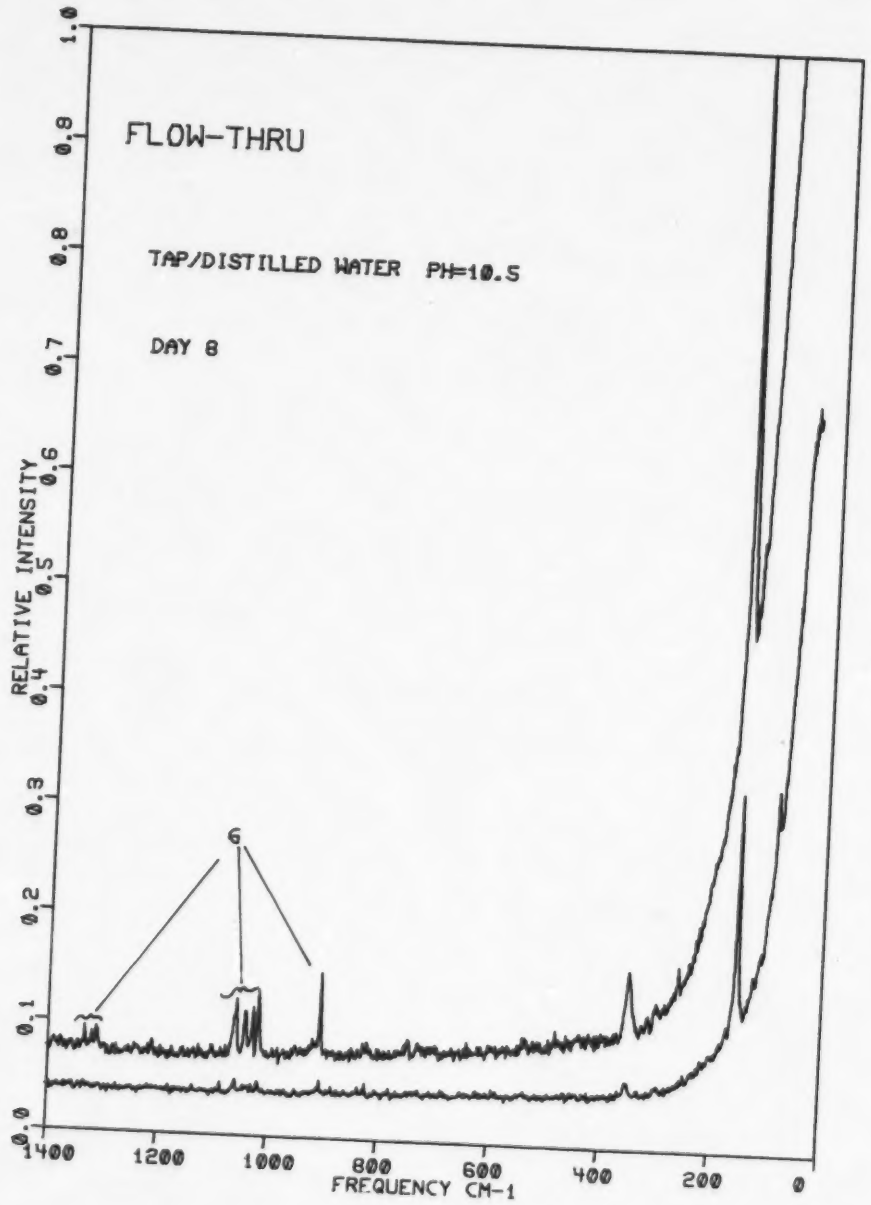

Figure 46. Raman spectra of electrode surface in experiment 4, day 8, pH = 10.5 (G = grating ghosts):
Top - Measured with slot widths consistent with previous spectra.
Bottom - Slit width cut by 1/3 to bring low frequency bands on scale.

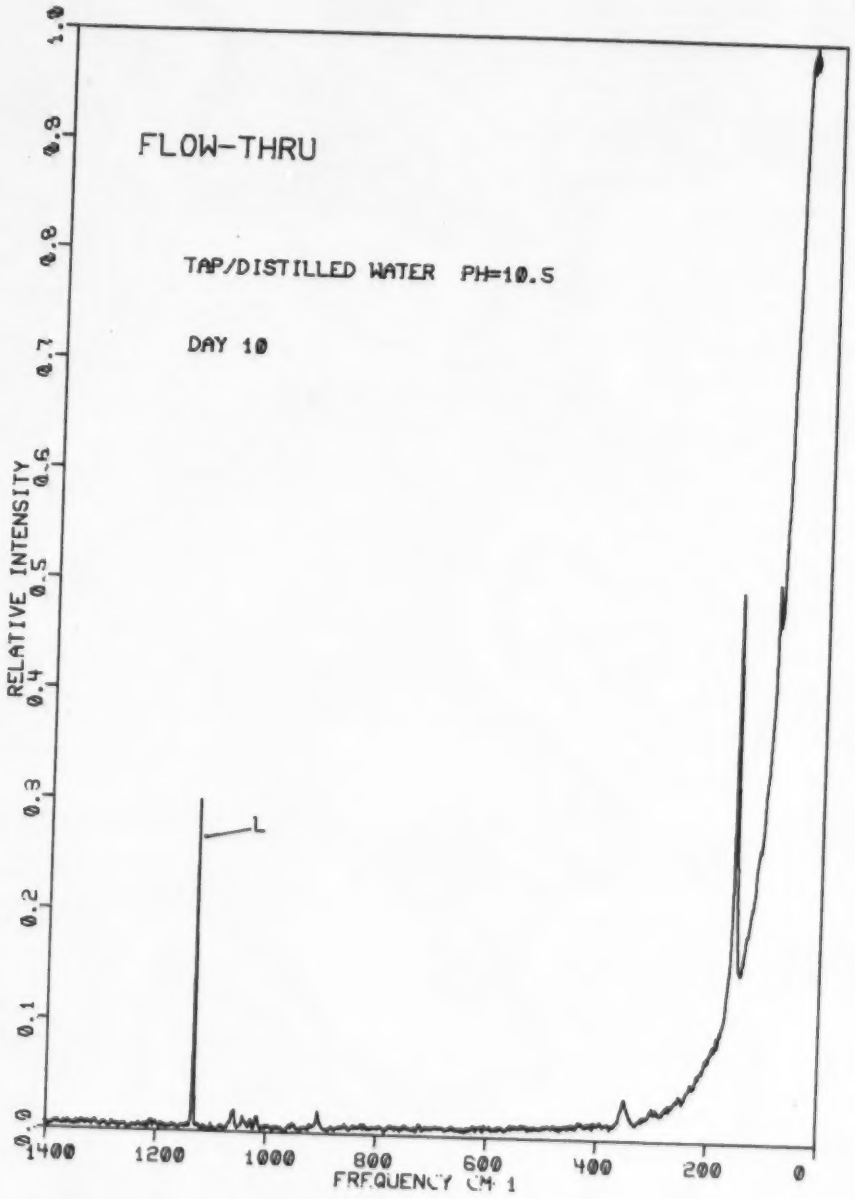

Figure 47. Raman spectrum of electrode surface, experiment 4, day 10, pH = 10.5 (L = room lights).

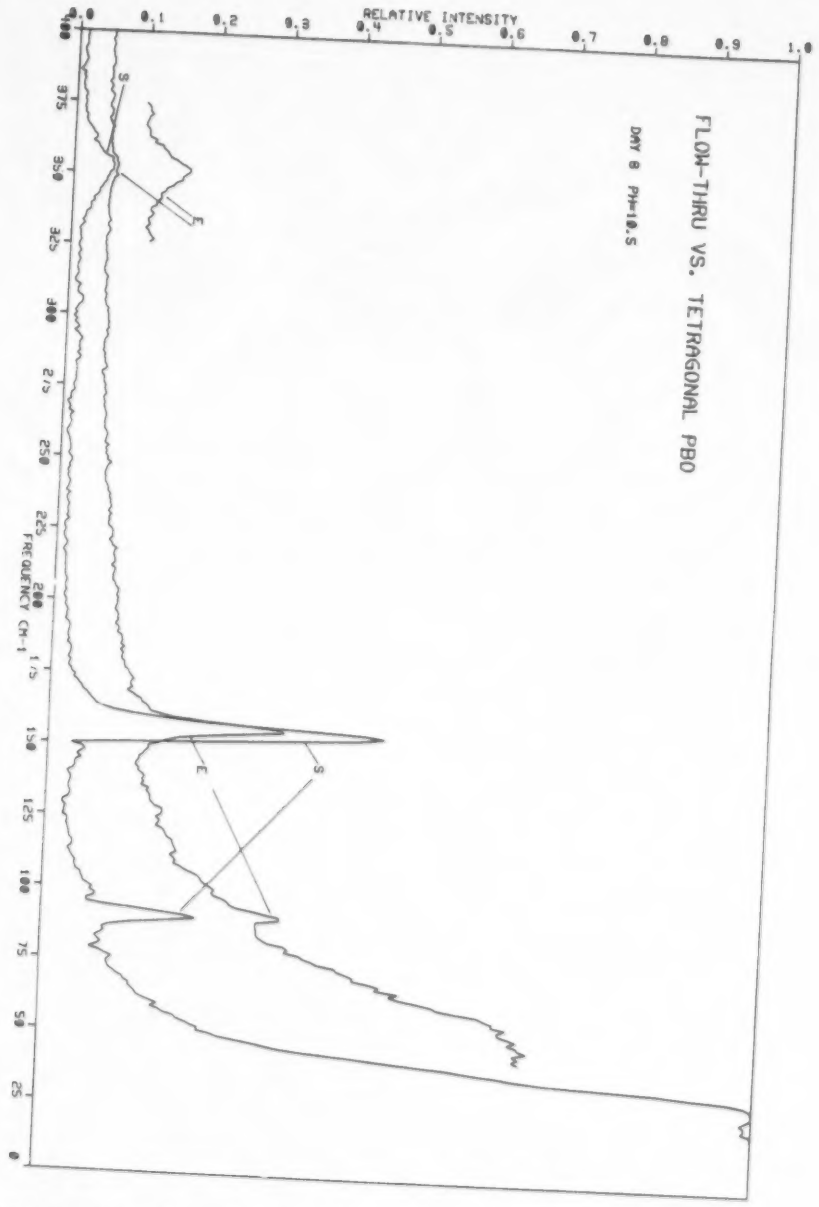

Figure 48. Raman spectra (expanded cm^{-1} axis) of:
Top - Electrode surface (E) in experiment 4, day 8, pH - 10.5.
Offset - Same electrode surface, measured with wider slits.
Bottom - Standard (S) tetragonal PbO.

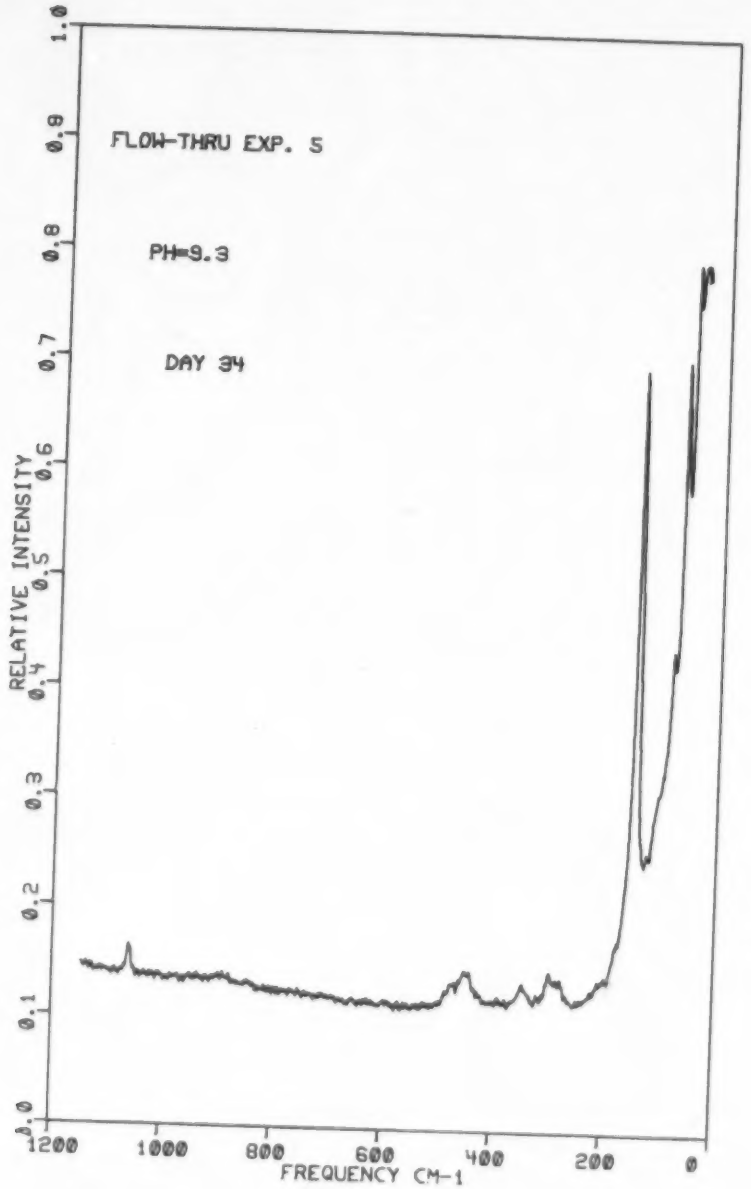

Figure 49. Raman spectrum of surface of lead pipe cell in large flow-thru tank, experiment 5, day 34.

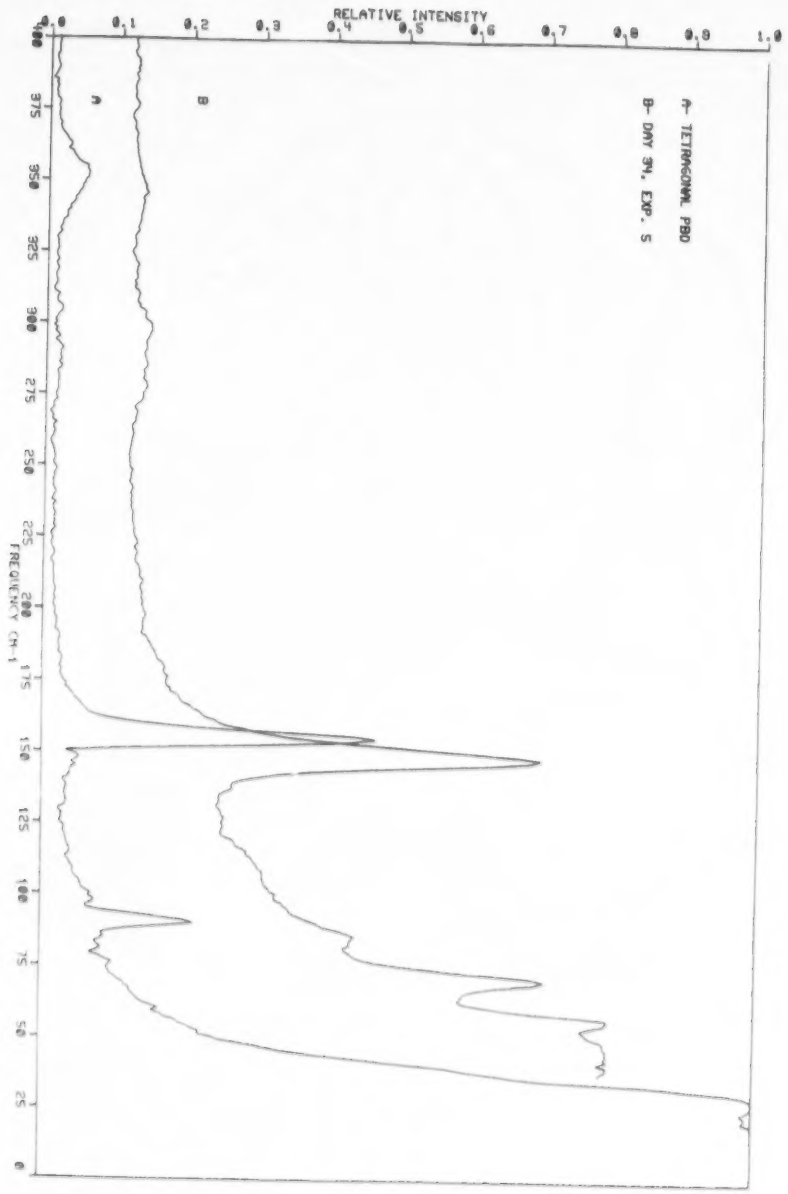

Figure 50.A. Raman spectrum of tetragonal PbO, expanded on the frequency axis.

B. Raman spectrum of surface of lead pipe from large flow-thru system expanded on frequency axis.

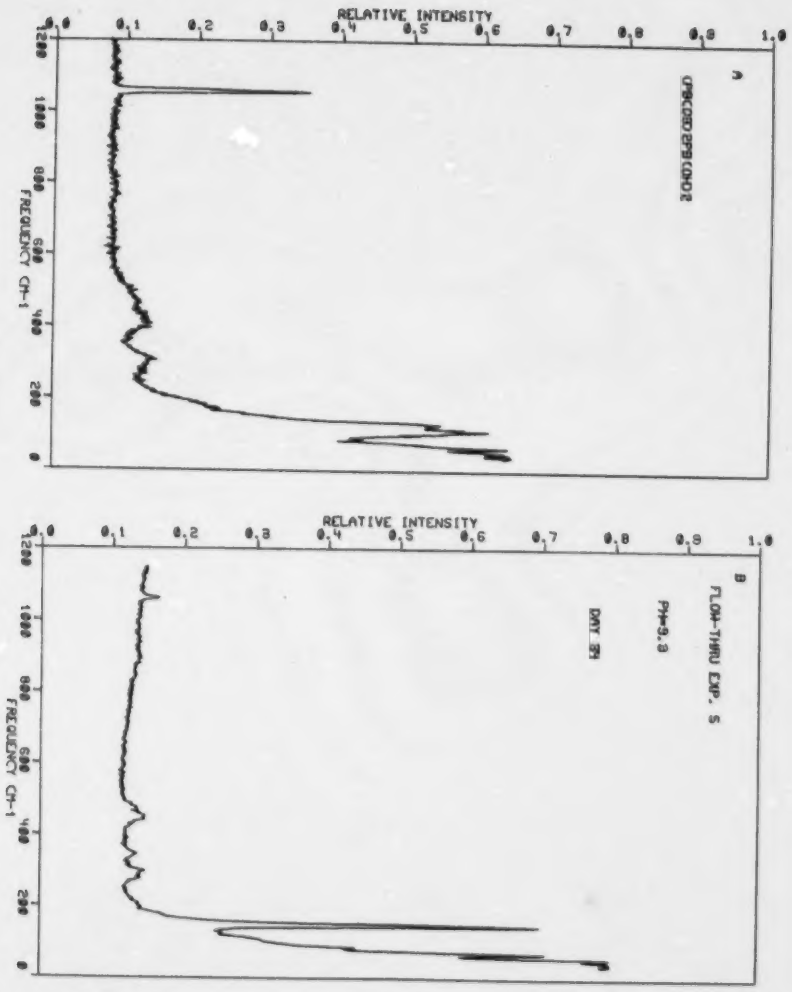

51.A. Reference Raman spectrum of lead carbonate.
B. Raman spectrum of surface of lead pipe from experiment 5.

Figure 52. Raman spectrum of surface of lead electrode after day 12 in experiment 6.

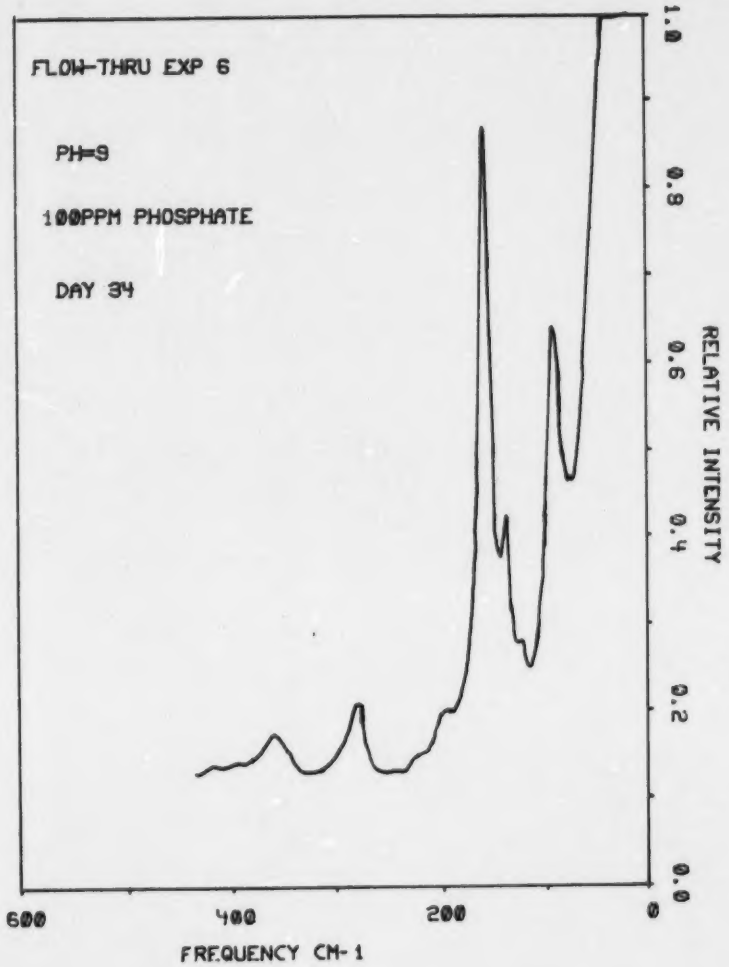

Figure 53. Raman spectrum of surface of lead electrode on day 34 of experiment 6.

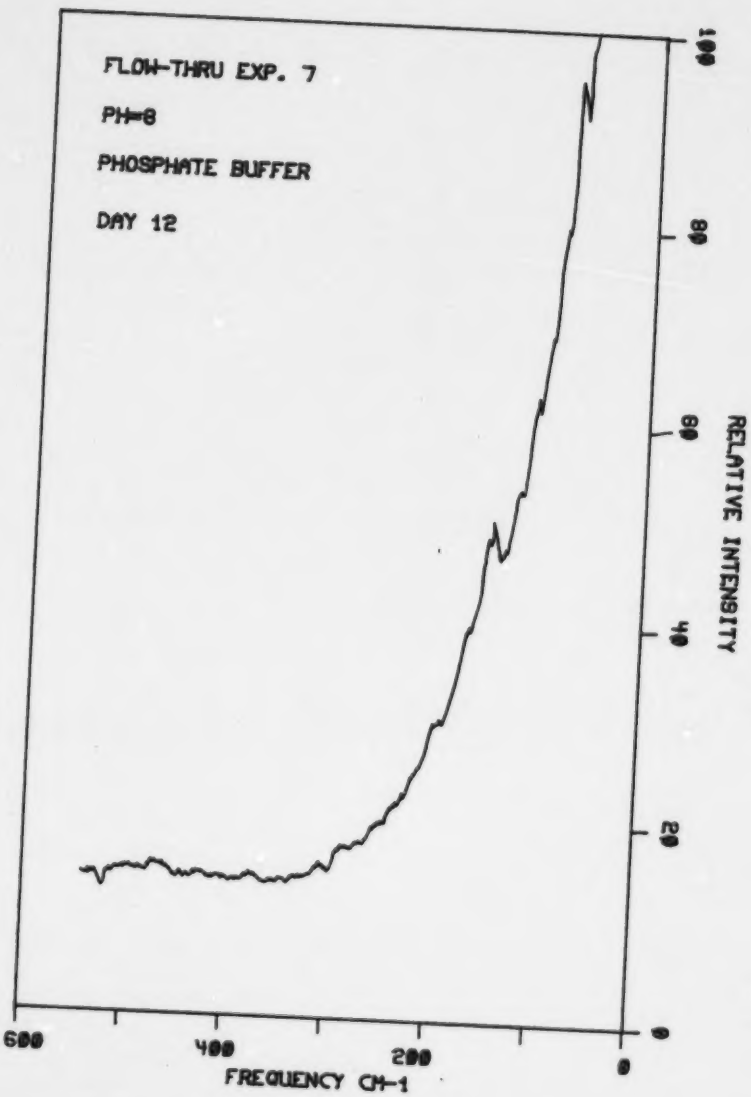

Figure 54. Raman spectrum of surface of lead electrode after day 12 in experiment 7.

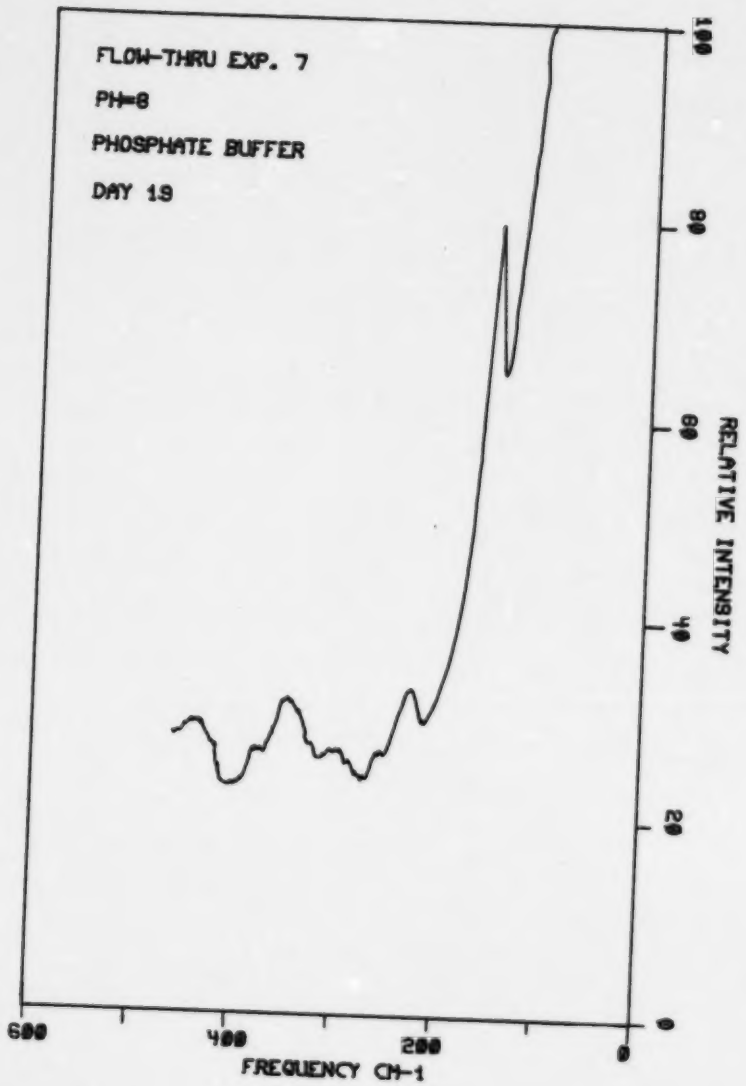

Figure 55. Raman spectrum of surface of lead electrode after day 19 in experiment 7.

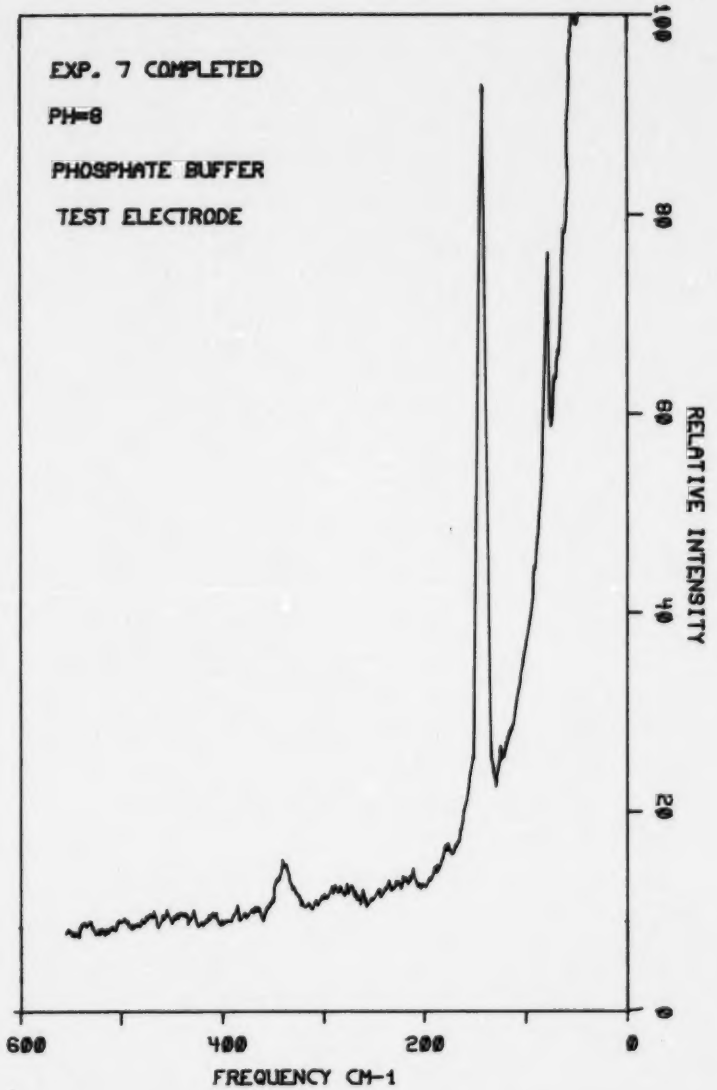

Figure 56. Raman spectrum of surface of the test lead electrode after experiment 7 was completed.

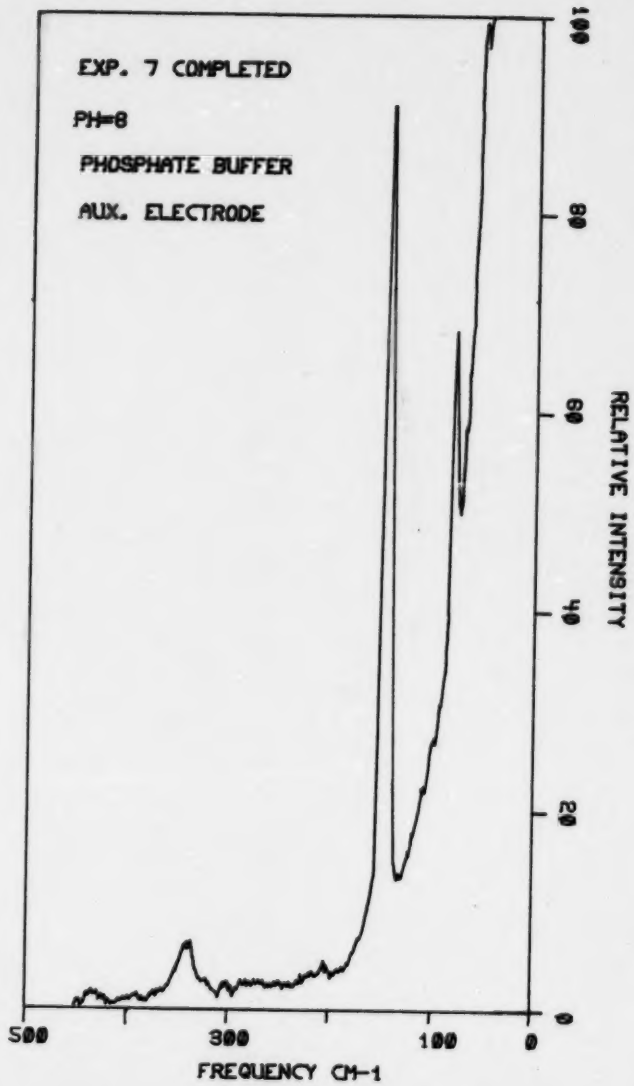

Figure 57. Raman spectrum of surface of the auxiliary lead electrode after experiment 7 was completed.

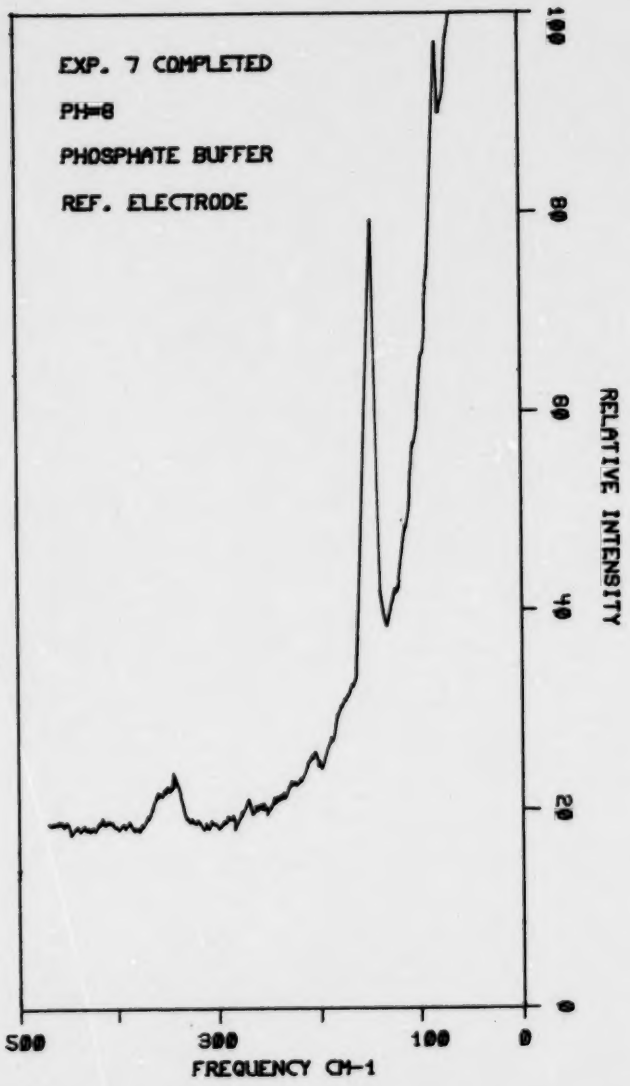

Figure 58. Raman spectrum of the reference lead electrode after experiment 7 was completed.

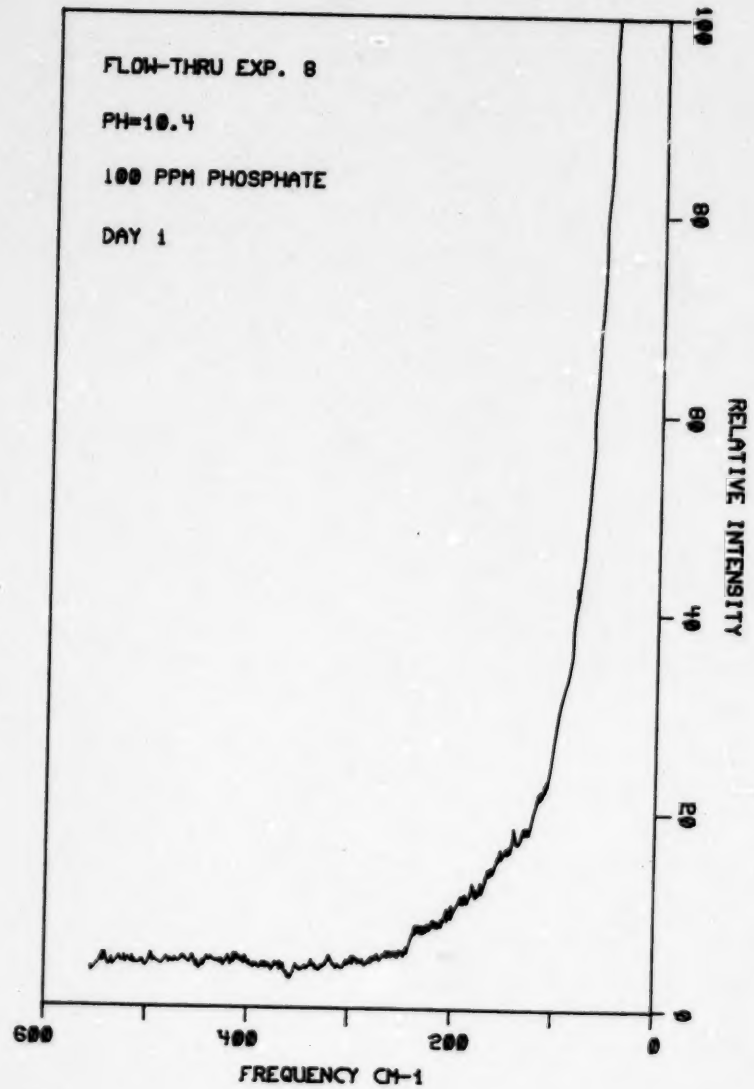

Figure 59. Raman spectrum of surface of lead electrode after day 1 in experiment 8.

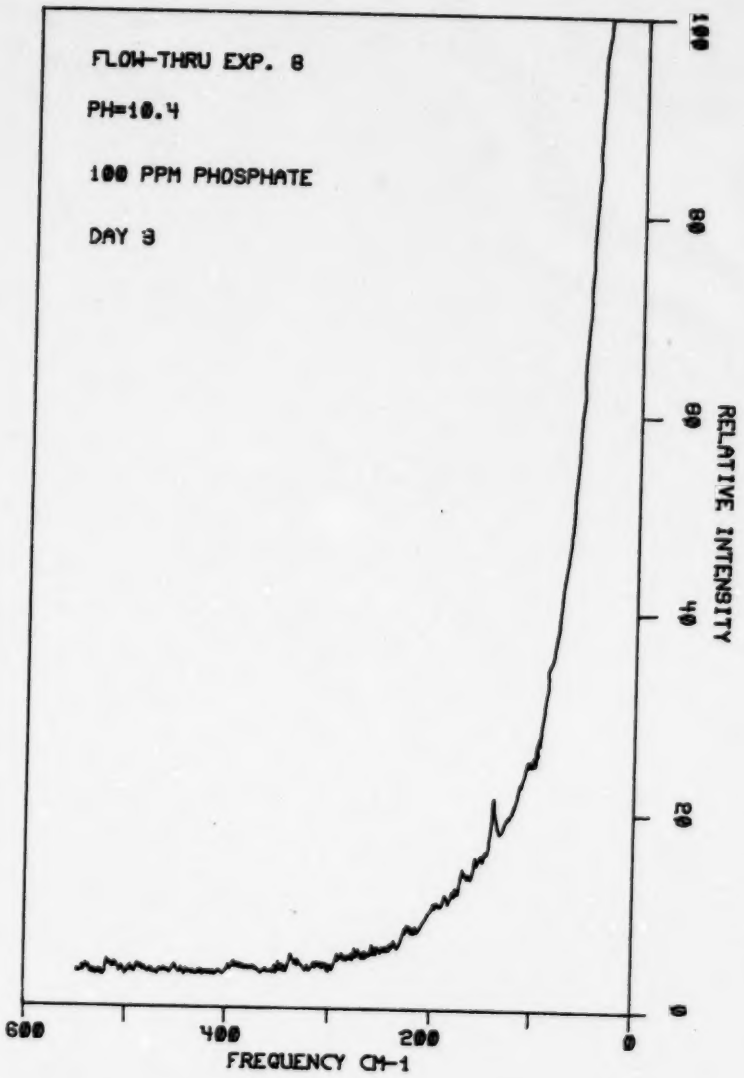

Figure 60. Raman spectrum of surface of lead electrode after day 3 in experiment 8.

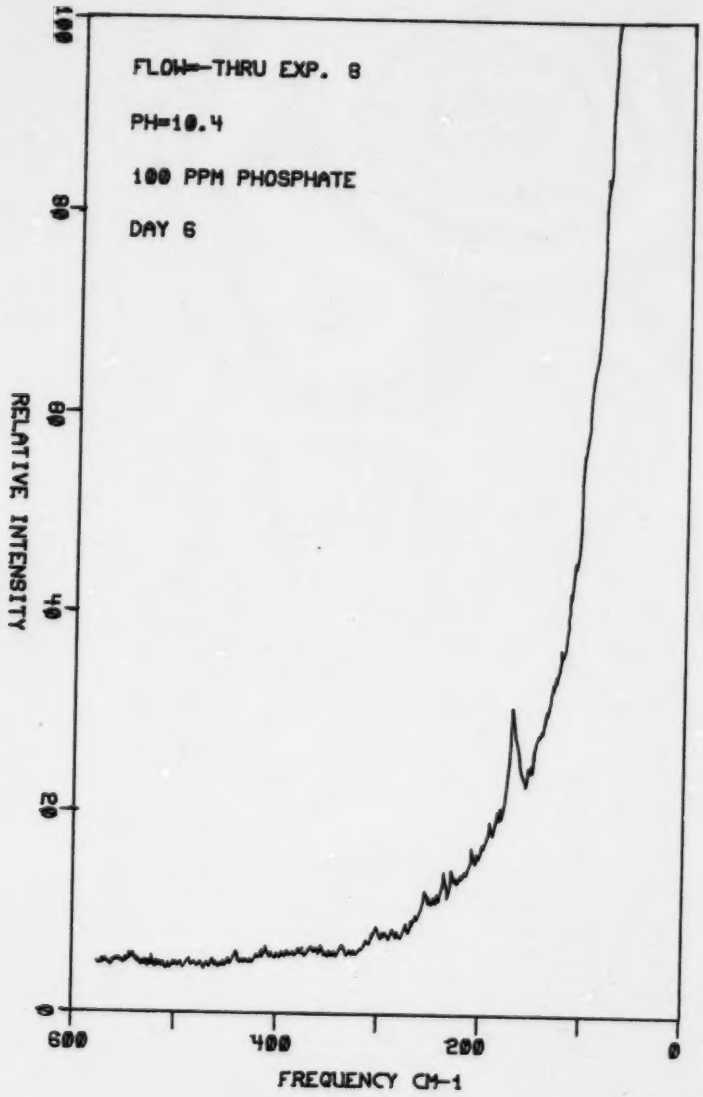

Figure 61. Raman spectrum of surface of lead electrode after day 6 in experiment 8.

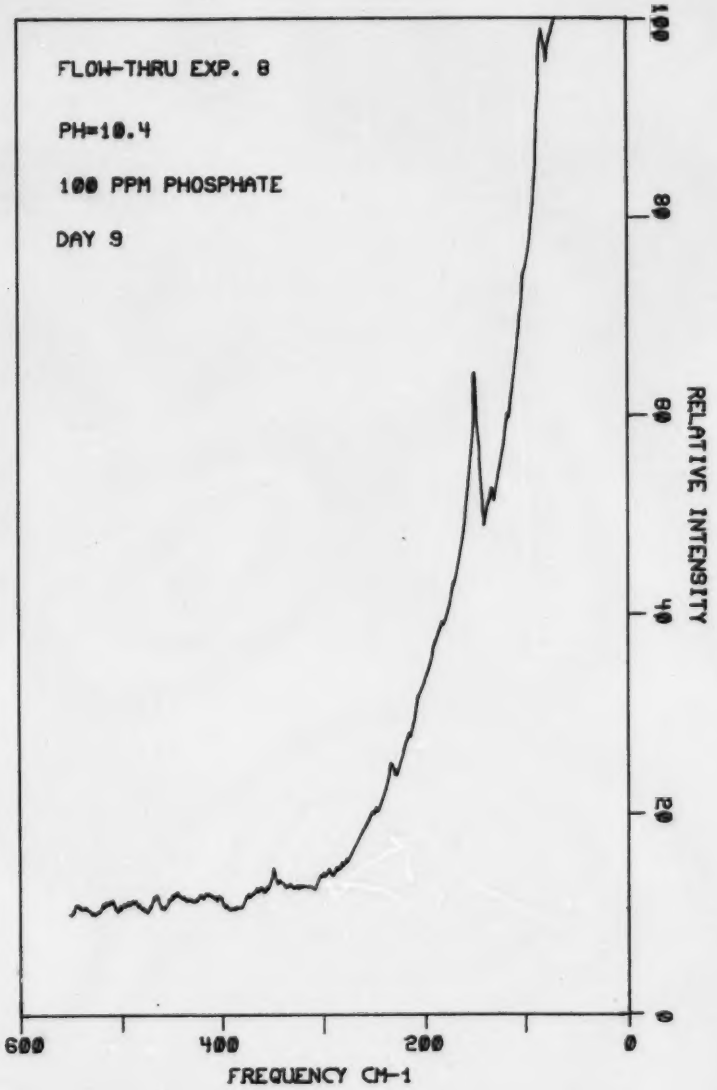

Figure 62. Raman spectrum of surface of lead electrode after day 9 in experiment 8.

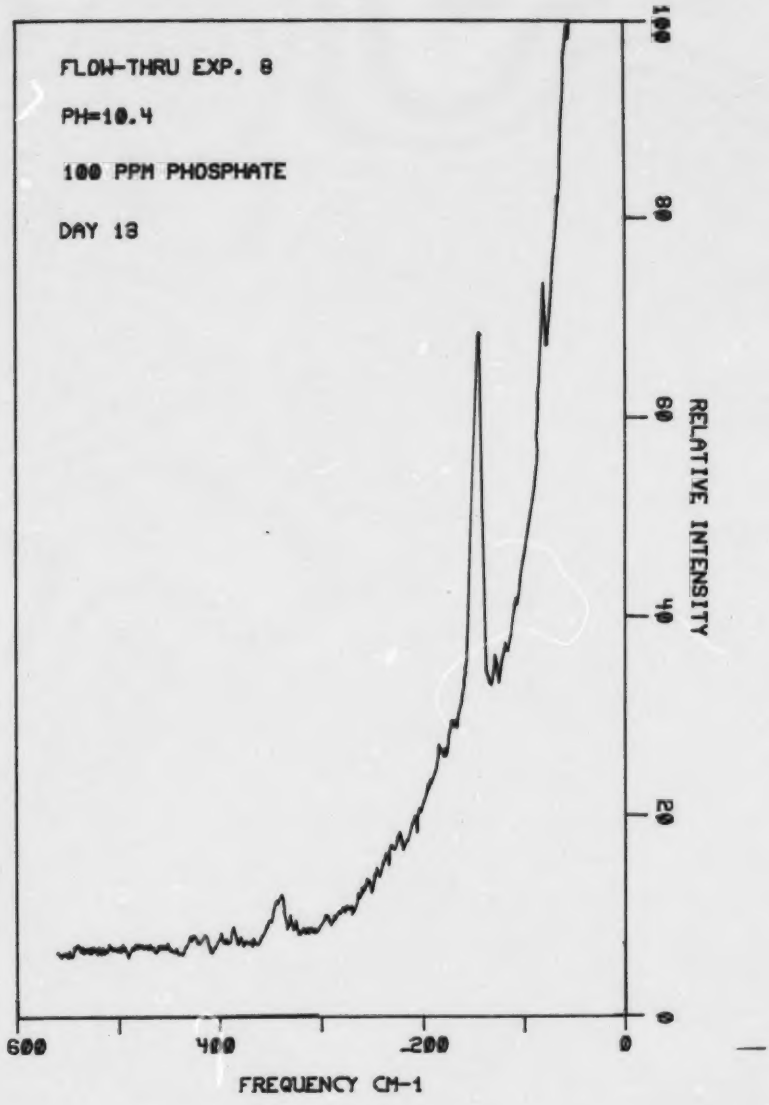

Figure 63. Raman spectrum of surface of lead electrode after day 13 in experiment 8.

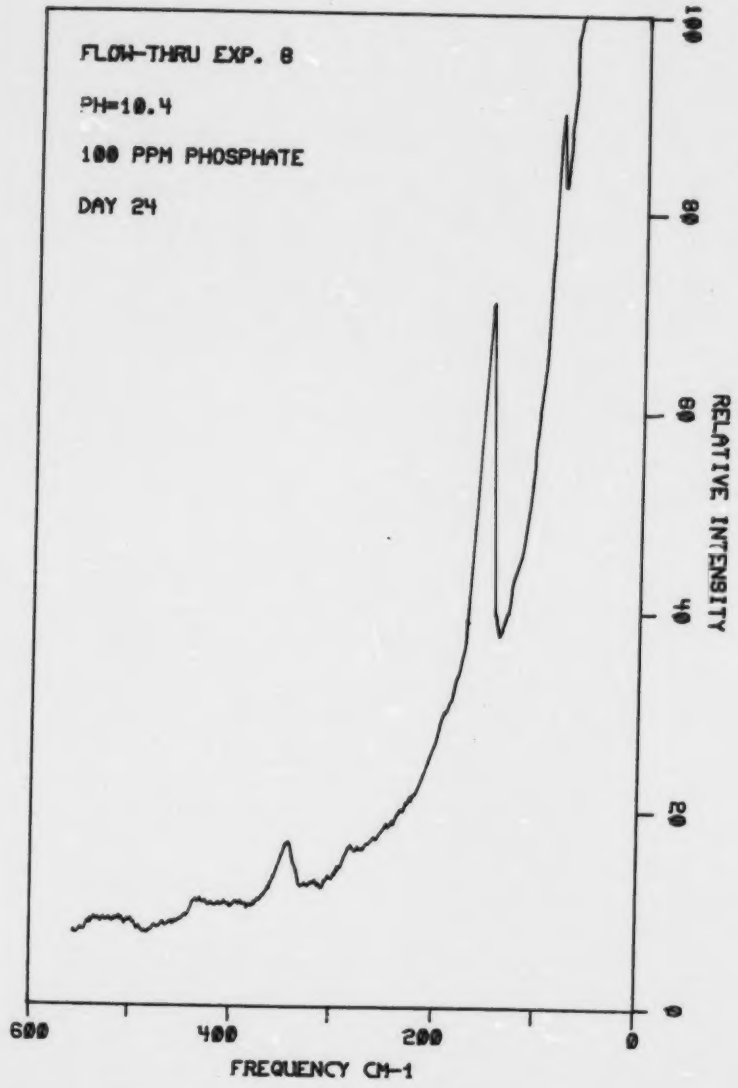

Figure 64. Raman spectrum of surface of lead electrode after day 24 in experiment 8.

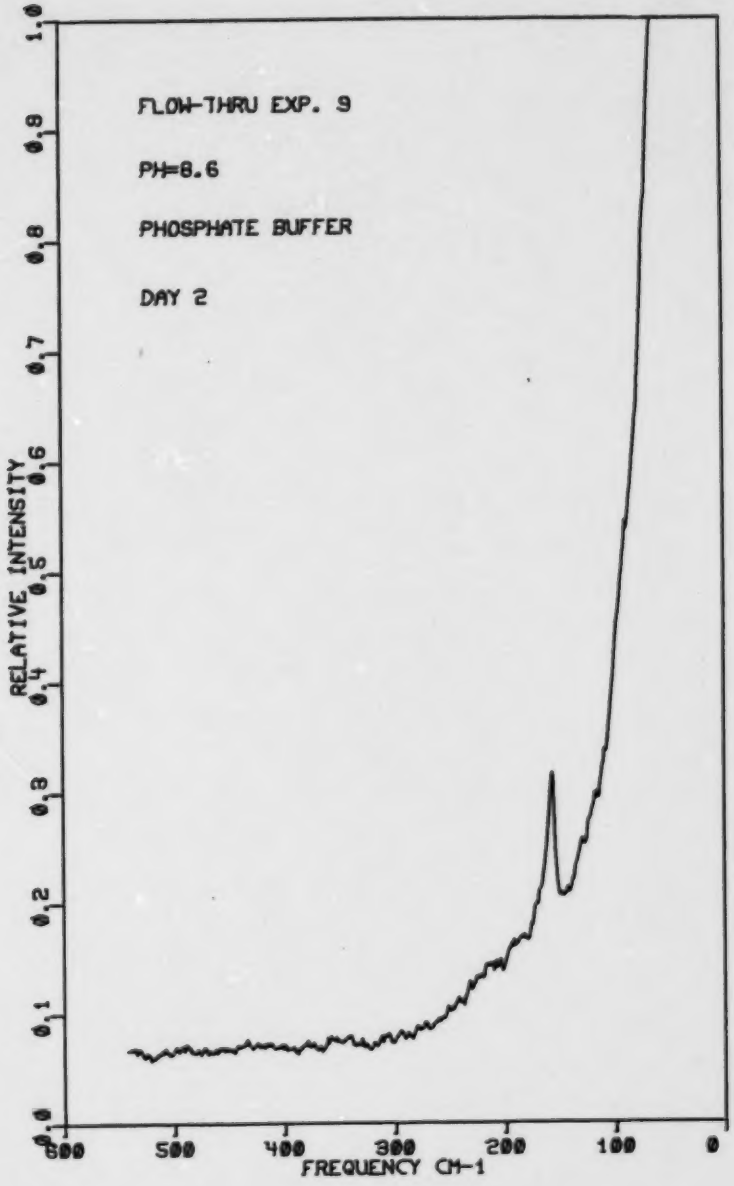

Figure 65. Raman spectrum of surface of lead electrode after day 2 in experiment 9.

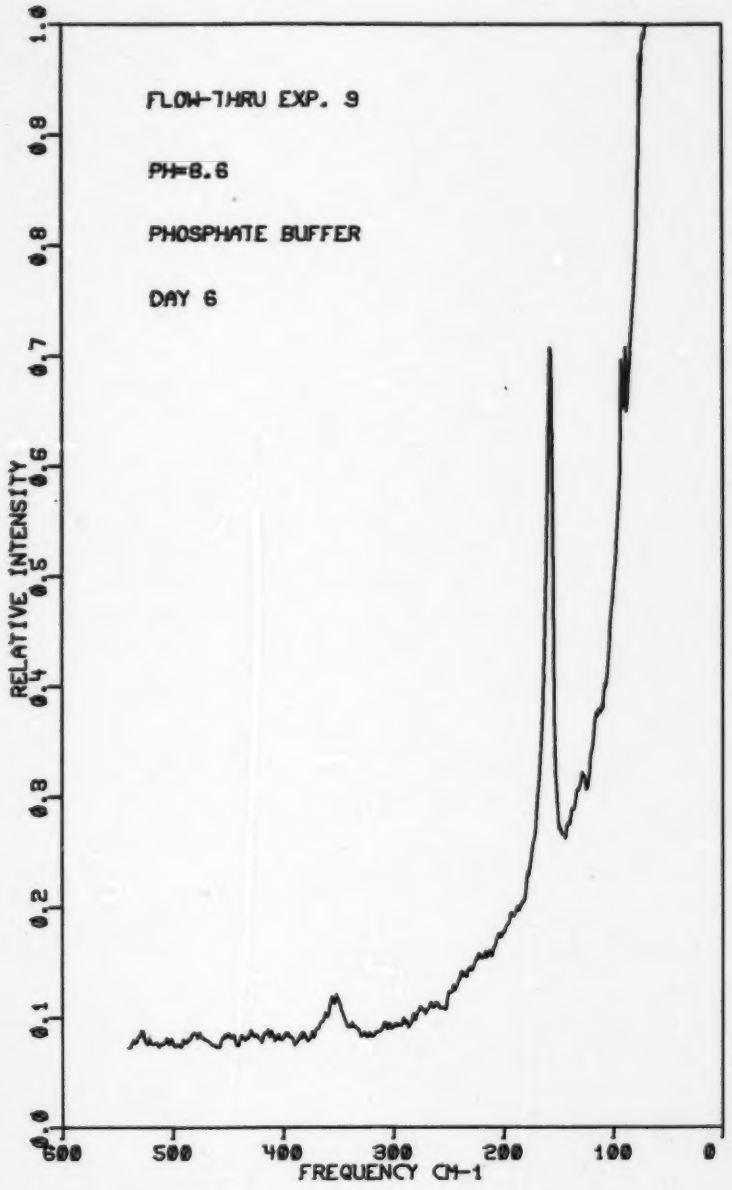

Figure 66. Raman spectrum of surface of lead electrode after day 6 in experiment 9.

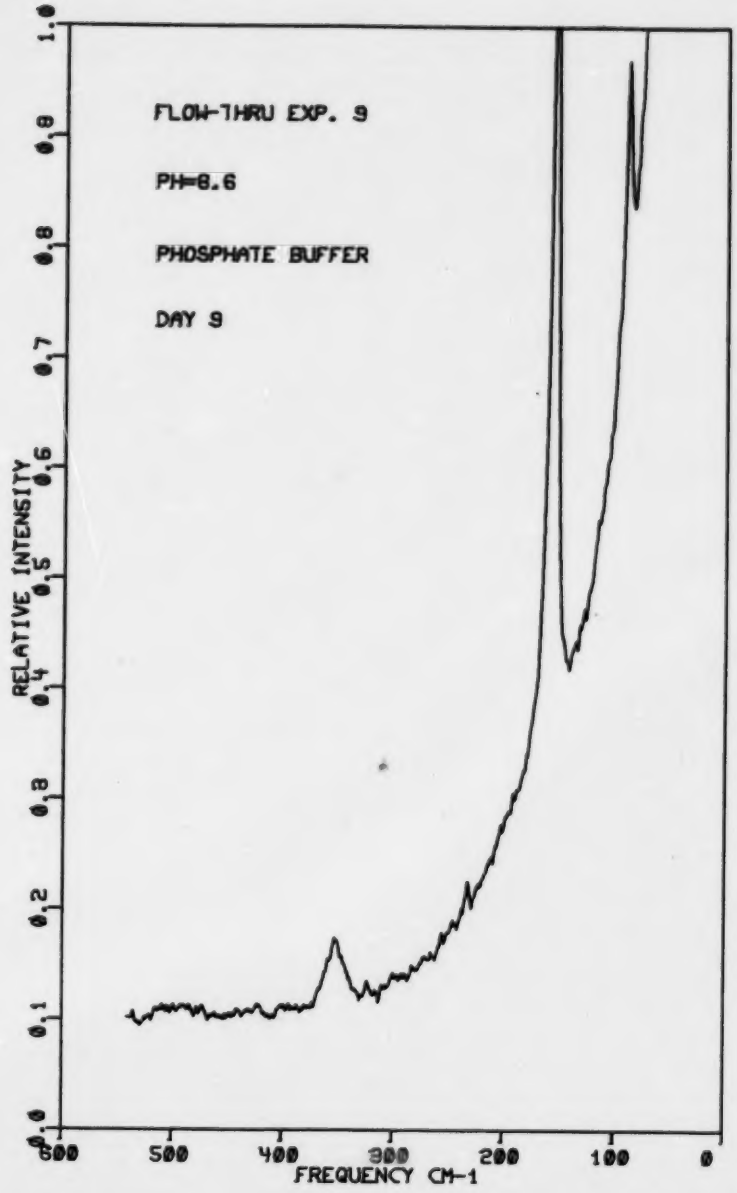

Figure 67. Raman spectrum of surface of lead electrode after day 9 in experiment 9.

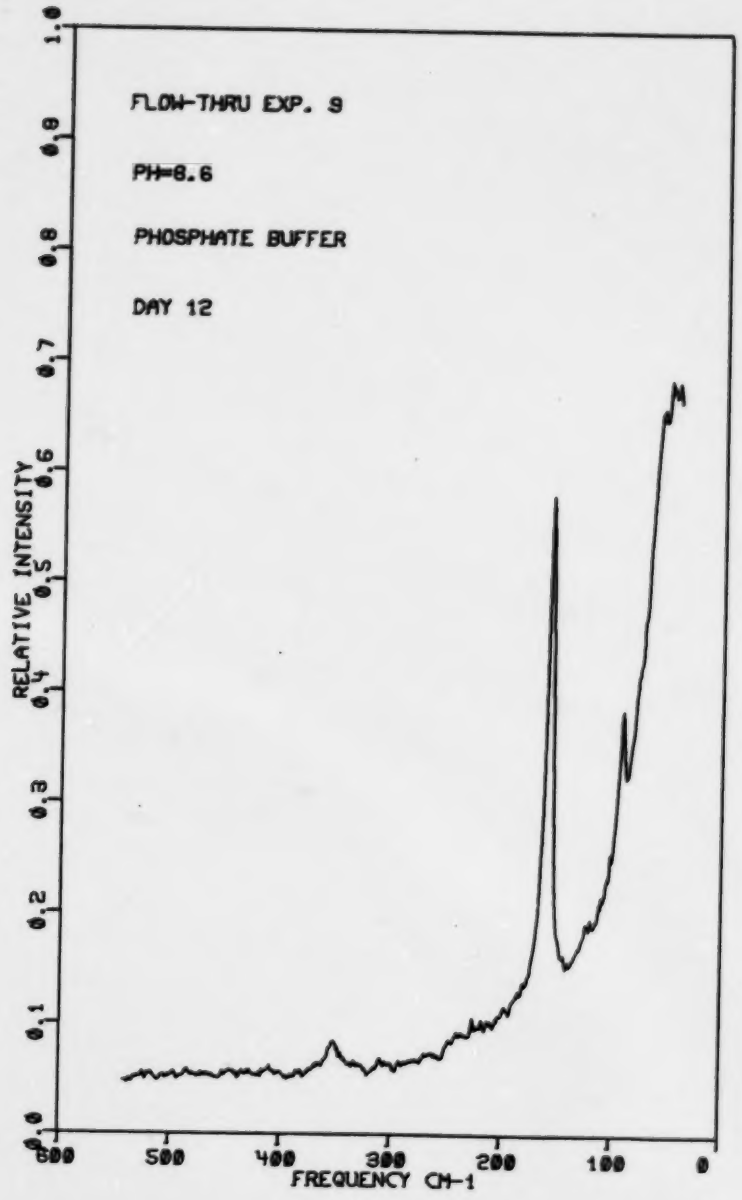

Figure 68. Raman spectrum of surface of lead electrode after day 12 in experiment 9.

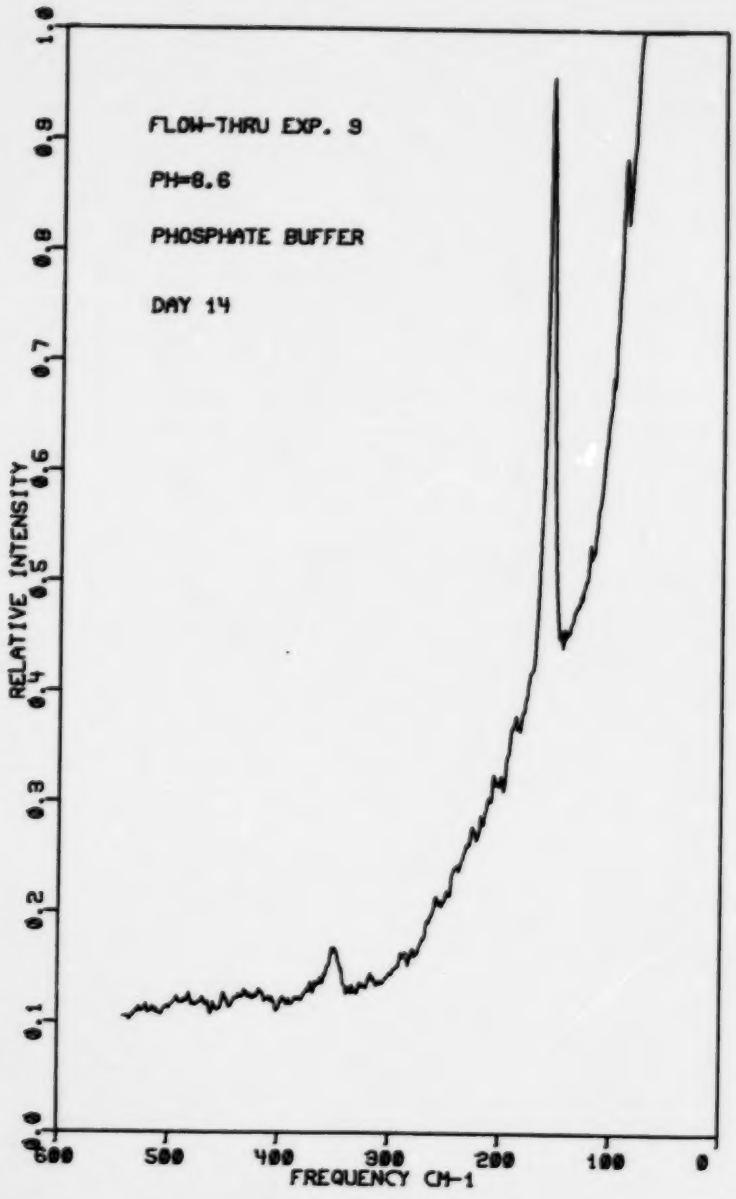

Figure 69. Raman spectrum of surface of lead electrode after day 14 in experiment 9.

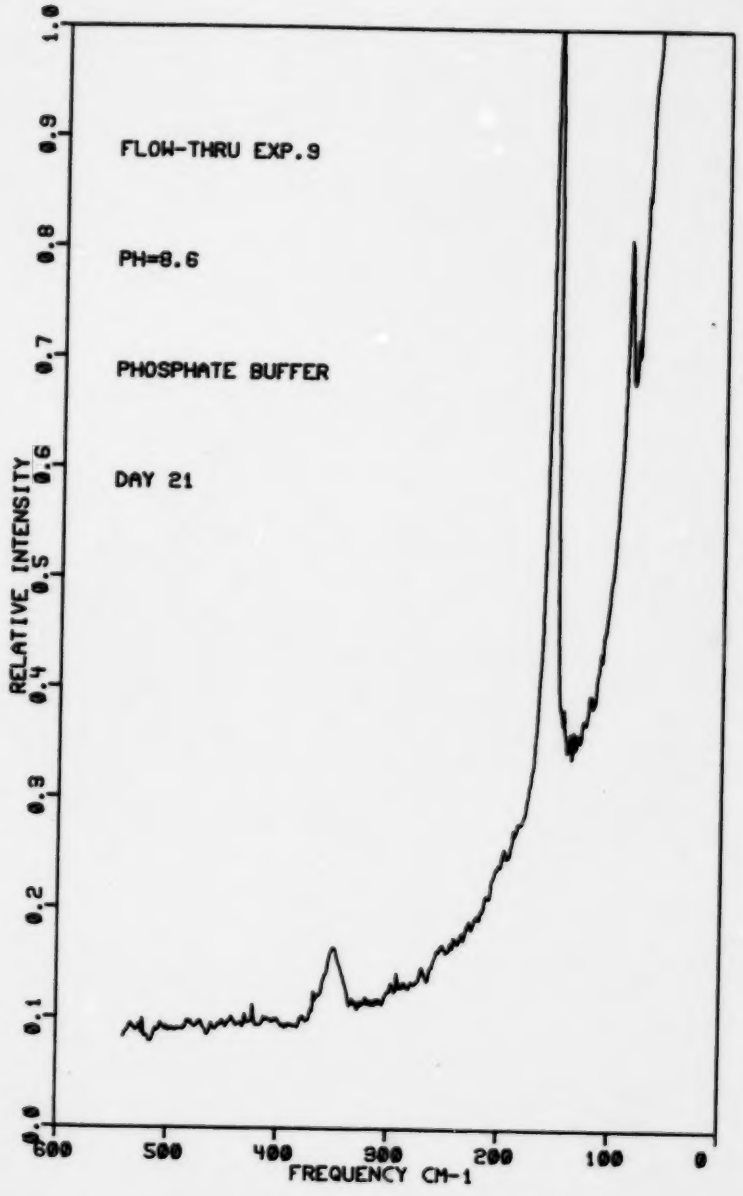

Figure 70. Raman spectrum of surface of lead electrode after day 21 in experiment 9.

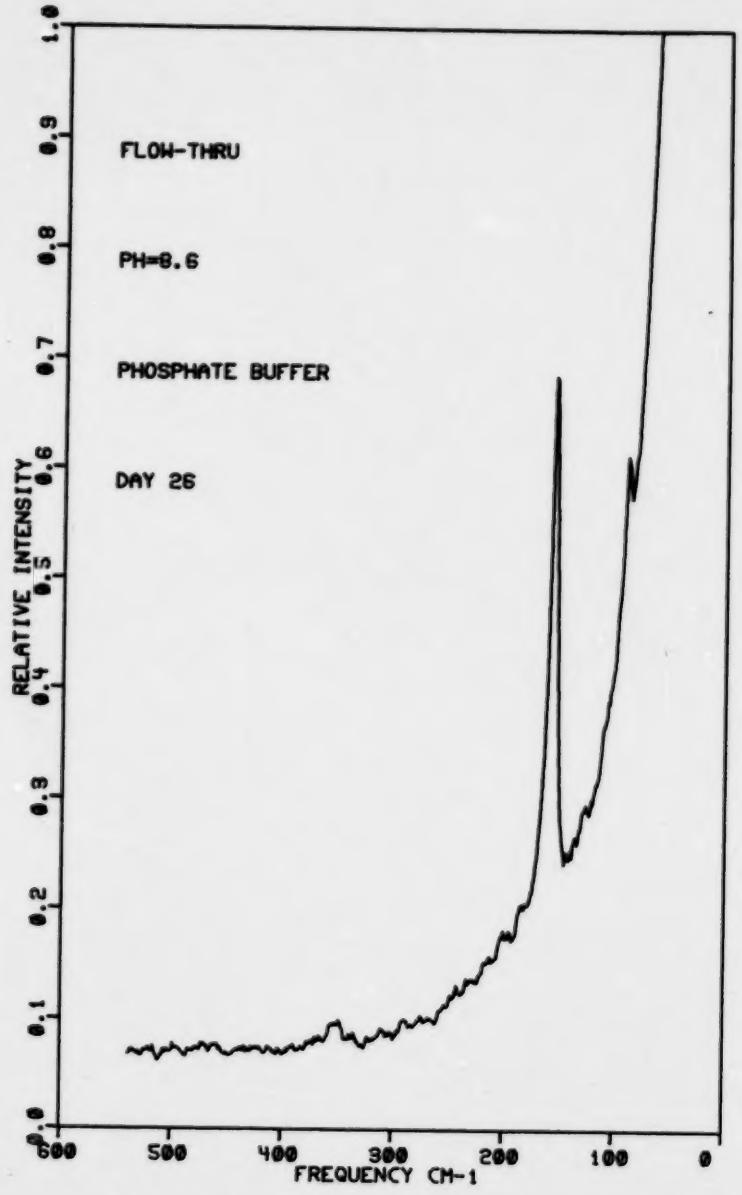

Figure 71. Raman spectrum of surface of lead electrode after day 26 in experiment 9.

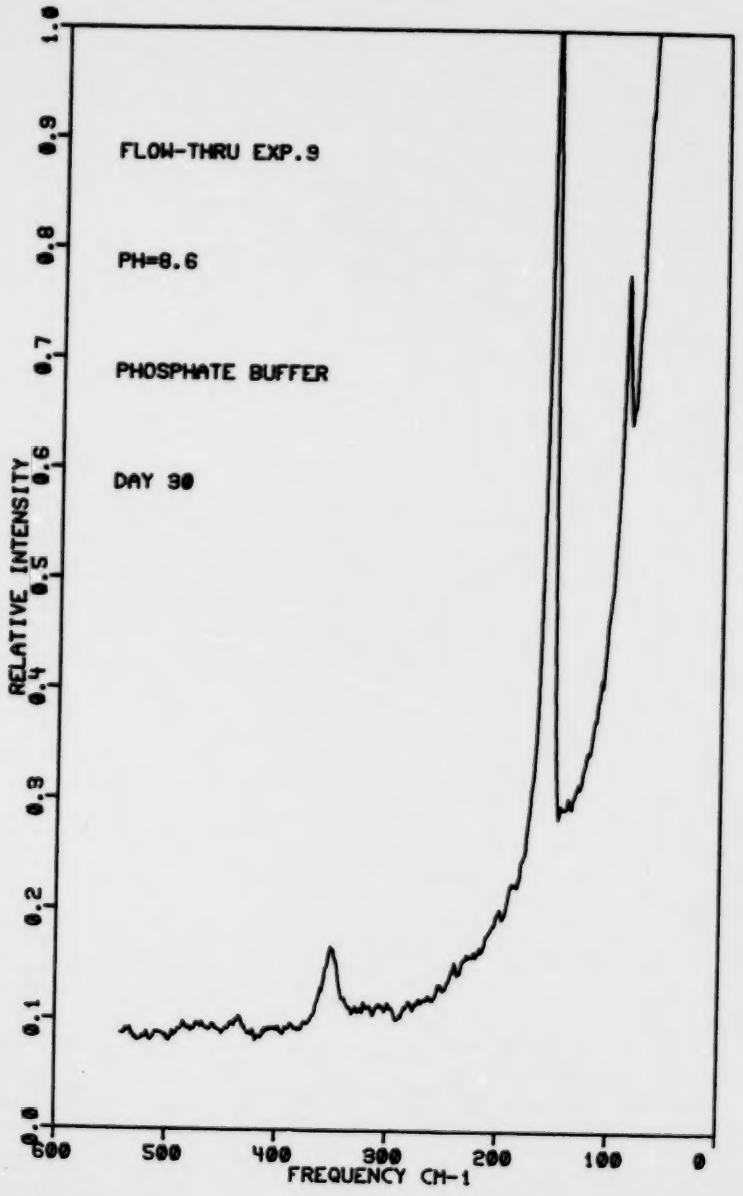

Figure 72. Raman spectrum of surface of lead electrode after day 30 in experiment 9.

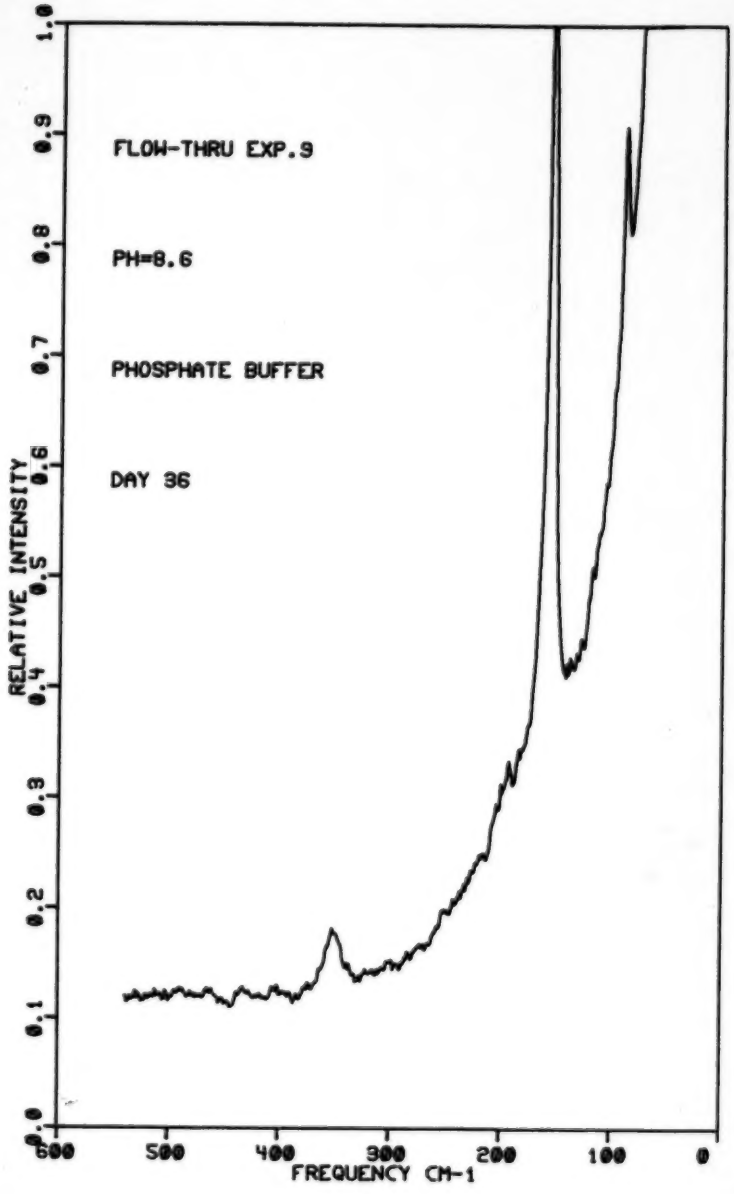

Figure 73. Raman spectrum of surface of lead electrode after day 36 in experiment 9.

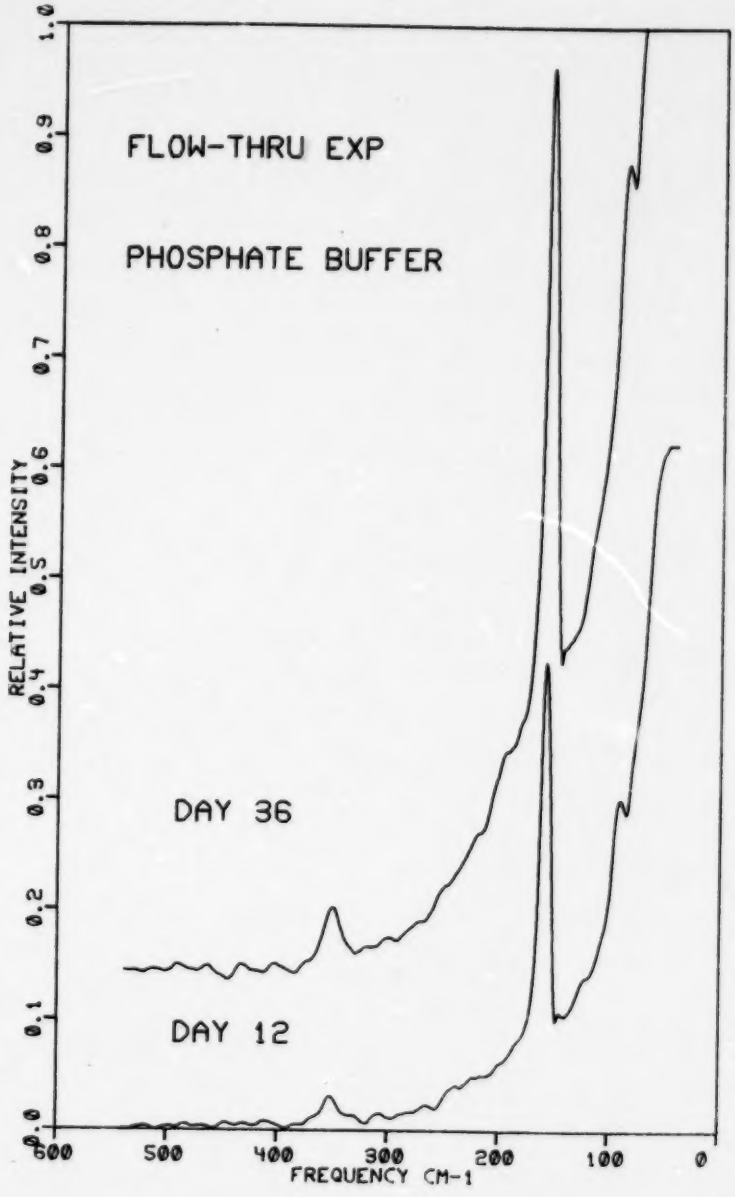

Figure 74. Comparison of Raman spectra from day 12 and day 36 in experiment 9.

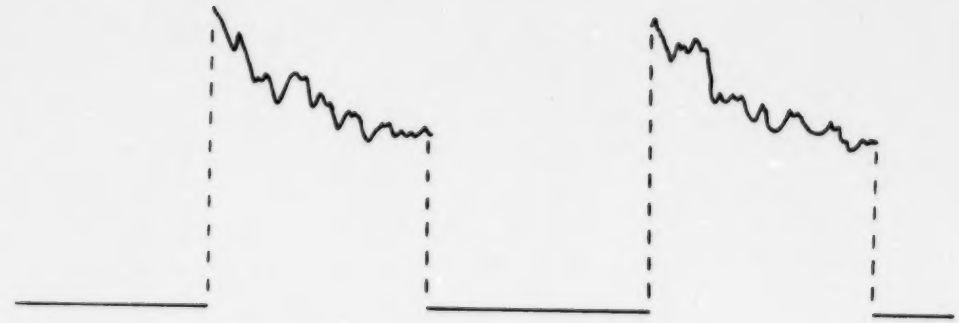

SURFACE AREA = 2 SQUARE INCHES

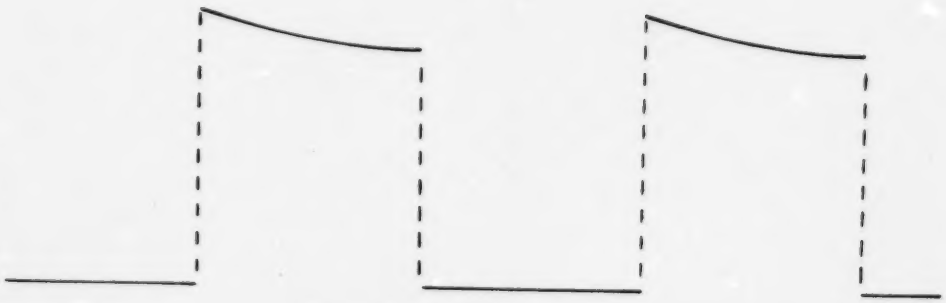

SURFACE AREA = 1 SQUARE CM

Figure 75. Enlargements of corrosion meter readings.

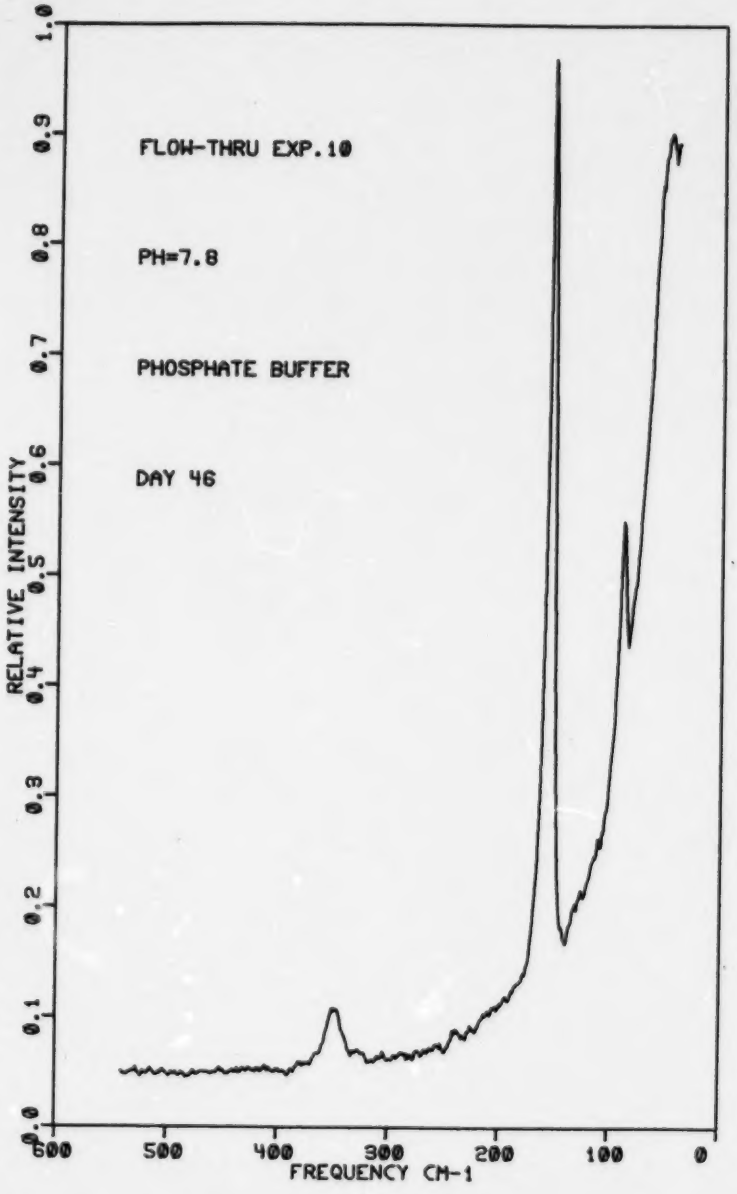

Figure 76. Raman spectrum of surface of lead electrode after day 46 in experiment 10.

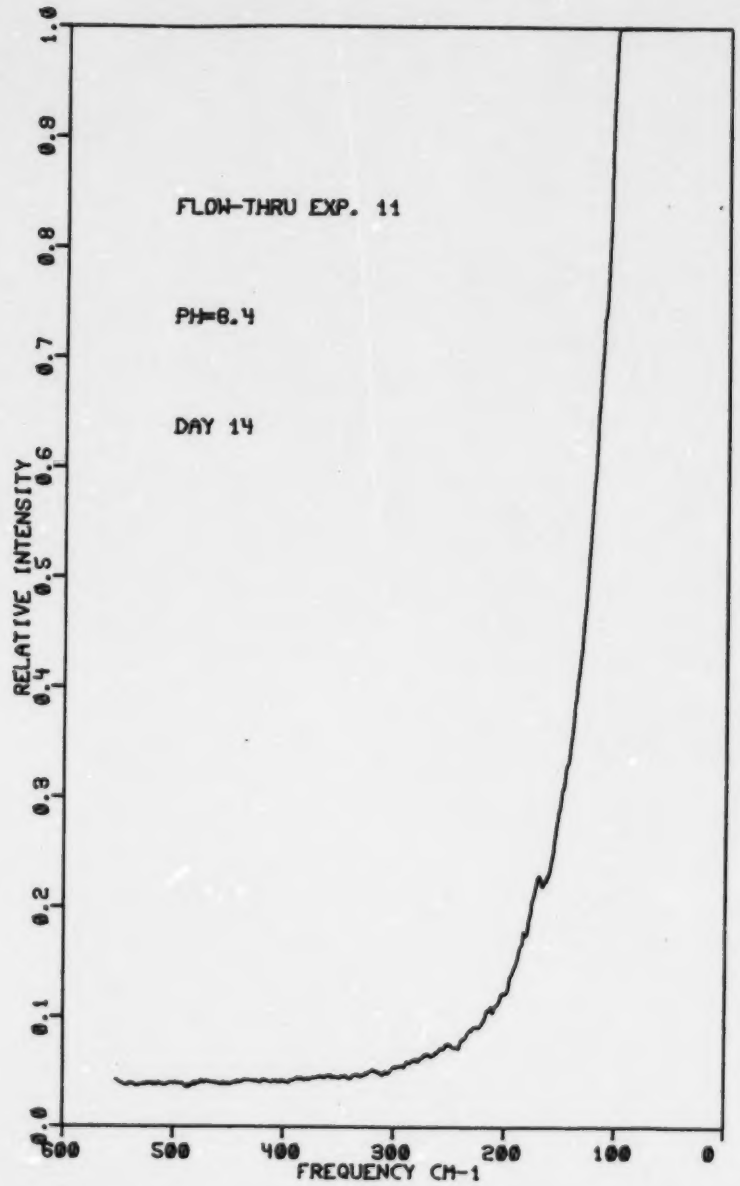

Figure 77. Raman spectrum of surface of lead electrode after day 14 in experiment 11

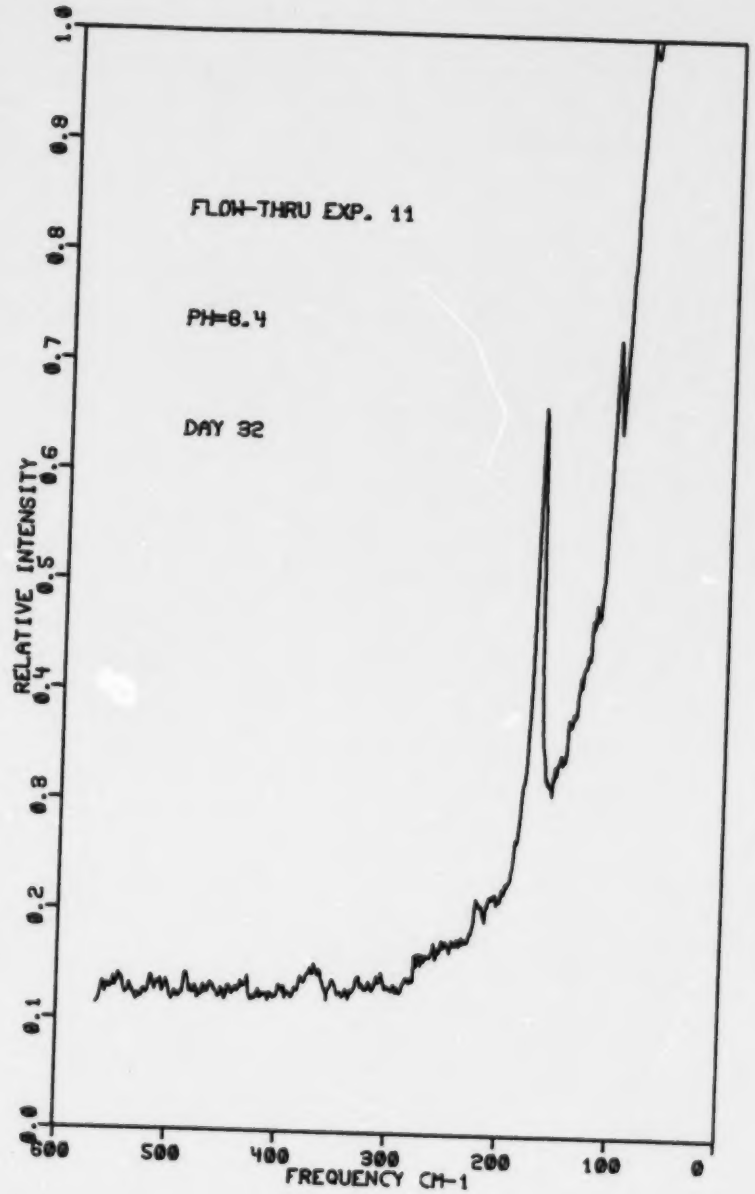

Figure 78. Raman spectrum of surface of lead electrode after day 32 in experiment 11.

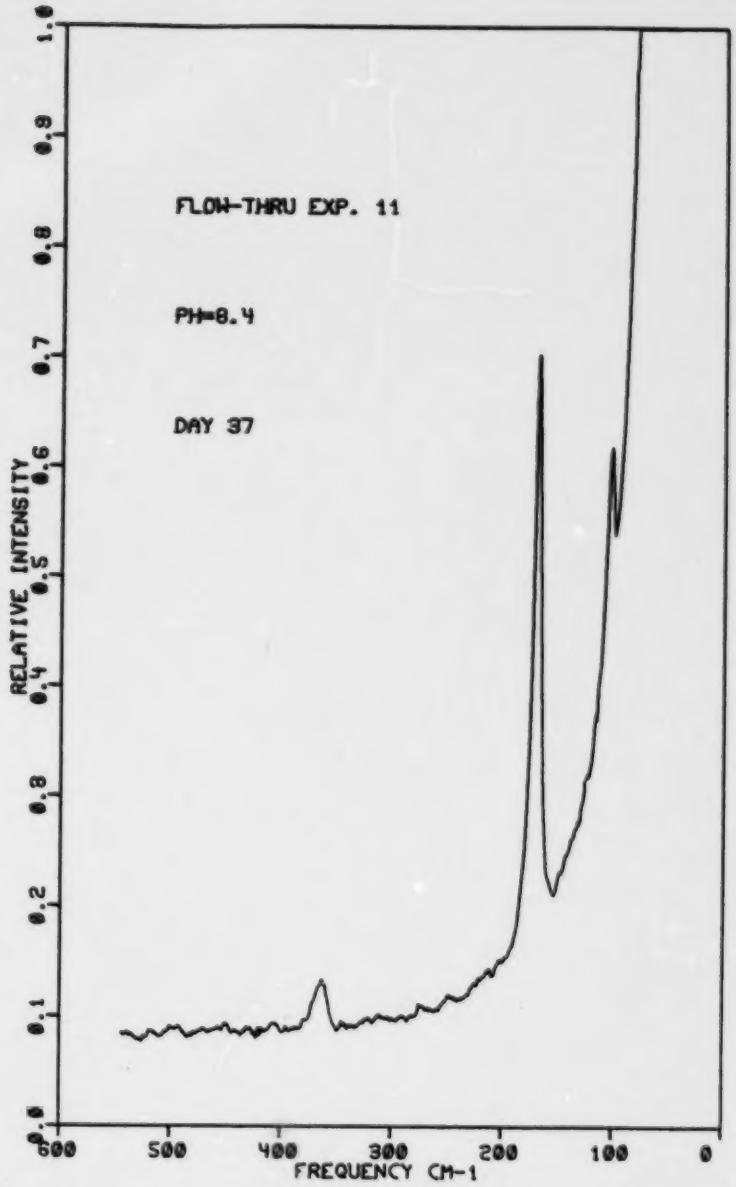

Figure 79. Raman spectrum of surface of lead electrode after day 37 in experiment 11.

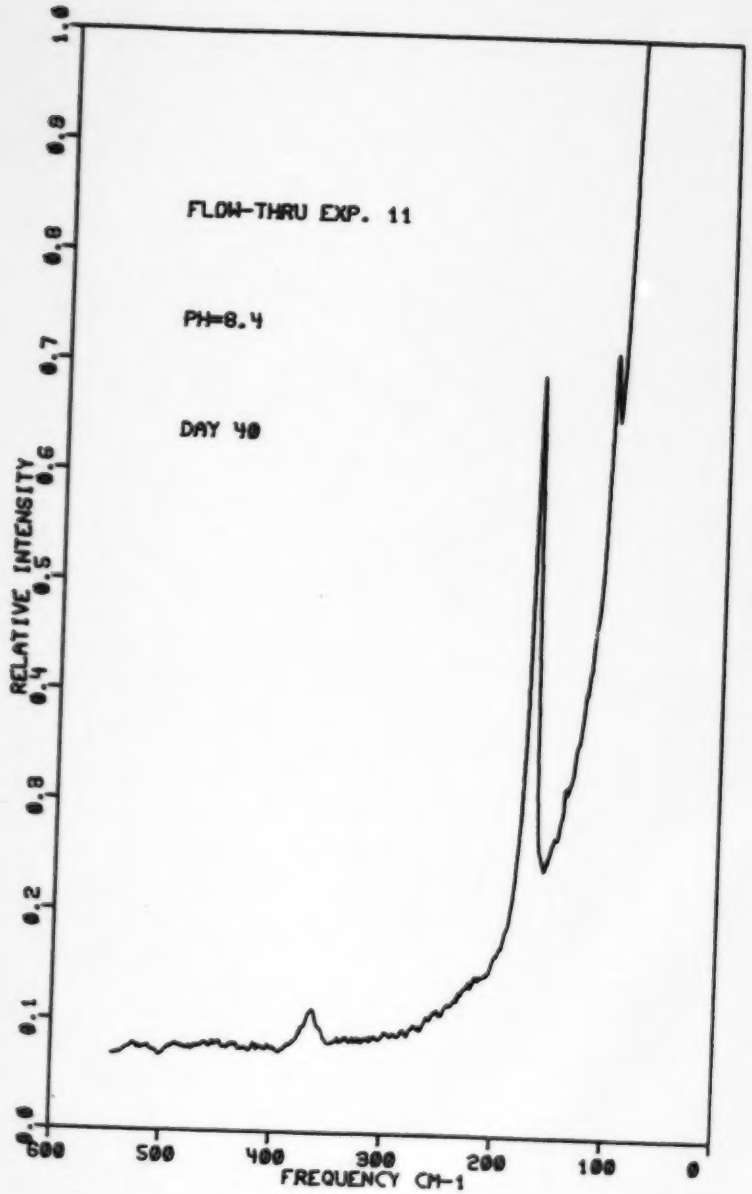

Figure 80. Raman spectrum of surface of lead electrode after day 40 in experiment 11.

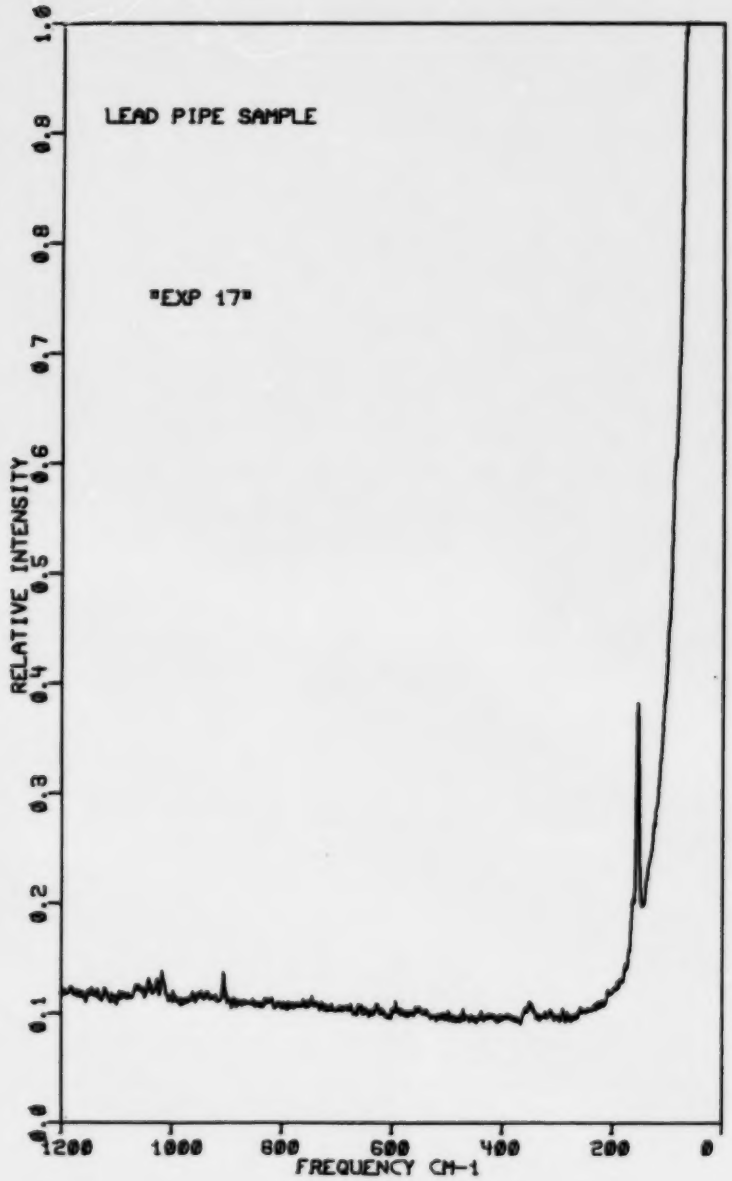

Figure 81. Raman spectrum of the surface of lead pipe labelled "Experiment 17.

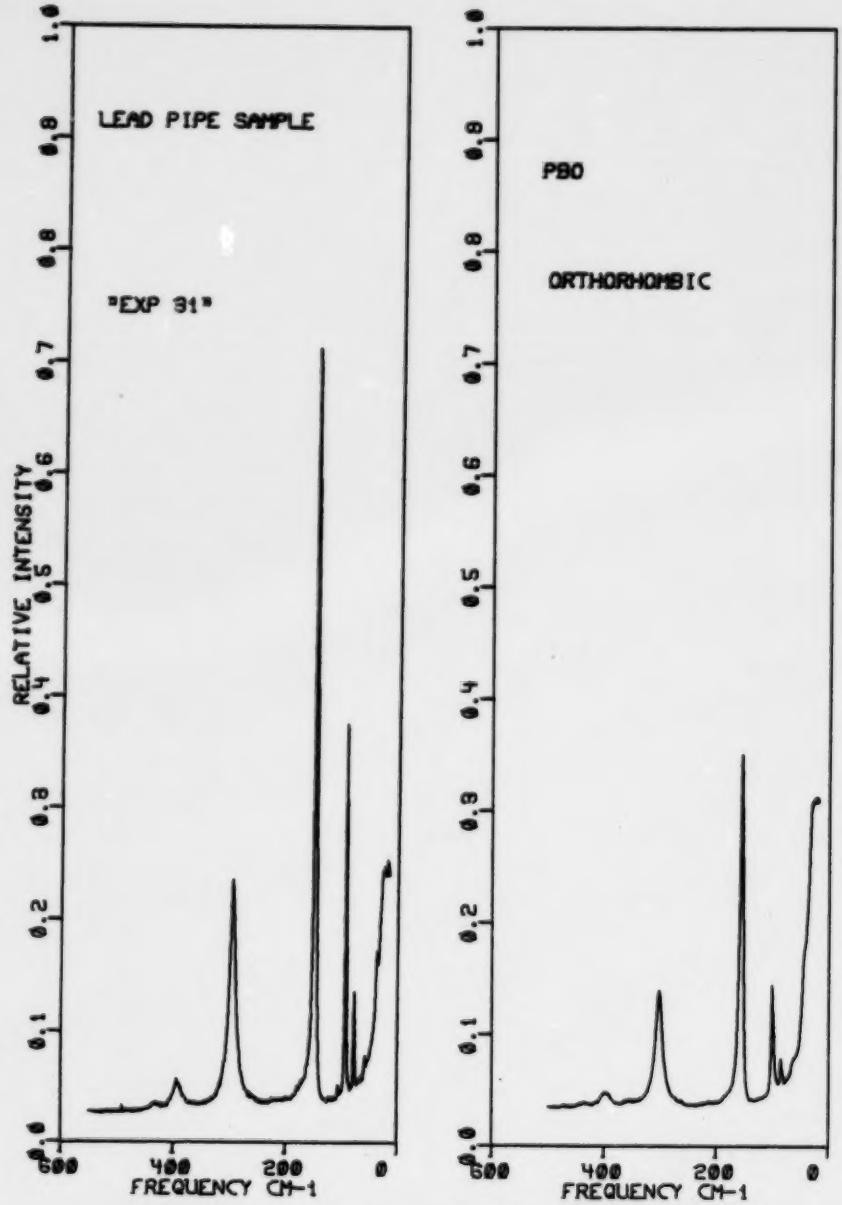

Reference Raman spectrum of orthorhombic PbO

Figure 82. Raman spectrum of the surface of the inside of lead pipe labelled "Experiment 31."

LEAD PIPE SECTION
EXP-32

Figure 83. Cross section of lead pipe labelled "Experiment 32"

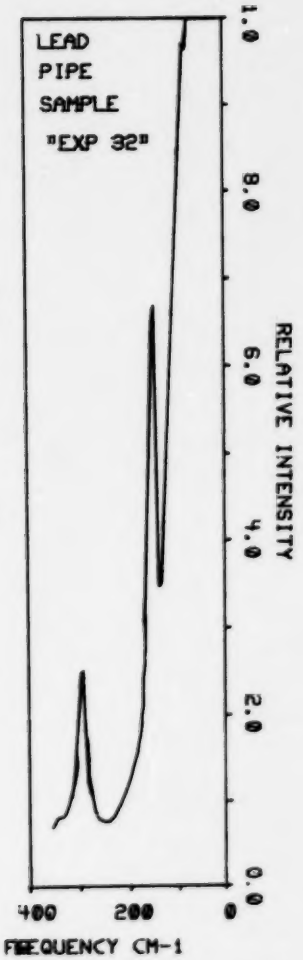

Figure 84. Raman spectrum of the inner surface of lead pipe labelled "Experiment 32."

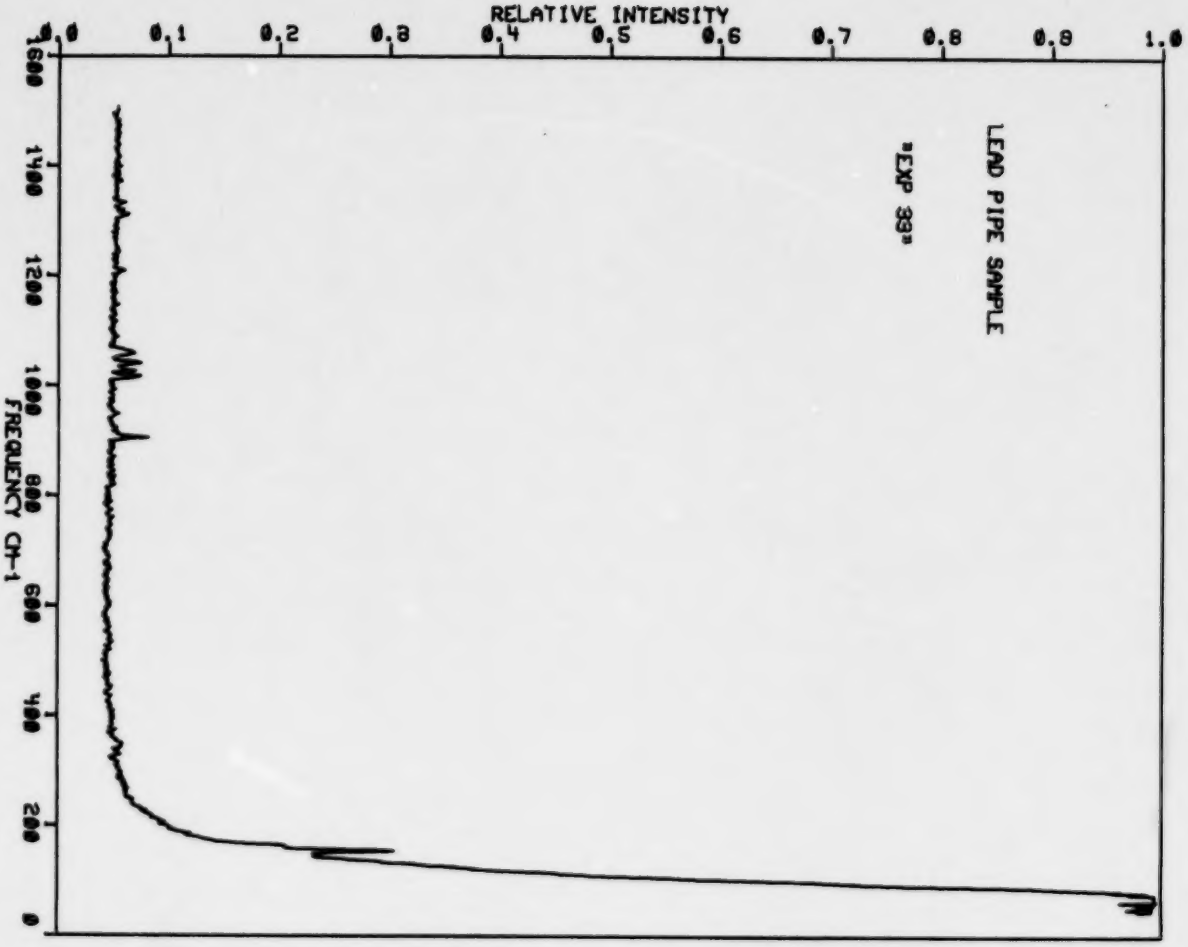

Figure 85. Raman spectrum of inner surface of lead pipe labelled "Experiment 33."

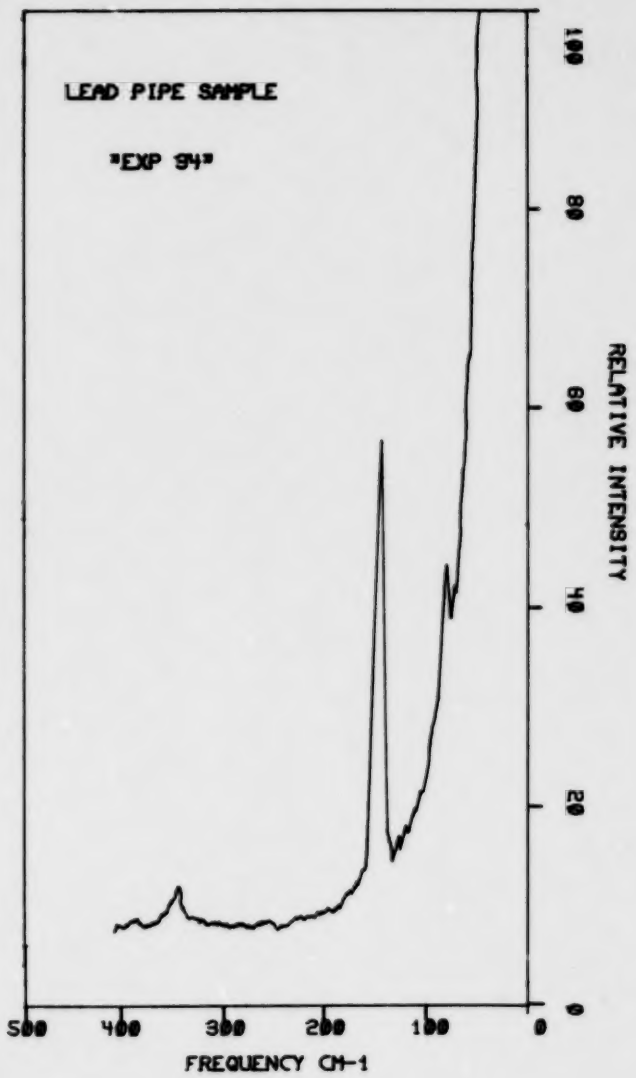

Figure 86. Raman spectrum of surface of lead pipe labelled "Experiment 34."

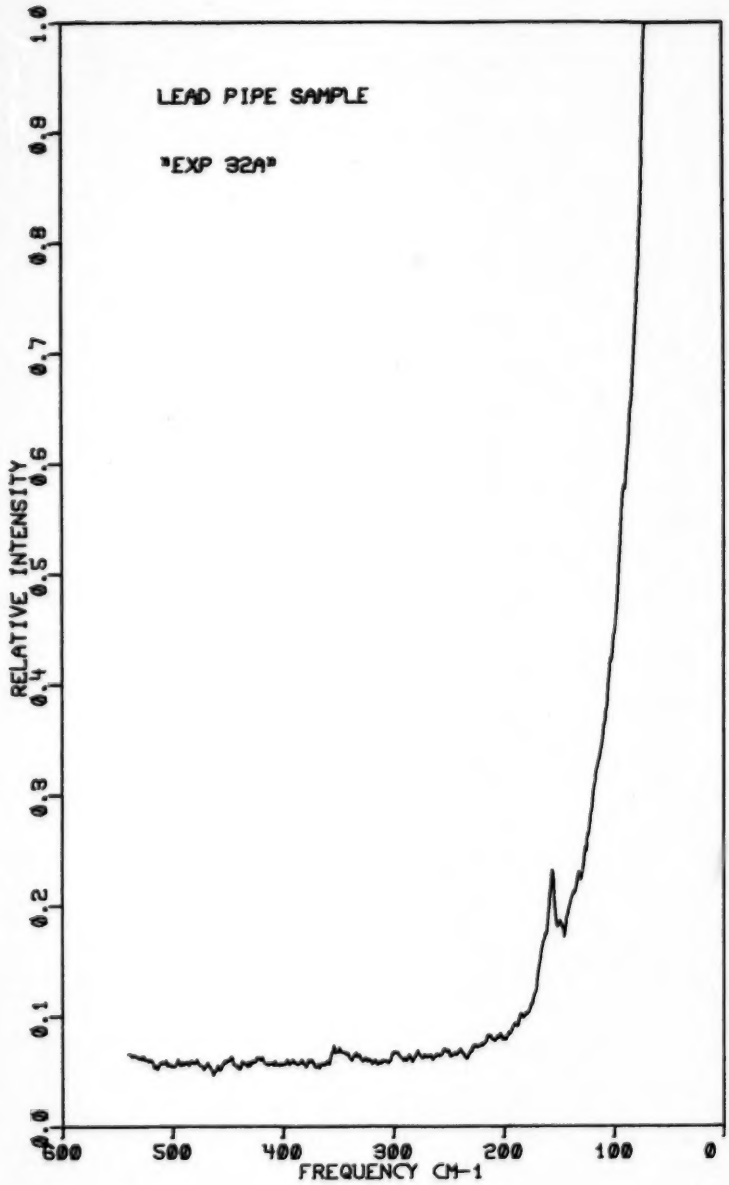

Figure 87. Raman spectrum of surface of lead pipe sample labelled "Experiment 32A."

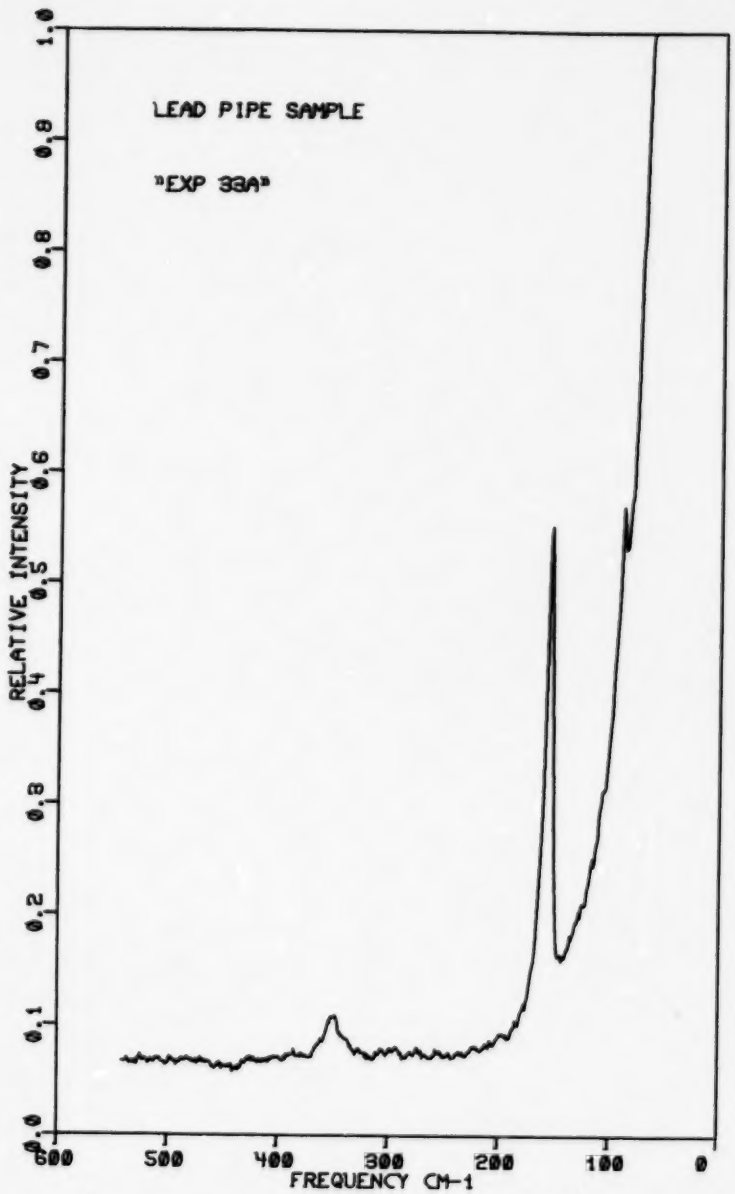

Figure 88. Raman spectrum of surface of lead pipe sample labelled "Experiment 33A."

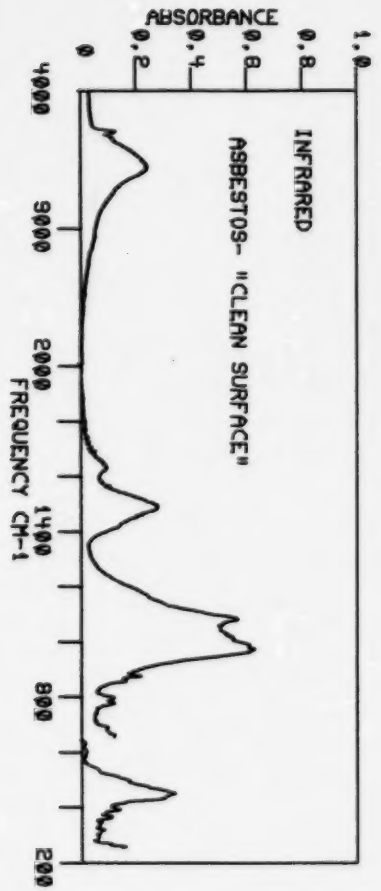

Figure 89. Infrared spectrum of a KBr pellet made from fibers scraped from surface of "clean" asbestos pipe.

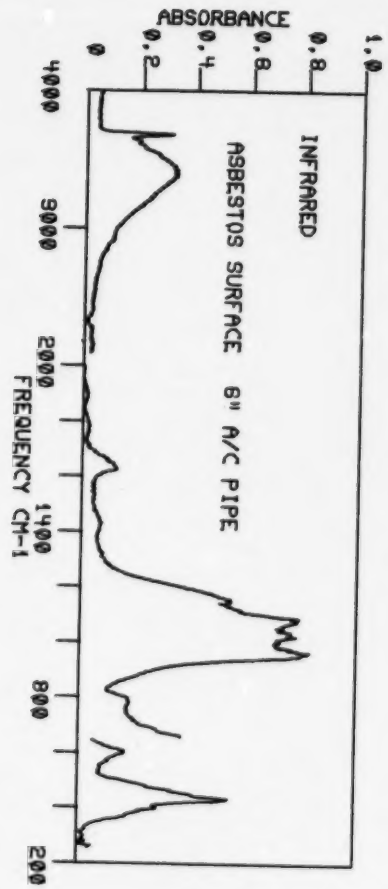

Figure 90. Infrared spectrum of a KBr pellet made from fibers scraped from surface of coated asbestos pipe labelled "6 A/C."

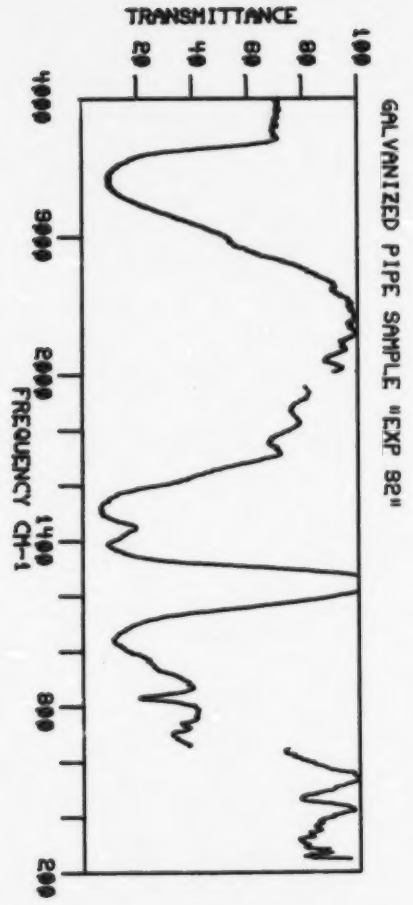

Figure 91. Infrared spectrum of surface material, in KBr pellet, of galvanized pipe labelled "Experiment 32."

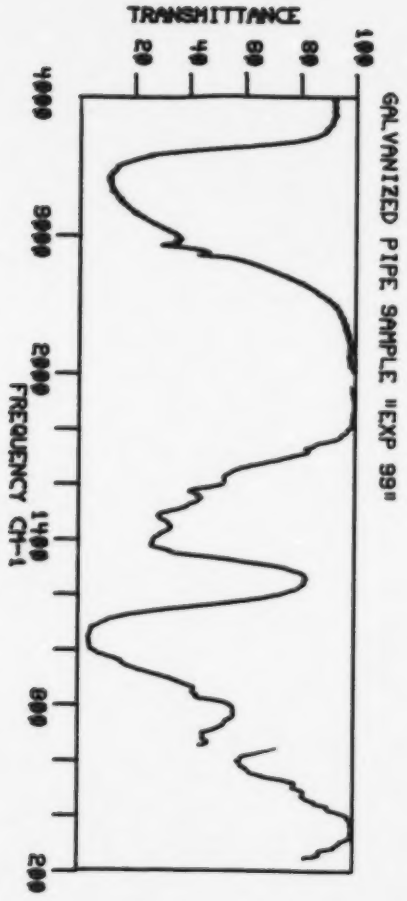

Figure 92. Infrared spectrum of surface material, in KBr pellet, of galvanized pipe labelled "Experiment 33."

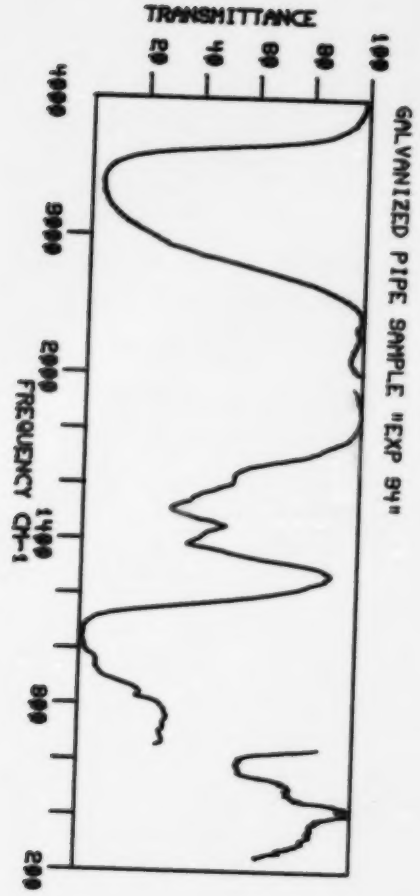

Figure 93. Infrared spectrum of surface material, in KBr pellet, of galvanized pipe labelled "Experiment 34."

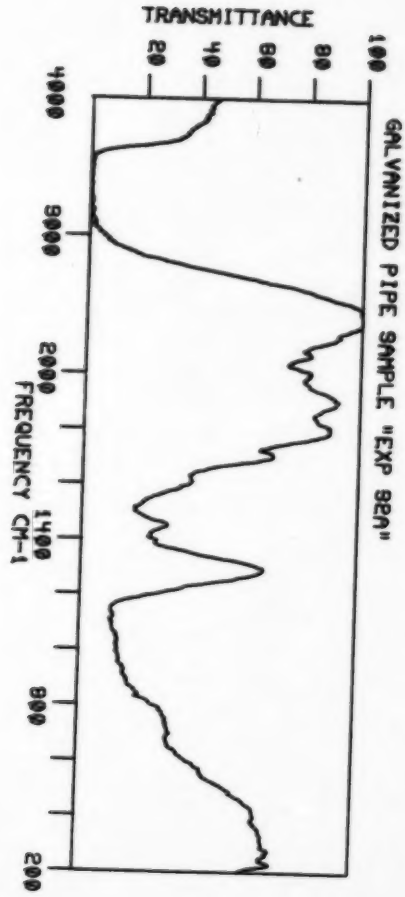

Figure 94. Infrared spectrum of surface material, in KBr pellet, of galvanized pipe sample labelled "Experiment 32A."

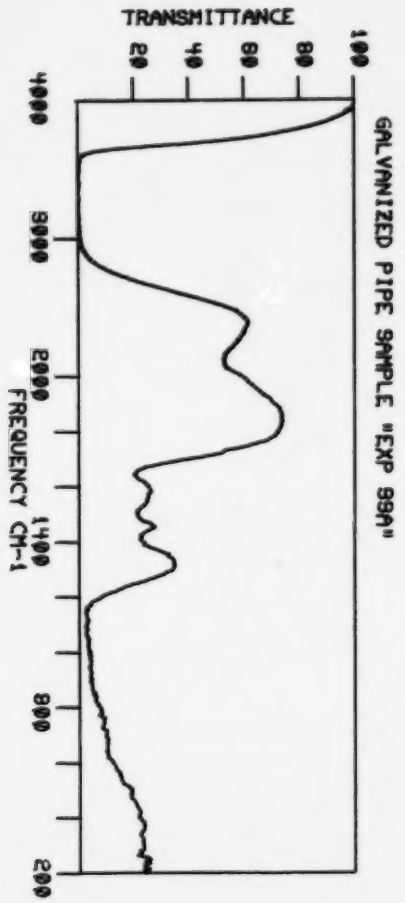

Figure 95. Infrared spectrum of surface material, in KBr pellet, of galvanized pipe sample labelled "Experiment 33A."

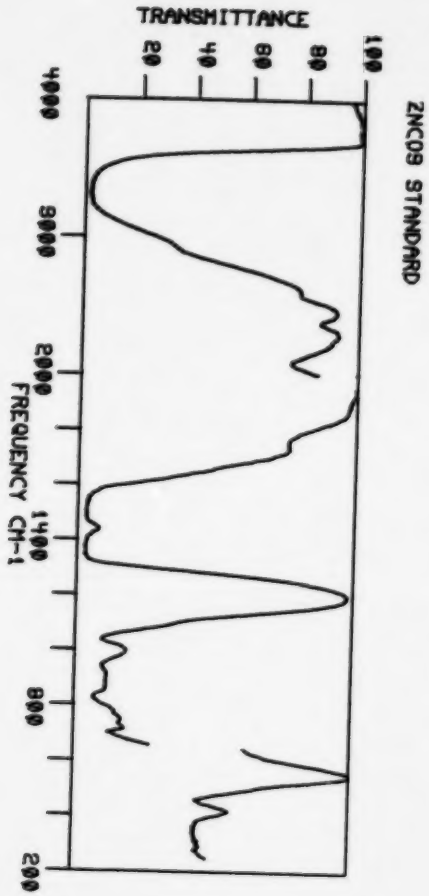

Figure 96. Infrared spectrum of $ZnCO_3$ in a KBr pellet.

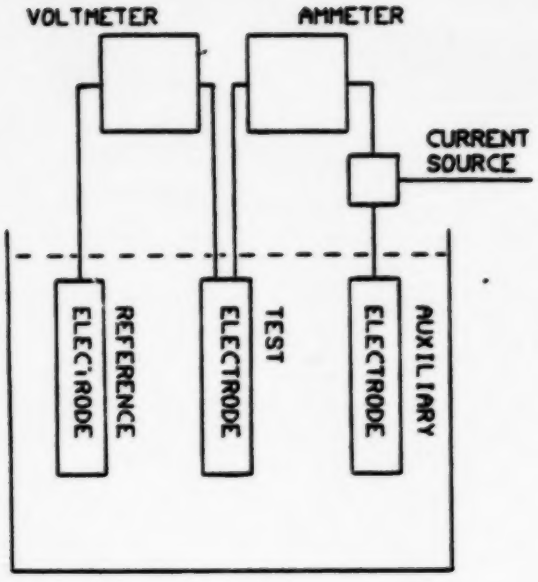

Figure 96. Schematic of interfacing Petrolite Corrosion Meter to electrodes.

REFERENCES

REFERENCES

1. P.C. Karalekas, C.R. Ryan, C.D. Larson, and F.B. Taylor, J. N.E. Water Work Assoc. 90, 150 (1976).

2. R.J. Thibeau, C.W. Brown, A.Z. Goldfarb, and R.H. Heidersbach, J. Electrochem. Soc., 127, 37 (1980).

3. R.J. Thibeau, C.W. Brown, A.Z. Goldfarb, and R.H. Heidersbach, J. Electrochem. Soc., 127, 1702 (1980).

4. M. Pourbaix, "Atlas of Electrochemical Equilibria in Aqueous Solutions," NACE, Houston (1969).

5. D.D. Wagman, W.H. Evans, V.B. Parker, I. Halow, S.M. Bailey, and R.H. Schummn, NBS Technical Note 270-3, U.S. Government Printing Office (1975).

6. W.L. Shirley, Practical Applications of Instantaneous Corrosion Rate Measurements in Industry, Petrolite Corporation, P.O. Box 2546, Houston, TX 77001 (1973).

7. M. Stern, Corrosion, 14, 440 (1958).

8. H.H. Uhlig, Corrosion and Corrosion Control, John Wiley & Sons, New York (1963).

9. D.R. Crow, Principles and Applications of Electrochemistry, Second Edition, John Wiley & Sons, New York (1979).

10. A.L. Whitted & C.F. Schrieber, Corrosion Rates by Electronic Methods, Dow Chemical Co., Freeport, TX.

11. A. Tamba, Br. Corros. J., 17, 29 (1982).

12. W.M. Gauntt, Technical Report C-13, Alpha Research Co., 1825 Wheaton Ave., Claremont, CA 91711.

13. E.L. Pye, Technical Report C-11, Alpha Research Co., 1825 Wheaton Ave., Claremont, CA 91711.